NTNU
Norwegian University of
Science and Technology

Benzotriazoles, Benzothiazoles and Inorganic Elements as Markers of Road Pollution Sources in a Sub-Arctic Urban Setting (Trondheim, Norway)

Johannes Asheim

Master of Science
Submission date: May 2018
Supervisor: Trond Peder Flaten, IKJ
Co-supervisor: Brynhild Snilsberg, Statens Vegvesen
Inga-Loise Sætermo Veivåg, Statens Vegvesen
Alexandros Asimakopoulos, IKJ

Norwegian University of Science and Technology
Department of Chemistry

Acknowledgements

This work was conceived and performed at the Department of Chemistry at the Norwegian University of Science and Technology (NTNU) in collaboration with the Norwegian Public Roads Administration, Trondheim.

The subject of the thesis was made possible with the help of my supervisor Trond Peder Flaten. I am grateful for all his advices both during the process of planning the thesis as well as sample preparation and analysis.

I am sincerely grateful to my co-supervisor Alexandros Asimakopoulos for the mentoring on both lab work and data analysis; and also for moral support, encouragement and excitement during the work of this thesis. The thesis would not be the same without it.

I am thankful for the help of Susana Villa Gonzalez and Kristine Vike in method development for LC-MS/MS. And grateful for all the help provided by Vishwesh Venkatraman for the principal component analysis.

The thesis would not be possible without the resources and help provided by Brynhild Snilsberg and the Norwegian Public Roads Administration. I am grateful for the help with the collection of road dust, and training of the Wet Dust Sampler provided by Inga-Loise Sætermo Veivåg; as well as help with the prall-test sampling.

Abstract

Road traffic emissions are known to contribute in environmental pollution and have adverse effects on humans. The emissions of organic and inorganic pollutants from traffic and road activity are established as the primary source of contamination in an urban environment. Abrasion of road materials, and tire and break wear are only some of thee contributing pollution factors in a road setting. Therefore, road dust is a promising environmental matrix for investigating sources of urban pollution. The road dust is a complex matrix composed of both natural and anthropogenic materials, and is a heterogeneous mix originating from diverse sources. Therefore, it is a great need for better characterization of the road dust, and a particularly need of good chemical markers for tire and brake wear.

In this study, a liquid chromatography tandem mass spectrometry (LC-MS/MS) method was developed for the simultaneous determination of six benzothiazoles (BTHs) and seven benzotriazoles (BTRs) primarily in road dust. The target benzothiazoles were benzothiazole, 2-hydroxy-benzothiazole, 2-mercaptobenzothiazole, 2-methylthio-benzothiazole, 2-amino-benzothiazole, and 2-Morpholin-4-yl-benzothiazole, and the target benzotriazoles were benzotriazole, 1-hydroxy-benzotriazole, 4-methyl-1H-benzotriazole (tolyltriazole), 5,6-dimethyl-1H-benzotriazole (xylyltriazole), benzotriazole-5-carboxylic acid, 5-chloro-1H-benzotriazole and 5-amino-1H-benzotriazole. Benzothiazoles and benzotriazoles are known pollutants in an urban environment. Benzothiazoles are previously proposed as potential chemical markers of tire wear, while benzotriazoles are well established anticorrosive chemicals linked to metal pollution. In addition, 66 elements were measured in the road dust samples by ICP-MS analysis in order to account for inorganic pollution sources.

The road dust samples analysed in this study were collected using a novel sampling instrument for road dust, the Wet Dust Sampler. Road dust samples were taken from both the non-studded tire season (summer) and the studded tire season (winter). The turbid road dust samples were filtered, extracted by sonication and prepared using solid phase extraction. In an attempt to pinpoint road dust pollution sources, different sample matrices were collected and analysed. In addition to road dust samples, air filters, tires, core-samples from asphalt, bitumen and background soil sample were analysed for both elements and/or organics. The tire samples, the asphalt samples, and the asphalt binding agent were also extracted by sonication and liquid extraction.

The concentrations both benzothiazoles and benzotriazoles and elements were higher in the winter season compared to the summer season. The concentrations of the benzothiazole and benzotriazole derivatives differed in the summer and winter season, indicating different transformation ratios based on season. Higher concentration of BTHs in the winter was probably attributed leaching from winter tires, possibly affected by road salt. This is described with a simple steady state kinetic model/equation in this study. The major source of most elements in road dust is the minerals in the coarse aggregate used in the pavement, and/or wear of car parts (chassis, shocks, brakes). The concentration of antimony (Sb) was approximately the same for both sampling seasons in dust, and it was associated to break wear. The increase in benzotriazoles, mainly tolyltriazole (TTR), in the winter season was probably attributed to the increased wear of car parts affected by road salt.

Making use of principal component analysis (PCA) it was possible to group adequately the sample matrices that were analysed. The PCA indicated associations between break wear and tire wear. 2-S-BTH and Sb were proposed as effective markers of break and rubber tire wear, while 2-OH-BTH, 2-Me-S-BTH, and Cl were proposed as possible markers of chemical leaching from tire rubber.

Sammendrag

Utslipp av organiske og uorganiske forurensninger fra trafikk og veiarbeid er den viktigste forurensningskilden i bymiljøet, og har klare negative virkninger på menneskets helse. Slitasje av veimaterialer, bildekk og bremsesystemer er noen av faktorene som bidrar til forurensning i en veisammenheng. På grunn av dette, er veistøv en lovende miljømatrise for å undersøke kilder til byforurensning. Vegstøvet er en kompleks matrise som består av både naturlige og menneskeskapte materialer, og er en heterogen blanding som stammer fra ulike kilder. Derfor er det et stort behov for bedre karakterisering av vegstøvet, og spesielt et behov for gode kjemiske markører for dekk- og bremselitasje.

I denne studien ble det utviklet en metode for væskekromatografi tandem massespektrometri (LC-MS/MS) for simultan bestemmelse av seks benzothiazoler (BTHer) og sju benzotriazoler (BTRer), hovedsakelig for veistøv. De analyserte benzothiazolene var benzothiazole, 2-hydroxy-benzothiazole, 2-mercaptobenzothiazole, 2-methylthio-benzothiazole, 2-amino-benzothiazole, og 2-Morpholin-4-yl-benzothiazole, og de analyserte benzotriazolene var benzotriazole, 1-hydroxy-benzotriazole, 4-methyl-1H-benzotriazole (tolyltriazole), 5,6-dimethyl-1H-benzotriazole (xylyltriazole), benzotriazole-5-carboxylic acid, 5-chloro-1H-benzotriazole og 5-amino-1H-benzotriazole. Benzothiazoler og benzotriazoler er kjente forurensninger i et urbant miljø. Benzothiazoler har tidligere blitt foreslått som potensielle kjemiske markører for dekkslitasje, mens benzotriazoler er veletablerte korrosjonshemmende kjemikalier koblet til metallforurensning. I tillegg, ble 66 grunnstoffer analysert i veistøvprøvene med ICP-MS for å kartlegge uorganiske forurensningskilder.

Veistøvprøvene analysert i denne studien ble innsamlet med et nytt prøvetakingsinstrument for veistøv, Wet Dust Sampler. Veistøvprøvene ble innsamlet fra både før og etter piggdekksesongen hadde startet (sommer og vinter). De turbide veistøvprøvene ble filtrert, ekstrahert ved hjelp av ultralydoppløsning og preparert med fast-fase-ekstraksjon. I et forsøk på å bestemme forurensningskildene til veistøv, ble forskjellige matriser innsamlet og analysert. I tillegg til veistøvprøvene ble luftfilter, bildekk, kjerneprøver fra asfalt, bitumen og jord-bakgrunnsprøve analysert for både grunnstoffer og/eller organiske stoffer. Dekkprøvene og prøven av asfaltbindemiddelet ble også ekstrahert med ultralydoppløsning og preparert med væske-ekstraksjon.

Konsentrasjonene av både benzothiazoler, benzotriazoler og grunnstoff var høyere i vintersesongen sammenlignet med sommer-sesongen. Konsentrasjonene av benzothiazol- og benzotriazol-derivatene varierte mellom sommer- og vinter-sesongen, som antyder forskjellige transformasjonsforhold avhengig av sesong. Høyere konsentrasjoner av BTHer i vinter-sesongen var sannsynligvis koblet til utlekking fra vinterdekk, mulig påvirket av veisalt. Dette er beskrevet i studien ved hjelp av en enkel ”steady state”-kinetikk-modell/ligning. Hovedkilden til de fleste grunnstoffene i veistøv er mineralene i grovtilslaget i veidekket, og/eller slitasje av bildeler (understell, fjæringer, bremser). Konsentrasjonen av antimon (Sb) var omtrent den samme i veistøv fra begge begge sesonger, og anslått til å komme fra bremseslitasje. Økningen av benzotriazoler, hovedsakelig tilyltriazole (TTR), i vintersesongen skyldes mest sannsynlig økt slitasje av bildeler påvirket av veisalt.

Ved hjelp av prinsipalkomponentanalyse (PCA) var det mulig å gruppere de analyserte prøvematrisene. PCAen indikerte en sammenheng mellom bremseslitasje og dekkslitasje. 2-S-BTH og Sb foreslås som effektive markører for bremse- og gummidekkslitasje, mens 2-OH-BTH, 2-Me-S-BTH og Cl foreslås som mulige markører for utlekking av kjemikalier fra gummidekk.

Table of contents

List of Figures

List of Tables

Abbreviations

Table 0.1: Abbreviation of the chemicals analysed in LC-MS/MS

Chemical	Abbreviation
Benzothiazole	BTH
Benzotriazole	BTR
5,6-Dimethyl-1H-benzotriazole monohydrate	XTR
4-Methyl-1H-benzotriazole	TTR
Benzotriazole-5-carboxyl acid	BTR COOH
5-Chlorobenzotriazole	5-Cl-BTR
2-Mercaptobenzothiazole	2-S-BTH
5-Amino-1H-benzotriazole	5-Amino-BTR
2-Aminobenzothiazole	2-Amino-BTH
1-Hydroxybenzotriazole hydrate	1-OH-BTR
2-Hydroxybenzothiazole	2-OH-BTH
2-(Methylthio)benzothiazole	2-Me-S-BTH
2-Morpholin-4-YL-benzothiazole	2-M-BTH
1H-Benzotriazole-(ring-d4)	BTR-d4

1 Introduction

Road dust and dust in suspension in cities have gained interest in the last 20 years. Many studies seek to find the sources of road dust, and how reduce the levels of pollution from vehicles. Increased amounts of road dust during winter has been mainly attributed to the use of studded tires that wear the road surface. Moreover, other sources of road pollution remain understudied.

The Swedish National Road and Transport Research Institute (VTI)has introduced a novel sampling device for collecting road dust, the Wet Dust Sampler (WDS). This device uses a high-pressure washer to collect road dust from the road into an aqueous sample matrix that allows a range of different analytic methods to be applied on (Per Jonsson, 2008). The WDS is distributed in Scandinavia, and Norway possess one such device located in Trondheim. Since this device is novel, its possibilities are still not fully investigated when it comes to its use as a road dust sampler for analytical/environmental chemistry purposes.

The first main aim of this study was to analyse both inorganic and select organic chemicals in the road dust collected by the WDS with an attempt to distinguish pollution sources. For the organic analysis, the analysed components were benzothiazoles (BTHs) and benzotriazoles (BTRs), as BTHs are established to be a possible indicator for tire wear, while benzotriazoles are well established anticorrosive chemicals linked to metals (Pant and Harrison, 2013). BTHs are also detected in previous studies in a variety of matrices, ranging from indoor dust and textiles to swimming pools and wastewater. In this study, a method was developed for the organics, including two benzotriazoles not previously studied in road dust.

Both elements (e.g. zinc) and organic chemicals (e.g. benzothiazoles) have been previously proposed as indicators for tire wear in road dust (Pant and Harrison, 2013). Specific elements are also suggested as key tracers for the wearing of different vehicle parts and emissions (e.g. brakes, deterioration, exhaust, emissions etc.) But a multitude of possible contributing pollution sources render it difficult to determine a sole key tracer (Pant and Harrison, 2013; Thorpe and Harrison, 2008). The second main aim of the study was to determine specific pollution sources by performing both elemental and select organic analysis in different seasons (summer, winter), and analysing a variety of sample matrices including asphalt, road dust, tires and air filters. The potential sources of exposure are elucidated through Principal Component Analysis (PCA) with the aim to identify the patterns within a specific data set, and cluster the sources based on their similar characteristics.

2 Theory

The theory chapter begins with the properties of benzothiazoles and benzotriazoles, and possible uses and sources, including previously detected levels. The road dust section gives a description of properties of road dust and differences between seasons, as well as information about elements relevant to traffic and use of vehicles. A brief description of the mineral composition of Elgeseter street follows, based on a previous study. Thereafter, a detailed description is given for both the sampling device and the instrumentation used for the road wear testing, as well as for the analytical methods used in this study. Since a multi-residue method was developed for the analysis of benzothiazoles and benzotriazoles, detailed quantification and quality assurance/validation information is presented in this work. For the statistical processing of the data, theory on data transformation, correlations, and principal component analysis (PCA) are given in the theory part.

2.1 Benzothiazoles and benzotriazoles

Benzothiazoles (BTHs) are aromatic heterocyclic compounds consisting of a 1,3-thiazole ring fused to a benzene ring. The chemical formula of the BTH ring structure is C_7H_5NS. Benzotriazoles (BTRs) are also heterocyclic compounds containing two fused rings and three nitrogen atoms. The chemical formula of the BTR ring structure is $C_6H_5N_3$ (**Figure 2.1**). BTHs are widely used as vulcanization agents in rubber, biocides in paper and leather manufacturing, and anticorrosive agents in antifreeze formulations (Herrero et al., 2014; Loi et al., 2013). BTRs can form a stable coordination complex with metals (e.g copper), resulting in anticorrosive properties, and applications in antifreeze formulations, cooling systems, hydraulic fluids and dishwasher detergents. BTHs can be derived from natural sources, in addition to anthropogenic sources. BTH is a known constituent of tea leaves and tobacco smoke (Asimakopoulos et al., 2013a). Some BTRs have specific chemical or biological properties, rendering them as particularly useful in the pharmaceutical industry (Herrero et al., 2014). BTRs and BTHs easily reach environmental media such as surface water bodies and wastewaters, due to their widespread use in various applications and consumer products (Herrero et al., 2014). BTRs and BTHs are classified as high-volume production chemicals, with an estimated worldwide production of BTRs in excess of 9000 tonnes/year (Loi et al., 2013). The production of BTHs was documented to be in the range of 4.5–450 tons in the U.S. in 1993 (Technical Resources International Inc., 1997). BTHs and BTRs have been found in indoor dust (Wang et al., 2013), outdoor air particles (Maceira et al., 2018), human urine (Asimakopoulos et al., 2013a,b), clothing (Liu et al., 2017), tobacco smoke (Schmeltz and Hoffmann, 1977; Seo et al., 2000) tap water (Wang et al., 2016) and even in swimming pool water (Lu et al., 2017). Previously detected levels of BTHs and BTRs, in selected matrices relevant to this study, are given in **Table 2.1**.

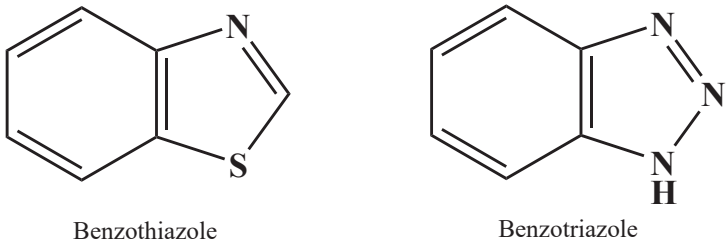

Figure 2.1: Chemical structure of benzothiazole and benzotriazole ring

Commonly known BTHs include benzothiazole (BTH), 2-hydroxy-benzothiazole (2-OH-BTH), 2-mercaptobenzothiazole (2-S-BTH), 2-methylthio-benzothiazole (2-Me-S-BTH), 2-amino-benzothiazole (2-NH2-BTH), and 2-Morpholin-4-yl-benzothiazole (2-M-BTH) (**Figure 2.2**). BTH and 2-OH-BTH are breakdown products from vulcanizing agents and antioxidants added to rubber materials during manufacturing (Reddy and Quinn, 1997). BTH and 2-OH-BTH are documented to be used as corrosion inhibitors in antifreeze liquids in commercial cars (Reddy and Quinn, 1997). 2-S-BTH is the BTH derivative most widely-used as a vulcanization accelerator in rubber products such as car tires, cables, seals, shoes, rubber gloves and toys (Herrero et al., 2014; Leng and Gries, 2017). 2-S-BTH and 2-NH2-BTH have proven good corrosion inhibitory efficiency for carbon steel applications (Jafari et al., 2014). 2-Me-S-BTH is a biomethylation product of 2-S-BTH, and a photolysis by-product of 2-(thiocyanomethylthio)benzothiazole (which is a commonly used herbicide) (Brownlee et al., 1992). 2-M-BTH is used as a vulcanizing accelerator in rubber (Zeng et al., 2004). It has low water solubility and is non-volatile, and has documented use in antifreeze liquids in cars (Reddy and Quinn, 1997). 2-M-BTH and its derivatives are toxic to living organisms including humans, and is a persistent substance in soil. (Umamaheswari and Rajaram, 2017). Reddy and Quinn (1997) found that BTH, 2-OH-BTH and 2-M-BTH are major organic components that leach from rubber, and asphalt containing 1-3% rubber. BTH biodegrades rapidly under aerobic conditions (HSDB, 2018). 2-S-BTH can undergo biomethylation to 2-Me-S-BTH, or photolysis to 2-OH-BTH and BTH. Specific microorganisms can transform BTH into 2-S-BTH before it is converted to a more stable methylated product (e.g 2-Me-S-BTH) (Felis et al., 2016). In water containing chloride it is suggested that BTH can undergo oxidation by hydrochloride to 2-OH-BTH (Brownlee et al., 1992). It is expected that 2-M-BTH is photodegraded to BTH, in a similar way as 2-S-BTH (Liao et al., 2018). Experiments on wastewater treatment has shown that 2-NH2-BTH rapidly degenerates (<5min) in solutions with chloride (molar ratio of 1000/1)(Nika et al., 2017). Aqueous photolysis tests show that 2-S-BTH is susceptible to direct photolysis, with a half-life of hours or less (at a surface) under full sunlight exposure (30-40 N latitude) (HSDB, 2018). Furthermore, BTH can be microbial degraded into 2-OH-BTH in natural waters. In experiments done by Reddy and Quinn (1997) with collected water from a highway settling ponds (collected during September) showed that 60% of the BTH was transformed into 2-OH-BTH. For water samples collected in November and December, both BTH and 2-OH-BTH degraded within 30 days. These results indicate that different bacteria that reside in the ponds or others seasonal factors (e.g. road salts), have an influence on the breakdowns of BTH and 2-OH-BTH (Reddy and Quinn, 1997). An overview of transformation pathways of BTHs in urban settings are demonstrated in **Figure 2.3**.

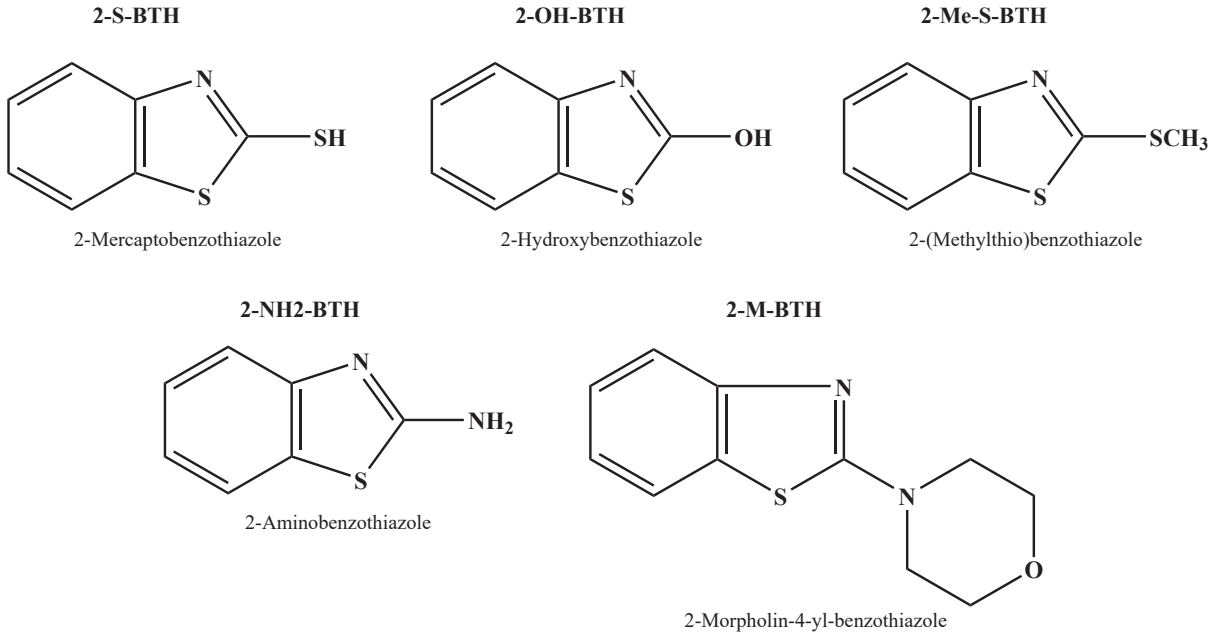

Figure 2.2: Derivatives of benzothiazole

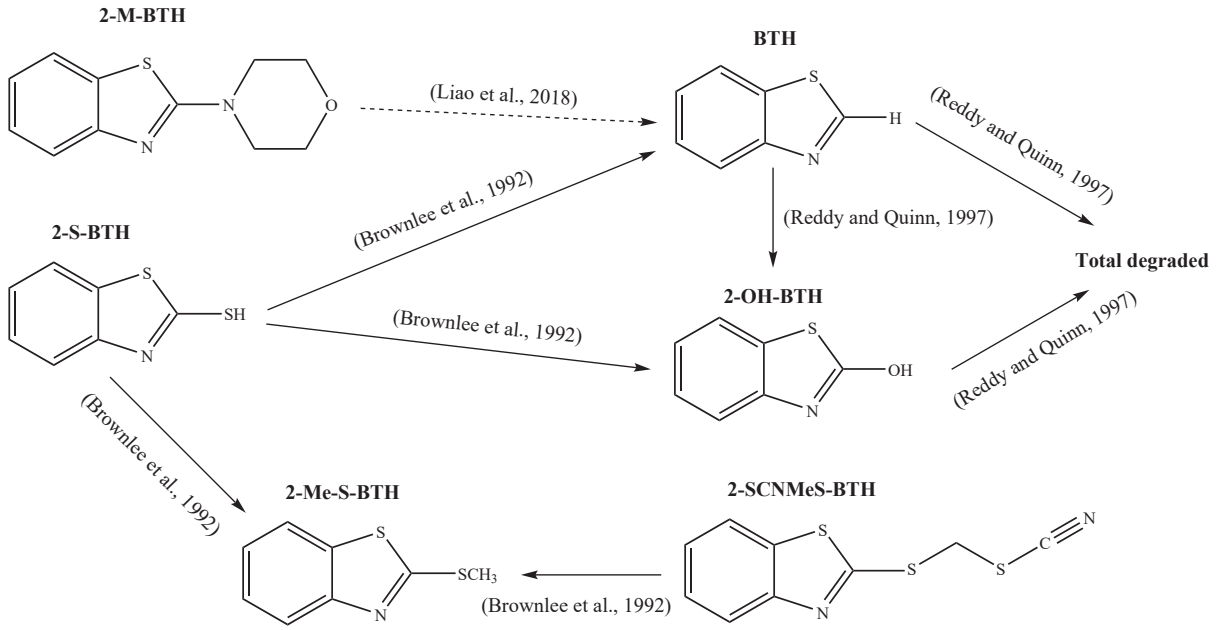

Figure 2.3: Overview of possible transformations of BTHs in environmental media

Table 2.1: Occurrence of BTHs and BTRs in different urban settings (means/range if not stated otherwise).

Matrix	Region	Date		BTH	2-S-BTH	2-OH-BTH	2-NH2-BTH	2-M-BTH	2-Me-S-BTH	Sum BTHs	Ref.
Summer tire (15 years old, rethreaded)	Norway		ng/g	23,500	12,300				460		(Avagyan et al., 2013)
Rubber tire, recycled	Spain		μg/g	6.16*					185*		(Llompart et al., 2013)
Commercial paver	Spain		μg/g	107*							(Llompart et al., 2013)
Urban dust	China		ng/g					15.9 - 45.8			(Pan et al., 2012)
	Spain[a]		ng/m^3	0.35		1.2	0.11		0.02	1.7	(Maceira et al., 2018)
Outdoor air[b]	Connecticut, USA	2009	ng/m^3	11,000-14,000							(Liao et al., 2018)
Road dust	Rhode Island, USA	1995	ng/g	78.7-149		2.46-90.2					(Liao et al., 2018)
Tire summer	Europe	2005-2011	μg/g	39.3-155[c]	554-1380[c]			0.80-2.04[c]			(Avagyan et al., 2014)
Stud tire	Europe	2005	μg/g	60.3-78.3[c]	53.3-2170[c]			0.88-1.10[c]			(Avagyan et al., 2014)
Tire winter	Finland	2005	μg/g	55.1	330			1.25			(Avagyan et al., 2014)
Asphalt	Stockholm, Sweden		μg/g	0.45	n.d			n.d			(Avagyan et al., 2014)
PM 10	Sweden	2013	μg/g	0.56	2.14			n.q			(Avagyan et al., 2014)
(particles $< 10\mu$m)	Tianjin, China	2016	μg/g*	13.07	0.42	7,91	0.19	21.31[c]	0.42	22.03	(Zhang et al., 2018)
PM 2.5 (particles $< 2.5\mu$m)	Tianjin, China	2016	μg/g*	15.7	1.9	7.32	0.57	31.01[c]	1.08	26.62	(Zhang et al., 2018)
Total suspended particulate	Sweden	2013	μg/g	4.58	13.3			n.q			(Avagyan et al., 2014)
(particles $< 75\mu$m)	Tianjin, China	2016	μg/g*	0.14	0.01	0.41	0.11	0.24[d]	0.01	0.68	(Zhang et al., 2018)

Matrix	Region	Date		BTR	TTR	XTR	5-Cl-BTR	Sum BTRs			Ref.
Summer tire (15 years old, rethreaded)	Norway		ng/g	n.d	n.d	n.d					(Avagyan et al., 2013)
Urban dust	Spain[a]		ng/m^3	1.5	0.16	0.15		2.8			(Maceira et al., 2018)
Snow from down-town/sub urban areas	Canada	2013	μg/L	0.08	0.59						(Alvey et al., 2016)
Melting water from "urban snow"	Canada	2013	μg/L	0.95-1.58	5.56-5.91						(Alvey et al., 2016)
Run off water, airport[e]	Norway		μg/L	1.2-1100							(Breedveld et al., 2003)

[a]: PM_{10} collected on quartz filters
[b]: sample taken over outdoor crumb rubber fields
[c]: low mean-high mean
[d]: ng/g
[e]: from de-icing pad, taken 1 year after de-icing operation ceased
*: median

Commonly known BTRs include 1H-benzotriazole (BTR), 1-hydroxy-benzotriazole (1-OH-BTR), tolyltriazole (TTR, a mixture of isomers of 4-methyl-1H-benzotriazole (4-Me-1H-BTR) and 5-methyl-1H-benzotriazole (5-Me-1H-BTR)), 5-chloro-1H-benzotriazole (5-Cl-BTR), and xylyltriazole (XTR or 5,6-dimethyl-1H-benzotriazole (5,6-diMe-1H-BTR)) (**Figure 2.4**). BTR and TTR are used as corrosion inhibitors for metals and steel, especially copper and brass (a metallic alloy that is made of copper and zinc), by forming a thin complexing film on the metal surface (Cantwell et al., 2015). BTR and TTR are particularly used in aircraft de-icing/anti-icing fluids. They are generally present to reduce the flammability hazard from corrosion of metal components carrying a direct current (Breedveld et al., 2003). BTR and TTR acts as a chelating agent in the reaction of silver (in silver-covered copper wires) and glycol (in de-icing/anti-icing fluids), by removing the silver ions. This prevents the creation of silver oxide and eventually silver fulminate, which is a sensitive detonator (Downs, 1968). BTR may undergo direct photolysis in the environment, and it is shown to be slowly photo-decomposed into aniline and o-anisidine by irradiation at 300 nm (HSDB, 2018). XTR is a methylated BTR, and possible transformation product of BTR (Huntscha et al., 2014). 1-OH-BTR (1-OHBTR), benzotriazole-5-carboxylic acid (BTR COOH) and 5-amino-1H-benzotriazole (5-Amino-BTR) are polar derivatives of the BTR class. It is found that BTR has an aerobic pathway to 1-OH-BTR and 4-hydroxybenzotriazole, by experiments with wetlands and artificial sunlight (Felis et al., 2016). BTR COOH, in particular, is proven to be a transformation product of 4-Me-1H-BTR (Huntscha et al., 2014). 5-Cl-BTR is used as a UV-stabilizer in various products, including building materials, vehicle components, waxes, paints, and adhesive agents (Fent et al., 2014).

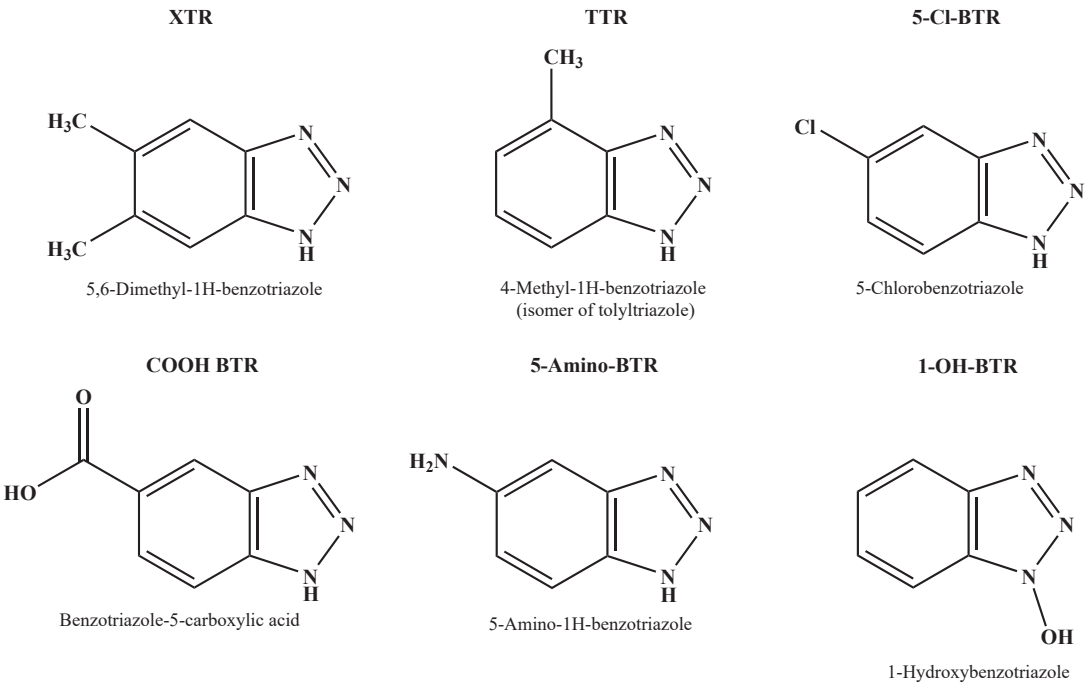

Figure 2.4: Derivatives of benzotriazole

2.2 Road dust

The road dust matrix is composed of both natural and anthropogenic materials that accumulate on the road surface mainly in proximity to the pavements (Valotto et al., 2018). The road dust is a heterogeneous mix originating from diverse sources, with a complex source characterisation. Some of the potential sources for road dust are erosion of surrounding soil, atmospheric deposition and anthropogenic activities including traffic related activities (Gunawardana et al., 2012). Snilsberg et al. (2017) analysed road dust from Kristiansund, Norway, collected by WDS (**section 2.3**). They found that the organic and inorganic content in the road dust obtained from the road edge (kerb) were 8.4-13.3% and 86.7-91.6% respectively, and the particle diameter of the road dust was in the range of 0.04-242 μm with a peak of 50 μm. Gunawardana et al. (2012) found that the organic content in road dust was higher in residential areas, compared to commercial and industrial areas, possibly because of the surrounding vegetation at the investigated sites of the study. The composition of road dust has been found to be dominated by elements normally associated with crustal materials. The element composition therefore often reflects the local geology and varies greatly with location. There can also be pronounced variation with seasons, especially in regions where road salting and use of studded tires is common practice in the winter months (Thorpe and Harrison, 2008).

The road dust comes from both exhaust and non-exhaust emissions and can be resuspended by wind and traffic (Valotto et al., 2018; Thorpe and Harrison, 2008). Emissions from road traffic constitute a substantial proportion of primary particulate matter within urban areas, with a considerable contribution to PM_{10} (particles with less than 10 μm diameter) and $PM_{2.5}$ (particles with less than 2.5 μm diameter) levels (**Table: 2.2**). Studies from European cities has shown that the road dust contribution from exhaust and non-exhaust emissions are of similar level of magnitude. In northern European cities, where sanding of roads and use of studded tires are common, the non-exhaust emission fraction of PM_{10} can be as high as 90% (Thorpe and Harrison, 2008; Omstedt et al., 2005). Non-exhaust emissions typically arise from abrasive sources, including wear and tear of vehicle parts (brakes, tires, clutch), wear of road surface and re-suspension of dust (Pant and Harrison, 2013; Thorpe and Harrison, 2008). Amato et al. (2014) identified three main sources for road dust build-up: (1) carbonaceous sources, mainly related to tire wear, with possible contributions from motor exhaust and brake wear; (2) road wear; and (3) brake wear. The sum of these three sources explained 96% of the observed road dust mass loadings.

Table 2.2: Yearly average road dust contribution to PM_{10} and $PM_{2.5}$ levels in different sites (Amato et al., 2014)

Rural		Urban-industrial		Urban		Traffic	
PM_{10}	$PM_{2.5}$	PM_{10}	$PM_{2.5}$	PM_{10}	$PM_{2.5}$	PM_{10}	$PM_{2.5}$
9-22%	7%	17-22%	6-16%	29-34%	11-31%	21-35%	21-31%

There have been reported high levels of metals, such as copper (Cu), lead (Pb) and zinc (Zn), in urban street dust from many countries, linked to the high motor vehicle traffic in these areas (Apeagyei et al., 2011). The wear of brakes and tires are an important source of trace metals in the urban environment (Thorpe and Harrison, 2008).

Exhaust emissions come from the combustion of vehicle fuel. Different types of engines emit fumes with different composition. Diesel engines produce a higher mass of particles since the

fuel is considered less clean and there is no catalytic treatment of the exhaust gases. More than 90% of the exhaust gases produced by diesel engines are nanoparticles (<50 nm) composed of metals, elemental carbon and semivolatile organic compounds. The organic compounds are formed when the exhaust is diluted and cooled after the gasses exit the tailpipe, and mainly consist of unburned lubricate oil (Forsberg et al., 2005; Matti Maricq, 2007). Diesel vehicles emit both a greater mass of PMs and a larger number of ultrafine particles if compared to gasoline vehicles (Pant and Harrison, 2013). In a study done by Suarez-Bertoa and Astorga (2018) gasoline vehicles emitted two times more solid particles than diesel vehicles (at cold start), explained by the improvement of particle filters in current diesel vehicles. Both trace elements and organic compounds have been used as source markers for exhaust emissions, but after the removal of Pb from gasoline trace metals have become less useful as source markers (Pant and Harrison, 2013). Metals can be emitted from different exhaust-related sources: fuel and lubricant combustion; catalytic converters; particulate filters and engine corrosion. Elemental markers used for vehicular emissions include Cu, manganese (Mn), iron (Fe), Zn, barium (Ba), tin (Sn), nickel (Ni), molybdenum (Mo) and antimony (Sb). Ni and vanadium (V) have also been reported to be present in exhaust emissions due to oil combustion (Pant and Harrison, 2013). Different studies suggest different markers for exhaust fumes, for both gasoline and diesel engines. Some elements are also suggested markers for exhaust fumes from both gasoline engines as well as diesel engines (e.g. Ba and V), making it difficult to distinguish a specific source. Studies have suggested bromine (Br), Ba, Sb and V as potential markers for gasoline engines (Cheng et al., 2010). Cu, Mn and strontium (Sr) in particles <0.1μm are reported to be strongly associated with gasoline, while silver (Ag), Ba, cadmium (Cd), Pb, Sb, V, and Zn contents in nanoparticles (0.01-0.056 μm) are strongly associated with diesel fuel (Lin et al., 2005). Metals in the platinum group (rhodium (Rh), palladium (Pd), and platinum (Pt)) are expected to come from catalytic converters (Schauer et al., 2006). However, due to very low levels of trace elements emitted in exhaust fumes, great care is needed to distinguish them from non-exhaust traffic emissions and other sources. Precise source attribution with trace elements alone is difficult without local information on source particle composition (Pant and Harrison, 2013). The number of particles emitted from vehicle exhaust is temperature dependent. The solid particle emission of both diesel and gasoline vehicles increases at cold temperatures; but literature is referring mainly to start-up conditions of engines. However, a study done by Li et al. (2005) stated that the fuel consumption increases with 1.4% in cold temperatures (winter).

Non-exhaust emissions are typically characterized by metals (e.g. Cu, Zn, Ba, Sb, Mn), and less commonly organic chemicals (e.g. benzothiazoles). The profile of trace metal concentrations in non-exhaust particulate is unique for every region, based on traffic volume, climate and geological characteristics (Pant and Harrison, 2013).

2.2.1 Asphalt wear

Asphalt is the top layer of the road surface, consisting of a mixture of gravel (aggregate) and bitumen. The bitumen is a black viscous mixture of hydrocarbons, usually made from petroleum residues, acts as the binding agent in the asphalt. A key component in road dust is crustal particles, consisting of primarily coarse particles derived from different sources (traffic, industrial emissions, mineralogical dust etc.) (Pant and Harrison, 2013). Several metals have been detected in road bitumen samples including V, Ni, Fe, magnesium (Mg), and calcium (Ca). However, the concentrations of these metals were significantly lower when compared with raw bitumen, indicating that these elements are incorporated into the road surface from other sources

(Thorpe and Harrison, 2008). The different kinds of tires have an impact on the magnitude of wear emissions, with studded tires causing more emissions compared to summer and friction tires (Pant and Harrison, 2013). The combination of sanding on the roads and use of studded tires in the winter season, substantially increases the wear of the road surface, resulting in an increase in coarse particle emission (Forsberg et al., 2005). The friction between studded tires and the road asphalt can generate particles <0.1 μm, and this friction has shown to increase the emissions of PM_{10} by a factor of 1.5 (Pant and Harrison, 2013). Laboratory tests have also shown that more particles are produced (more wear) under wet conditions than under dry conditions (Snilsberg et al., 2008).

2.2.2 Tire wear

The tire wear particles are predominantly coarse ($PM_{2.5-10}$) and are generated mostly by shear forces between the tire thread and road surface, and also by volatilization (Pant and Harrison, 2013). Since tires contain a vast array of organic components and several inorganic components, much research has been done to investigate the physico-chemical characteristics of tires and tire wear particles, but the current understanding is still incomplete (Thorpe and Harrison, 2008).

The key tracer components of tire wear include BTHs and trace metals. The BTHs used as tracer components are: benzothiazole (BTH), 2-hydroxybenzothiazole (2-OH-BTH) 2-(4-morpholinyl)benzothiazole (2-M-BTH) and N-cyclohexyl-2-benzothiazolamine (Pant and Harrison, 2013). Zn is added to the tire thread as zinc oxide and organozinc derivatives to facilitate the vulcanization process. Zn is reported to reach up to nearly 1% by weight in rubber tires. Even though Zn is a ”major component” in car tires, it cannot be used as a sole tracer for tire wear as it is also emitted from brake wear, motor oil and other sources (Pant and Harrison, 2013). Other metals reported in tire wear debris are Mn, Fe, Co, Ni, Cu, Cd and Pb, but since there are other significant sources of these elements related to traffic, the use of these elements as individual or collective tracers for tire wear will most likely be ineffective (Thorpe and Harrison, 2008).

2.2.3 Other non-exhaust emission sources

The frictional contact between the brake system components during deceleration is an important source of particulate matter emissions from motor vehicles. During the braking of the vehicle, wearing occurs to both brake lining materials and brake discs (Thorpe and Harrison, 2008). Amato et al. (2014) found the contribution of brake wear to road dust to be 12% on average. Analyses of brake dust and crushed brake pads show high concentrations of Fe and Cu. The elements with the highest concentrations in brake dust are Ba, Cu, Zn and Sb (Thorpe and Harrison, 2008). Brake pads contain 13-45% of metallic Fe, and Cu, Sn, Sb, chromium (Cr) and Ba are used in lubricant formulations in brake pads manufacturing (Amato et al., 2014). Schauer et al. (2006) found Cu, Ba and Sb to be more strongly correlated to each other than to crustal elements, indicating that they are likely to originate directly from brake wear.

The Cu:Sb ratio has been suggested as a method to distinguish brake wear particles. Sternbeck et al. (2002) proposed the Cu:Sb ratio 4.6 as a diagnostic criterion for brake wear particles, but other ratios have been reported ranging from about 1-10. Some of the reported ratios are: 5.6 (Germany, 1990); 4.4 (Denmark, 2006); 5.3 (Sweden, 2007); and 9.1 (London, 2010). Differ-

ences can arise from different compositions in brake pads, and contribution from other sources (e.g ambient air) due to natural occurrence (Pant and Harrison, 2013).

In the winter season road salts are often applied to the road surface to remove snow and ice and therefore improve the tire friction. The most commonly used road salt for preventing/removing ice is sodium chloride (NaCl), both as dry and moisturised salt. Calcium chloride ($CaCl_2$), magnesium chloride ($MgCl_2$) and calcium magnesium acetate (CMA) are some of the other de-icing chemicals used on road. The de-icing chemicals also act as dust binding agents, by keeping the surface wet or humid and therefore retaining the road dust (Lundberg, 2018).

The road salts have been associated to corrosion of motor vehicles and unprotected steel structures (Kogel et al., 2006). $MgCl_2$ is the road salt which leads to the highest weight loss (corrosion) of steel, and use of $CaCl_2$ and $MgCl_2$ has been associated with an increase in vehicle corrosion (Prošek et al., 2007). The chassis of personal vehicles mainly consists of steel (iron and carbon), with an increasing use of Al alloys. Steel and titanium (Ti) is used in shocks. Wheels made of Al now make up over 50% of road wheels in cars and light trucks (Cole, 2017).

2.2.4 The urban road setting at ”Elgeseter street”

A previous study performed in Trondheim by Erichsen et al. (2004) found that the airborne dust was dominated by mineral matter. They also stated that the dust most likely comes from the tearing/wearing of the aggregate (rocks/gravel in asphalt recipe) used in the asphalt pavement. In Elgeseter street the mineral composition is almost 50/50 mylonite and gabro in the coarse aggregate. In the fine aggregate the content of gabbro is 65%. From the aggregate used in Trondheim, mylonite is composed of 40% plagioclase and 25% quartz as the main components. The gabbro is composed of 40% amphibole and 35% plagioclase as the main components. The dust collected and filtered ($< 10\mu$m) consisted of 31% quartz and 26.4% plagioclase (Erichsen et al., 2004). So, the most abundant mineral in the coarse aggregate is plagioclase, thereafter amphibole and quartz.

Plagioclase consists of a mixture of the minerals $Na(AlSi_3O_8)$ (albite) and $Ca(Al_2Si_2O_8)$ (anorthite) ranging from pure albite to pure anorthite. Amphibole minerals consists of Mg, Fe and a silica group. Quartz consists primarily of silica (silicon dioxide, SiO_2) (Encyclopædia Britannica, 2018).

2.2.5 Data from previous studies

Table 2.3 shows levels of elements found in some studies on road dust, tires, brake pads and brake dust, to give a rough overview of detected elements in the different matrices, and the amounts detected.

Table 2.3: Occurrence of elements in road related matrices (means/range if not stated otherwise).

Matrix	Car brake dust	Passenger tire tread	PM 10	Road dust			Used brake pads	Tires	Urban road dust
Region			Portugal -2014	Australia	Oslo, Norway - 1994	London, UK - 2014			Massachusetts, USA
	mg/kg	mg/kg	wt%	mg/g[a]	ppm (dry weight)[b]	mg/g[b]	ppm	ppm	ppm
Al	330-2500	7-129	1.10-4.23	1.40-5.88	59,527	18.53			
Ba	5900-74,400	10.4-166	0.06-1.12		526		49,960		148
Ca	920-8600	100-1680	0.68-3.93		42,691		2,843		12,712
Cd	<0.06-2.6	<0.05-0.34		0.19-0.54*	1.4	0.012	84[b]		
Co	12-42.4	0.5-4.1	<LOD		19		537[b]		
Cr	135-1320	<1-2	<LOD	3.16-14.8*		0.175	263[b]	140	119
Cu	70-39,400	<1-2	0.03-0.22	65.5-131.4	123	0.337	58,810	50	104
Fe	1.1-53.7 (%)	40-220	2.16-3.04	2.98-7.22	51,452	27.32	102,080	670	28,542
K	190-5100	110-410	0.55-0.84				12,106	690	7,363
Mg	83,000	<4-37	0.10-0.16		13,188	6.96			
Mn	620-5640	0.8-2.5	0.02-0.04		833	0.375	2,086		412
Mo	5-740				4			60	5[b]
Na	80	120-530	0.293		19,295				
Ni	80-730	<1-3	<LOD	4.53-7.92*	41	0.031			
Pb	4-1290	1-5.7	0.010-0.028	25.7-38.4*	180	0.227	80	11[b]	69
Sb	4-16,900	<0.2-0.9	0.005-0.015		6		300[b]		
Sr	300-990	<0.5-2.6	0.003-0.004		344		2,380	40	143
Ti		560	0.096-0.110		7,452		94,360	200	2,216
Zn	12-27,300	5650-9640	0.074-0.259	90.4-296.6*	412	1.15	1,152	17,720	296
Zr			<LOD				26,840	30	173
Ref	(Thorpe and Harrison, 2008)	(Thorpe and Harrison, 2008)	(Alves et al., 2018)	(Gunawardana et al., 2012)	(Miguel et al., 1997)	(Crosby et al., 2014)	(Apeagyei et al., 2011)	(Apeagyei et al., 2011)	(Apeagyei et al., 2011)

*: μg/g
[a]: low average-high average
[b]: mean

2.3 Wet Dust Sampler (WDS)

The wet dust sampler is used for sampling of dust and other dissolved substances in an impermeable surface. WDS III (version 3; **Figure 2.5**) is using a high-pressure washer to spray a small area of the surface and pneumatically (use of air) transfer the road dust to a sample bottle (Per Jonsson, 2008; Snilsberg et al., 2017).

The WDS is equipped with a control box that regulates the time of the high-pressure washer and the compressor settings (Per Jonsson, 2008); this ensures that each sampling is made in a similar manner. The diameter of the chamber, and the area washed, is approximately 20 cm^2 (circle with $\sim$ 51 mm). Each sample-shot consist of 340 mL distilled water, and a sample consist of six consecutive sample-shots reaching a total of 2.5 L (Snilsberg et al., 2017).

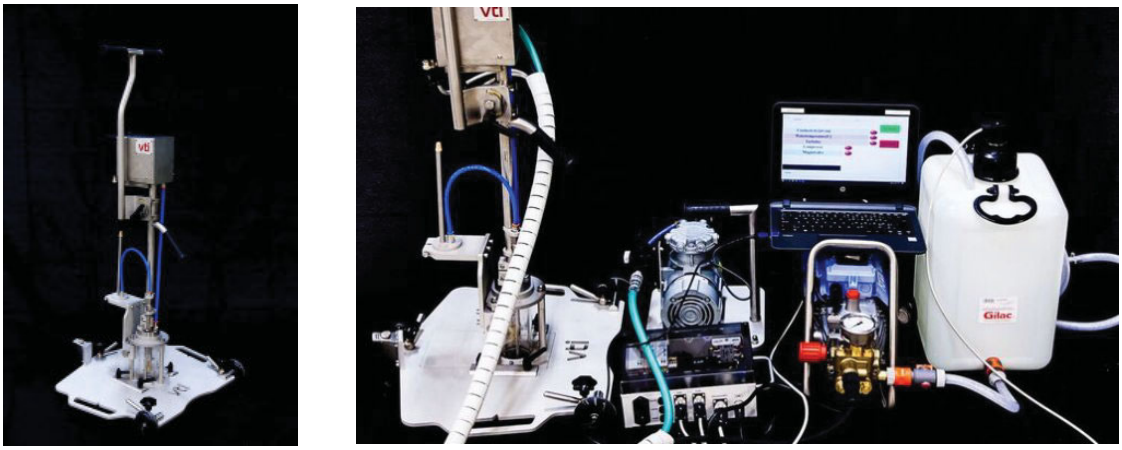

Figure 2.5: The Wet dust sampler, (Photo: Mats Gustafsson, VTI)

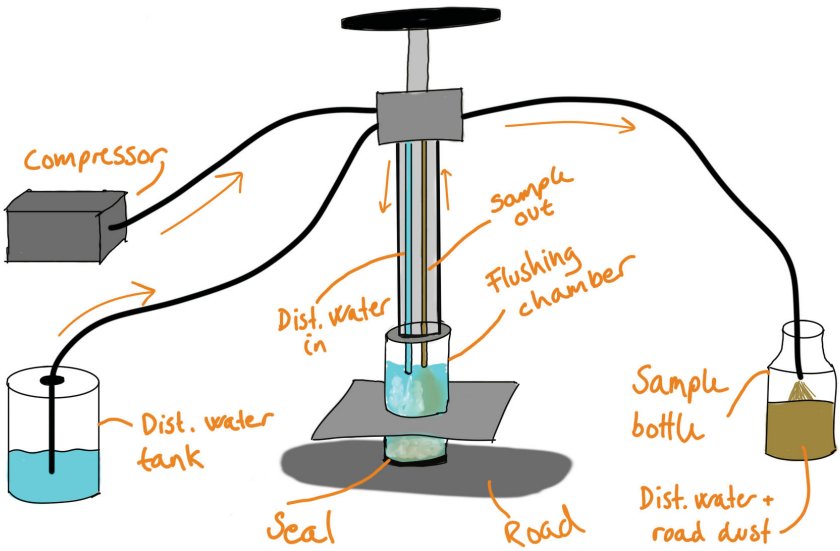

Figure 2.6: Description of the WDS instrument.

Figure 2.6 demonstrates the WDS instrument. The sampler is connected to a tank of distilled water and a compressor. The sampler first flushes the spot where the sample is being collected,

using high-pressure. Thereafter, the flushing chamber is kept sealed and air tight making it possible to transfer the sample from the flushing chamber into the sample-flask by the use of compressed air.

2.4 Prall

The ”prall”-test is a laboratory method for determining the wear of the asphalt pavement. The core sample is placed in a test chamber with 40 steel balls (12 mm diameter each). The steel balls hammer the sample, driven by a stay rod with a rotation of 950 RPM. The sample is cooled down with distilled water flushing through the chamber with a flow of 2 L per minute. The particles produced by this process are washed out from the chamber and collected (Snilsberg et al., 2008).

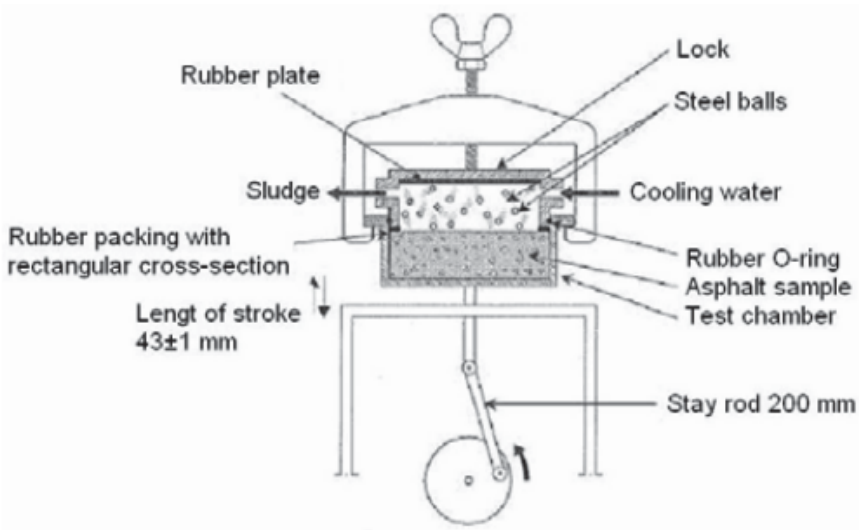

Figure 2.7: Description of the ”prall”-test instrument (Snilsberg et al., 2008)

2.5 Sample preparation and organic instrumental analysis

Performing trace analysis of samples is always challenging due to the complexity and diversity of the sample matrix, and the multiplicity of interfering compounds (Pérez-Fernández et al., 2017). Matrix effects might have a profound impact on the performance of the method, such as the limit of detection, limit of quantification, accuracy, precision and linearity. During environmental analyses sample treatment and enrichment processes are crucial because of the typically low concentrations found. Sample preparation may include clean-up and pre-concentration procedures to ensure that the analytes are found at a suitable concentration level (Padrón et al., 2014). There are several goals of sample extraction prior to analysis. Firstly, there is the necessity to separate the target analytes from a complex matrix such as road dust samples to remove interfering components. The second task is the enrichment of the target analytes in the sample, especially when analytes in trace levels are to be determined. Sample extraction and concentration are applied steps used to improve instrumental sensitivity. Lastly, the compatibility between the sample matrix and the instrumental analysis must be considered. The most common detection techniques for analysis of organic and inorganic compounds are based on mass spectroscopy analysis (Mitra, 2003).

2.5.1 Solid-liquid extraction

Solid-liquid extraction (SLE) is a classic extraction technique, used to extract organic compounds from a solid sample into a liquid phase. Solid-liquid extraction allows soluble components to be removed from solids using a solvent. The choice of solvent is critical when doing the SLE separation. In general, good selectivity and low miscibility with the sample matrix, are highly desirable properties of the extraction solvent. The efficiency of the extraction is also dependent on solvent/solid ratio, temperature, time of contact and the particle size of the solid matrix (Ballesteros et al., 2013).

Ultrasound is an important aid in sample preparation procedures, facilitating and speeding up extraction of organic and inorganic compounds. Ultrasound-assisted solid–liquid extraction is an effective and time-saving extraction method. Sonication accelerates the mass-transfer process between two phases. With the use of ultrasound operating temperature is reduced, allowing the extraction of temperature-sensitive components (Baranowska, 2016, p. 136).

2.5.2 Liquid-liquid extraction

Liquid-liquid extraction (LLE) is based on partitioning of the analytes between two immiscible solvents. Most common is that the sample containing the analytes is an aqueous solution, while the extraction phase is an organic solvent. The partitioning coefficient K_{LLE} is given by the equation:

$$K_{LLE} = \frac{[\text{analyte}]_{\text{organic}}}{[\text{analyte}]_{\text{aqueous}}} \tag{2.1}$$

Where $[\text{analyte}]_{\text{organic}}$ and $[\text{analyte}]_{\text{aqueous}}$ are the concentrations of the analyte in the immiscible phases. High K_{LLE} mean that the analyte is mainly in the organic phase, and low K_{LLE} mean that the analyte is manly in the aqueous phase (Lundanes et al., 2014).

2.5.3 Solid phase extraction

The solid phase extraction (SPE) method requires a measured volume of the liquid state sample to be passed through a cartridge tube packed with a suitable solid adsorbent material. The chemicals in the sample are adsorbed onto the solid surface from which they are eluted by a properly selected eluent (Baranowska, 2016, p. 126). The sample is applied at the top of the tube and drawn through the bed, maintaining a flow rate of 1–2 drops/second. Alternatively, larger pore size particles may be used to allow fast flow rates for large volume samples. The tube is washed with a nonpolar solvent for polar analytes, and with a polar solvent for nonpolar analytes. SPE has become increasingly common when performing sample preparation for trace level analysis. This is mainly attributed to the lower solvent consumption of the SPE technique (Zdravkovic, 2017). Other advantages of SPE is that it eliminates emulsions, and it is considered to improve selectivity, specificity and reproducibility. The most common SPE packing materials used for trace level analysis of organic compounds, consists of nonpolar pores of chemically bound silica, with a carbon chain length from C-8 to C-18. The head of the carbon chain usually has an ion-exchange head (e.g., Strata X cartridge).

The general procedure of SPE consists of four steps (**Figure: 2.8**): First is the conditioning of the SPE material by means of methanol or acetonitrile, followed by water. The second step is to apply the aqueous sample to the SPE material. The third step is to remove hydrophilic interferences by washing with water or 5% aqueous acetonitrile, the fourth and last step is to elute the analytes from the SPE material (Niessen, 2006, p. 17).

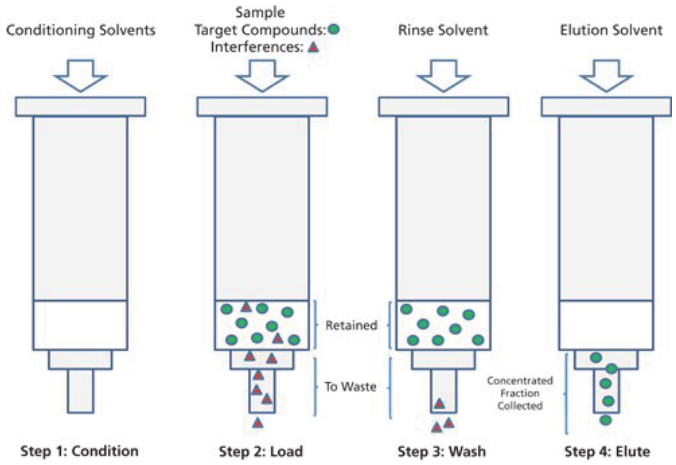

Figure 2.8: The four steps of the SPE procedure (Zdravkovic, 2017)

2.6 Sample preparation for elemental analysis

A decomposition procedure is required in inorganic analysis to alter the original environment of a sample into a solution where the analyte is homogeneously distributed. Criteria for a good decomposition technique include that the decomposition must be as complete as possible, inorganic materials should be converted to soluble compounds, and organic material must be totally mineralized. Residual matrix components that interfere in detection must be removed (Baranowska, 2016, p. 75). Liquids can be analysed directly without dissolution, if the total dissolved solids (TDS) are below 0.5%. With a higher content of TDS, the solids can precipitate in the nebulizer of an ICP instrument, or overload the plasma and alter the processing of the sample in the plasma (Thermo Fisher Scientific, 2018).

Microwave-assisted acid digestion has proven to be the most suitable method for the digestion of complex environmental matrices such as soils and sediments containing oxides, silicates and organic substances. Closed vessel microwave-assisted digestion systems under high temperature and pressure for digestion with acid has now become routine for determining metals in environmental samples. The procedure allows shorter digestion times, good recoveries even for volatile elements, and it reduces the risk of external contamination. It also requires smaller quantities of acids, thus improving detection limits and the overall accuracy of the analytical method (Hassan et al., 2007). HNO_3 is a strong oxidant that dissolves all common metals with the exception of aluminium and chromium (Skoog et al., 2003, p. 1043).

2.7 Analytical techniques

2.7.1 LC-MS/MS

A mass spectrometer coupled to HPLC (abbreviated LC-MS) is a common technique because of its robustness, automation and performance (Lundanes et al., 2014). The LC-MS combination gives high sensitivity, providing a ”fingerprint” of a particular eluent, instead of relying on the retention time as in conventional HPLC (Skoog et al., 2003, pp. 980-981). The central pillar of the LC analysis system is the chromatographic column where the actual separation occurs (**Figure 2.9**). The ability to separate compounds in a sample using chromatography is an essential step in analysing compounds in complex matrices. The efficient separation of different

target analytes from each other, and from the matrix components, is essential to avoid or reduce background noise in the analysis. It also diminishes the risk of false positive or negative results (Kuster et al., 2009). The HPLC separates the compounds contained within a sample based on their difference in polarity.

The HPLC system consists of different components, which perform different tasks in the HPLC system (**Figure 2.9**). First, a carrier stream of solvent (the mobile phase) is pumped into an injector, from which the sample is introduced. The sample is dissolved in the mobile phase or in a similar solvent. After the sample has been introduced into the mobile phase, the sample goes through the column, where the separation of the individual components (analytes) occurs, based on the polarity of the different components (Lundanes et al., 2014, pp. 47-71). The composition of the mobile phase is an important factor to obtain separated peaks in LC (Ramos, 2013, p. 209). After the sample has been separated into its individual components, the different components are detected. Separation is specific for each column design/type and the separated peaks elute flowing into the detector. A typical LC column has a length of 15-25 cm, with an internal diameter in the range of 2-5 mm (Lundanes et al., 2014, p. 54). The most common tube packing for LC is small silica particles, which have an average diameter of 3 to 10 μm (Skoog et al., 2003, p. 978). Due to the different interactions between the components in the sample and the stationary phase in the column, different components migrate through the system at different speeds and elute from the column at different retention times. Retention time is the time between the sample injection into the mobile phase until the separated component is observed by the specific detector (Lundanes et al., 2014, p. 2). Among the most common approaches for improved peak shape in chromatography, is an acidic condition with acetonitrile–water and methanol–water mixtures with gradient elution. Attempt to improve the sensitivity of MS detection have been accomplished with acetic acid, formic acid or ammonium acetate modification of the mobile phase (Ramos, 2013, p. 209).

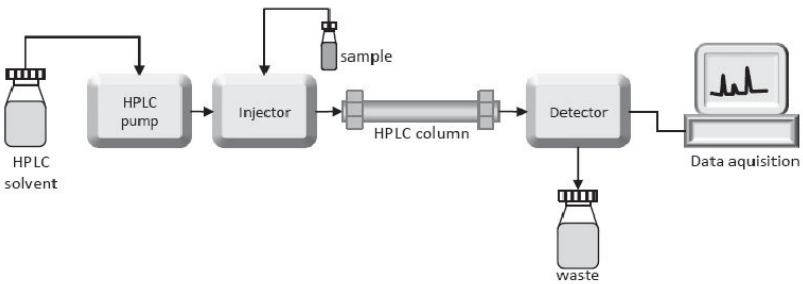

Figure 2.9: General instrumentation of a HPLC-system (LaboratoryInfo.com, 2018)

In this study, a tandem mass spectrometer (triple quadrupole) was used for the detection and quantification of the target analytes. Often, the retention times and molecular-weight information from the total ion chromatogram of a mass spectrometer are insufficient to completely identify all the compounds present in the chromatogram of the effluents. A LC-MS/MS system with collision-induced fragmentation of the molecular ion to produce daughter ions, can provide a greater sensitivity than what can be provided by a mass range scan. The fragmentation to daughter ions from the molecular ion results from fragment-induced cleavage and rearrangements resulting in the loss of neutral molecules. The structures of the daughter ions can then be estimated by examining the mass intervals and isotopic patterns between the product ions. (McMaster, 2005, p. 103)

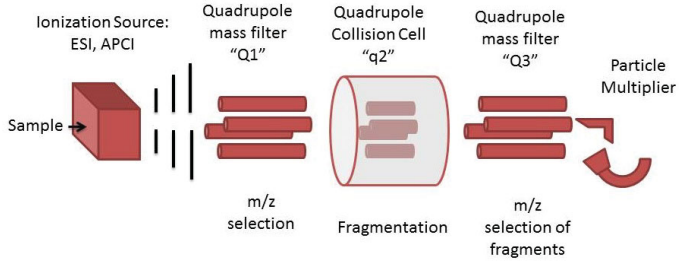

Figure 2.10: Schematic of a triple quadrupole mass spectrometer

The triple-quad LC-MS/MS system (Figure **2.10**) was designed to cleave ions into their daughter ions. The system consists for a scanning Q1 quadrupole analyser, separating the original precursor ion(s), an unscanned Q2 quadrupole, serving as a collision cell to fragment the ions sent to it by collision with a heavy gas molecule, and a scanning Q3 quadrupole, separating the fragments produced in the Q2 unit. The first quadrupole, Q1, can be operated in a full-scan or SIM mode to select ions to pass on to the other analysers in the system. The Q2 unit is flooded with an inert heavy gas, either krypton or xenon, and fragmentation is induced as the ions from Q1 pass to Q2 where they undergo collision with the inert gas. The final analyser, Q3, can also be run in either full-scan or SIM mode (McMaster, 2005, p. 104).

There are four possible modes of operating the two analysers: Q1 scan/Q3 SIM (daughter mode/precursor scanning), Q1 SIM/Q3 scan (parent mode/product scan), Q1 scan/Q3 scan (neutral loss scanning mode) and Q1 SIM/Q3 SIM (multiple reaction monitoring (MRM) mode). The scan/SIM mode makes it possible to determine which primary fragments that are related to each other. Q1 is scanned over the mass range, and all fragments formed enter the collision cell to form secondary fragments. The Q3 is set at a specific mass/charge position, and only primary fragments that breaks down to a specific m/z value will be detected. The common daughter ion points out interrelated primary fragments, and makes it easier to understand which fragments are formed when a large primary fragment breaks down. The SIM/SIM mode is designed to analyse specific components of very impure mixtures without having to purify them completely. Detection can be done at very high sensitivity, since both analysers are set at different specific single m/z values, and a greater number of scans can be summed in determining their position. When examining a chromatographic peak, in which we expect a specific compound to appear, the first quadrupole is used to separate a primary fragment characteristic of the compound of interest before it is passed to the collision cell, and finally the last quadrupole is used to identify it by looking for only one of its specific daughter ions. For each compound to be analysed, an individual primary and secondary fragment on a time basis is selected in step with their expected chromatographic retention time (McMaster, 2005, pp. 104-106).

Electrospray ionization

Electrospray ionization (ESI) is one of the most common interfaces in LC-MS, and has a wide range of applications. ESI is carried out under atmospheric pressure conditions and used mainly for compounds with polar groups. Under given conditions, neutral components either accept or donate a proton to yield positive or negative ions. This can happen either in the mobile phase or during the ESI process. For acids and bases the ionization process occurs in the mobile phase by pH adjustments (Lundanes et al., 2014).

In ESI, the mobile phase with the analytes enters a capillary where a high voltage is applied (typically +5 or -5 kV). A nebulizing gas (mostly N_2) is mixed with the mobile phase at the outlet of the capillary to facilitate formation of droplets. A dry gas is introduced in the opposite direction of the flow. When the repulsive forces inside the drop exceed the surface tension, the droplets explode into smaller droplets. This repetitive process results in yielding ions in the gas phase. Detection can be set to positive mode, to detect protonated ions, or negative mode, detecting deprotonated ions (Lundanes et al., 2014).

2.7.2 ICP-MS

Inductively coupled plasma-mass spectrometry (ICP-MS) is a technique for elemental chemical characterization of virtually any material. ICP-MS has the ability to precisely identify and measure almost all elements in the periodic table including the refractory elements, which often are difficult to analyse. It can also detect and measure concentrations of analyte elements at very low levels (down to 1-10 ng/L, in solution). It has a wide linear dynamic work range, high accuracy and precision of measurement, and minimal interference, making this a powerful and useful trace analysis tool (Taylor, 2001, pp. 1-2).

All atomic spectroscopic techniques require atomization of the sample, converting it into gas-phase atoms and ions. The sample enters the atomization source in solution, and the atomization device must then convert the analyte species in solution into gas-phase free atoms and/or elementary ions (West et al., 2014, p. 776).

Plasma is an electrically neutral gas made up of positive ions and free electrons. It has a sufficiently high energy to atomize, ionize an excite virtually all elements in the periodic table. The inductively coupled plasma (ICP) is the most useful ionization source for mass spectrometry. To sustain plasmas, inert gases are often desired due to their ionization properties and availability in a relatively pure form, resulting in low spectral interference. Argon specifically, has the advantageous property of minimal chemical reactivity with various analyte species, leading to less interference with the analytical results (Taylor, 2001, p. 15). Once argon ions are formed in plasma, they are capable of absorbing enough power from an external source to maintain the temperature level at which further ionization sustains the plasma indefinitely. In this way, temperatures as high as 10 000 K are achieved (West et al., 2014, p. 778).

Samples can be introduced into the ICP by argon flowing through the central quartz tube (**Figure 2.11**; C). The most common sample introduction is by means of a nebulizer. A high-velocity gas breaks the liquid into fine droplets of various sizes, which are then carried into the plasma (West et al., 2014, p. 779).

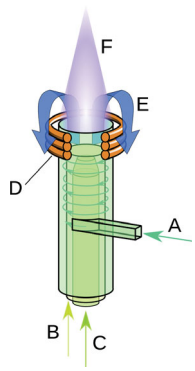

Figure 2.11: The inductively coupled plasma torch. A: cooling gas tangential flow to the outer quartz tube B: discharge gas flow (usually Ar) C: flow of carrier gas with sample D: induction coil which forms the strong magnetic field inside the torch E: force vectors of the magnetic field F: the plasma torch (the discharge). Retrieved (02.05.2018) from `https://en.wikipedia.org/wiki/Inductively_coupled_plasma\#/media/File:ICP_torch.svg`

The ICP-MS system has high-temperature argon plasma as the atomic ion source, and a quadrupole as a typical mass analyser. The ions formed in the plasma are introduced into the the mass analyser, where they are sorted according to their mass-to-charge (m/z) ratio and detected. The interface usually consists of two metal cones, the sampler and the skimmer. Each cone has a small orifice, approximately 1 mm, to let the ions pass through to ion optics which guides them into the mass analyser. ICP-MS spectra are used to identify and quantify the elements present in the sample. Usually, quantitative analysis is based on a calibration curve made from plotting the ratio of the ion signal for the analyte and internal standard as a function of concentration (West et al., 2014, pp. 808-809).

2.8 Quantitation and quality assurance

2.8.1 LC-MS/MS

Retention time (RT) and relative retention time (RRT)

The RT of a compound is not fixed, it is dependent on the applied chromatographic system and can fluctuate between consecutive injections. Factors that can cause fluctuation is: instability of the mobile phase flow rate; instability in column temperature; column degradation; air bubbles in the mobile phase; and column length differences. These factors can make it difficult to compare absolute RT. With the use of RRT, the RT of the analyte is compared to the RT of an internal standard (**Equation 2.2**). This reduces the fluctuation impact, since the same fluctuations impact the internal standard and the ratio should be the same (Asimakopoulos, 2014).

$$RRT = \frac{\text{RT analyte}}{\text{RT interal standard}} \tag{2.2}$$

Relative response (RR)

The relative response (RR) is a factor used to compensate for variations in the signal intensity of a target analyte. This can be due to variations during sample preparation (e.g., loss of sample volume) and/or variabilities in instrumental response. To compensate for these variations, a

ratio between the signal intensity of the analyte and the internal standard can be calculated (**Equation 2.3**). This ratio is called relative response ratio.

$$RR = \frac{\text{Response analyte}}{\text{Response interal standard}} \tag{2.3}$$

Ion ratio (IR)

The ion ratio is an additional confirmation parameter for the target analytes. The ion ratio is a specific ratio unique for each compound in a sample matrix. The ratio is calculated by dividing the area of confirmation ion with the area of the quantification ion multiplied by 100 (**Equation 2.4**).

$$IR\% = \frac{\text{Area of confirmation ion}}{\text{Area of quantification ion}} \tag{2.4}$$

Repeatability and Reproducibility

Repeatability of measurements refers to the variation in consecutive measurements made on the same sample under identical conditions (Bartlett and Frost, 2008). Reproducibility refers to the degree of agreement between the results of experiments conducted under different conditions. Herein, by the term reproducibility the measurements taken in between different days are indicated. A measurement is repeatable when this variation is smaller than a pre-determined acceptance criterion. Repeatability can be calculated using the standard deviation formula (**Equation 2.6**) or the relative standard deviation (**Equation 2.7**). The mean value is calculated using **equation 2.5**.

$$\bar{x} = \frac{\sum_{i=1}^{n} x_i}{n} \tag{2.5}$$

$$STD = \sqrt{\frac{\sum_{i=1}^{n} (x_i - \bar{x})^2}{n-1}} \tag{2.6}$$

Where $x_1, x_2 \ldots x_n$ are the observed values for the repeated test, $\bar{x}$ is the mean of the data sample, n is the number of samples and n-1 is the degree of freedom. Standard deviation is used to measure precision, and measures the amount of variation or dispersion in a data set (Skoog et al., 2003).

The relative standard deviation (RSD%), also known as coefficient of variation, often gives a clearer picture of the data quality than STD. The RSD% is given as **equation 2.7** (Skoog et al., 2003).

$$RSD\% = \frac{STD}{\bar{x}} \times 100\% \tag{2.7}$$

Absolute and relative recovery

Recovery is a measure of how effective an analytical method, and particularly the sample preparation, is to recover and measure an analyte spiked into a blank matrix (Meier and Zünd, 2005). The absolute recovery is given by **equation 2.8** and the relative recovery is given by **equation 2.9**.

$$\text{Absolute recovery}\% = \frac{A_{Pre-ext}}{A_{Post-ext}} \times 100\% \tag{2.8}$$

Where $A_{Pre-ext}$ is the area of analyte in the pre-extraction spiked sample and $A_{Post-ext}$ is the area of the analyte in the post-extraction spiked sample (Matuszewski et al., 2003).

$$\text{Relative recovery } \% = \frac{A_{Pre-ext}/IS_{Pre-ext}}{A_{Post-ext}/IS_{Post-ext}} \tag{2.9}$$

Where $IS_{Pre-ext}$ is the area of internal standard in the pre-extraction spiked sample and $IS_{Post-ext}$ is the area of internal standard in the post-extraction spiked sample.

The absolute recovery is the "real" recovery, and is typically characterized by higher uncertainty than its respective relative recovery, which is the "corrected" recovery. The relative recovery compensates effectively for the analyte(s) losses during sample preparation.

Instrumental level of detection (LOD) and lower level of quantification (LLOQ)

The limit of detection (LOD), is the smallest quantity of an analyte that is "significantly different" from a blank. The lower level of quantification (LLOQ), called (lowest) limit of quantitation, is the smallest amount of analyte that can be measured with a reasonable accuracy (Harris, 2006).

The calculation of LODs and LLOQs can vary within a matrix due to matrix effects and needs to "fit the purpose" of the analytical method. (Asimakopoulos et al., 2014). In this study the LLOQ was set to the lowest concentration detected in the calibration curve, as done by Asimakopoulos et al. (2014), and the LOD calculated from the equation:

$$LOD = \frac{LLOQ}{3} \tag{2.10}$$

Matrix effect

When developing an LC-MS/MS method, evaluating matrix effects is of the utmost importance. Coeluting compounds from the matrix can cause either signal enhancement or suppression. The ionization efficiency of the analyte may also be affected when matrix compounds and the analytes enters the ionization source at the same time. Because of this, the matrix effect can affect both the reproducibility and accuracy of the method. The best option to tackle matrix effects is the use of isotopically labelled internal standards (Steene and Lambert, 2008).

The effect on the analytical signal from the other compunds, except the main analyte in the matrix, is expressed as a matrix factor by the equation (Silvestro et al., 2013):

$$MF = \frac{Area_{post-ext-spike}}{Area_{IS}} \tag{2.11}$$

Where $Area_{post-ext-spike}$ is the area of analyte in the post-extraction spiked sample, and $Area_{IS}$ is the area of analyte in the standard solution (in solvent matrix) fortified with the same concentration as spiked sample (Silvestro et al., 2013).

The matrix effect percentage can then be expressed by this equation (Asimakopoulos et al., 2014):

$$ME\% = (MF - 1) \times 100\% \tag{2.12}$$

Internal standard method

The internal standard method consists of using a calibration curve in matrix, constructed for every target analyte, from the ratio of the analyte response and the internal standard response in a set of standard solutions, plotted against the concentration of the spiked analyte. Validation criteria (i.e. reproducibility, accuracy) can be calculated in accordance to this ratio (Asimakopoulos et al., 2014).

The internal standard is a compound that is very similar, but not identical to the chemical species of interest in the samples. A known amount of the internal standard can be added to the sample, and the signal from the analyte can be compared with the signal from the standard to determine the amount of analyte present. The internal standard method is useful when the instrument signal varies from run to run, or if sample losses occur during sample preparation (Harris, 2006, pp. 90-92).

2.9 Statistics

2.9.1 Data transformation

Transformation of data is frequently used to normalize the data to a more bell-shaped curve. By transforming data, regression line plots can also achieve a more linear form instead of a curvilinear form. For aggregated data it is usually found adequate to transform the data by a logarithmic transformation. Log transforming the data can make positively skewed data distributions more normal in form; the data becomes more symmetrical (Bakus, 2007, p. 66).

2.9.2 Correlation

Correlation is widely used to measure the amount of association between two variables. The strength of the correlation can be evaluated from the correlation coefficient (r). A rule of thumb is that a r-value from 0.90 to 1 is a very high correlation, 0.70-0.89 a high correlation, 0.50 to 0.69 a moderate correlation, 0.30 to 49 a low correlation and 0.00 to 0.29 little if any correlation (Asuero et al., 2006). The p-value of a correlation coefficient states the probability of finding a correlation if there is none (null hypothesis). The lower the p-value, the lower the probability of ”false” correlations.

2.9.3 PCA

PCA is a multivariate technique, used to analyse a data table representing observations described by several dependent variables. The variables in the data table are in general inter-correlated. The goal of PCA is to (1) extract the most important information from the data table; (2) compress the size of the data set by keeping only this information; (3) simplify the description of the data set; and (4) analyse the structure of the observations and variables. PCA also represents the similarity of the observations and the variables by displaying them as points in maps (score plots).

To achieve these goals, PCA computes new variables called principal components, obtained as linear combinations of the original variables. The first principal component is required to have the largest possible variance of the variables, and will then explain the majority of variance

in the data table. The second component is computed to have the largest possible variance, under the constraint of being orthogonal to the first component. The other components are computed the same way. The values of these new variables is called factor scores. These factor scores can be interpreted geometrically as projections of the observations on to the principal components.

The data table used for PCA analysis is represented by a $\boldsymbol{I} \times \boldsymbol{J}$ matrix $\boldsymbol{X}$ containing $\boldsymbol{I}$ observations described by $\boldsymbol{J}$ variables. The rank of the matrix $\boldsymbol{X}$ is $\boldsymbol{L}$, where $\boldsymbol{L} \leq \boldsymbol{min\{I, J\}}$. The data is generally pre-processed before analysis, almost always by centring the column of $\boldsymbol{X}$, done by subtracting the mean of each variable from the data, so that the mean of each column is equal to 0. The components in PCA are obtained from the singular value decomposition (SVD) of the data table $\boldsymbol{X}$:

$$\boldsymbol{X} = \boldsymbol{P}\boldsymbol{\Delta}\boldsymbol{Q}^T \tag{2.13}$$

where $\boldsymbol{P}$ is the $\boldsymbol{I} \times \boldsymbol{L}$ matrix of left singular vectors (normalized eigenvectors[1] of the matrix $\boldsymbol{X}\boldsymbol{X}^T$), $\boldsymbol{Q}$ is the $\boldsymbol{J} \times \boldsymbol{L}$ matrix of right singular vectors (normalized eigenvectors of the matrix $\boldsymbol{X}^T\boldsymbol{X}$), and $\boldsymbol{\Delta}$ is the diagonal matrix of singular values (square root of the diagonal matrix of the eigenvalues[2] of matrix $\boldsymbol{X}\boldsymbol{X}^T$ and $\boldsymbol{X}^T\boldsymbol{X}$ (as they are the same)) (Hervé and Williams Lynne, 2010).

The main principal component (with the highest variance) becomes the x-axis in the new plot, and the other principal component (with the second highest variance) becomes the y-axis (as this is orthogonal to the main component). The ”plot” is then rotated, so that the x-axis is horizontal and the y-axis vertical, by multiplying the original data by the eigenvectors (which indicate the direction of the principal components). For the plot, there are two eigenvectors (one for each axis) each corresponding to an eigenvalue, whose magnitude indicates how much of the data’s variability is explained by its eigenvector.

PCA is used to identify patterns within a data set, aiming to cluster similar observations. The goal is to project and visualize the data to a two-dimensional space with a minimal loss of information. To achieve this, the number of variables is decreased to a few linear combinations of the data set, with linear combination corresponding to a principal component. The loading plot (shown in **Appendix H**) shows the variables influential for the PCA model (score plot) and how the variable correlates to each other. Points close to each other in the loadings plot indicate a similar data profile; increase or decrease of one of the component, will lead to the same change for proximal components (Asimakopoulos et al., 2016).

[1] non-zero vector that changes only by a scalar factor, and not in direction, when linear transformation is applied to it

[2] scale factor corresponding to the eigenvector

3 Experimental

3.1 Sample collection

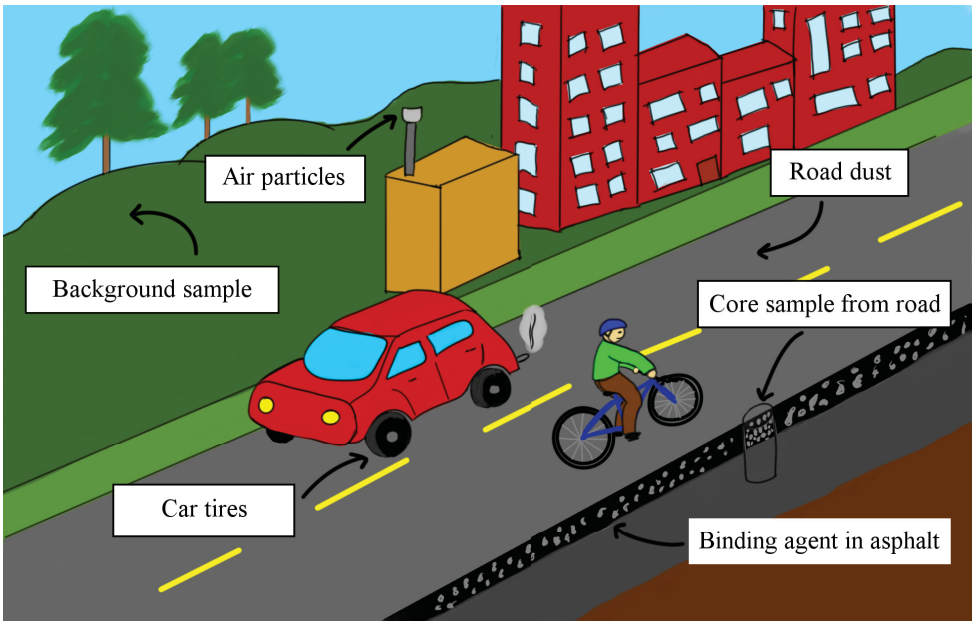

Figure 3.1: Description of all the types of samples collected.

The different types of samples collected are shown in **Figure 3.1**. The main part of the samples is road dust collected with WDS. Air filters (passive samplers) were collected from an ”air-filtering”-station located at Elgeseter street. Core samples were collected from the road by drilling, and they were analysed with the prall-test. Tire samples were collected from a tire distributor, and asphalt binding agent was obtained from the Norwegian road department. A background sample was collected from a forest located outside Trondheim, with the basic aim to establish natural occurring background levels.

3.1.1 Road dust

Road dust samples were collected during two different seasons, with the aim to compare the road dust generated by traffic with summer and winter tires. The use of studded tires in Norway is regulated, by law, from the beginning of November to mid-April (unless the conditions require studded tires) (Norwegian Road Departement, 2014). The samples representing the non-studded tire season were collected in the beginning of October (02.10.17) and later in the text called ”summer samples”. The samples representing the winter season were taken in late November (23.11.17). The samples were taken at Elgeseter street in Trondheim, Norway [63°25’10.5”N, 10°23’45.2”E] (**Figure 3.2**). The sampling area was close to an intersection and is the main road to the city centre. Each sample batch consisted of 16 samples that were consecutively collected

near the pavement edge (kerb) from an approximately 15 metres of road stretch. Each sample was collected using the Wet Dust Sampler (WDS, **section 2.3**) in plastic bottles (polyethylene, high density) with a total sample volume of approximately 2.1 L.

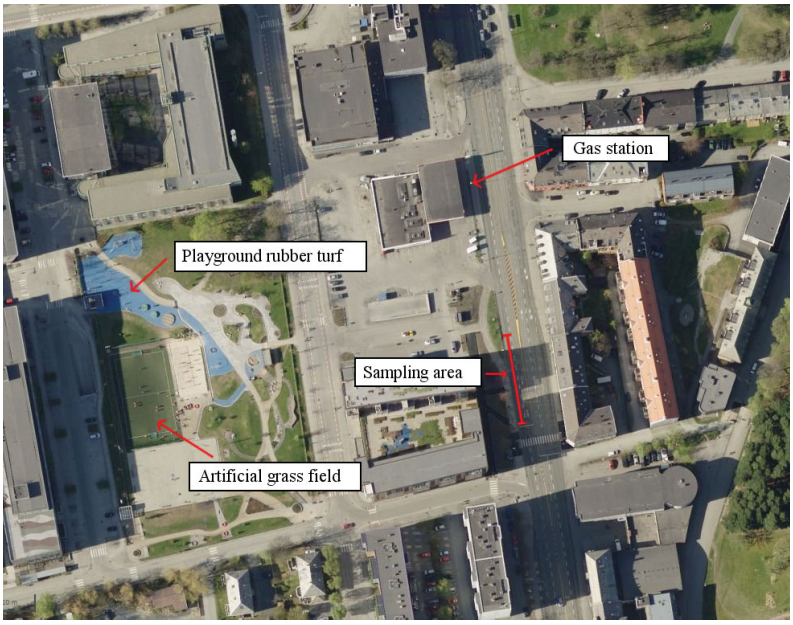

Figure 3.2: Location of sample collection. Elgeseter street, Trondheim, Norway.

3.1.2 Asphalt

During the sampling campaign in summer, four core samples were collected from the road (asphalt). A column with diameter of ∼10 cm and height of ∼ 50 cm was drilled out from the road. The top layer of each core sample (3 cm) was obtained and submitted to a ”prall”-test. Before the test, the sample was stored in a water bath in the refrigerator (4-5 °C), to simulate saturated road (full of rain water) which is most susceptible for stud tire wear. The ”prall”-test was performed by an instrument that contains 40 metal balls (14 mm diameter each), that are set to spin at 950 RPM for 15 min. Two of the samples (P1 and P2) were collected with pre-flush (core sample flushed with distilled water before wearing; 2 min) and two samples without pre-flush (P3 and P4). The collected water sample was transferred to two 25 L cans, and from these 2 L was transferred to 2 L plastic bottles for analysis (shaken before transferring to obtain as homogeneous mixture as possible).

Figure 3.3: Top layer asphalt sample before (left) and after (right) ”prall”-test.

A sample of the same binding agent (bitumen) used for the pavement recipe in Elgeseter street, was retrieved from the Norwegian Road Department for analysis.

3.1.3 Tires

Tire samples for both personal vehicles and heavy-duty vehicles were obtained from an importer of tires. There were three types of tires from both types of vehicles: Summer tire, studded tire and stud free tire. All tires tire samples were cross section samples of new tires. Labelling of samples was T1 (personal, summer), T2 (personal, studded), T3 (personal, stud free), T16 (heavy, summer), T17 (heavy, studded) and T18 (heavy, stud free).

3.1.4 Air filters

Two sets of filters were collected from the air-filtering-station at Elgeseter street. The first set of air filters was collected in mid-September, after a collection period of $\sim$10 days. The other set of filters had a collection period of 14 days, and was collected the same day as the collection of road dust in summer season (02.10.17). The sets of air filters consist of four filters: $PM_{2.5}$, PM_{coarse}, volatile $PM_{2.5}$ and volatile PM_{coarse}. The PM_{coarse} consists of particles ranging from PM_{10} to $PM_{2.5}$. The $PM_{2.5}$ (FE-1, FE-5) and PM_{coarse} (FE-2, FE-6) filters were kept at 30°C during sampling. The filters collecting volatile $PM_{2.5}$ (FE-3, FE-7) and PM_{coarse} (FE-4, FE-8) particles were kept at 4°C during sampling.

3.2 Sample preparation

3.2.1 Filtering of samples

For filtering the samples, a 589/3 Blue Ribbon ashless filter ($<2\mu m$, Whatman) was used in a ”funnel” attached to a Büchner flask via an elastomer adapter. The flask was then connected to a vacuum pump. Before filtering, the filters were weighed on a Petri dish. 50 mL of sample was transferred to a measuring cylinder and thereafter to the ”filtering device”. Duplicates were obtained from each sample bottle. The filtered sample (50 mL) was then transferred to a 50 mL polypropylene plastic tube (PP). After the process the equipment used for filtering was washed with soap-water, followed by methanol and MilliQ water (Q-option, Elga Labwater, Veolia Water Systems LTD, UK). The same method was used for all the road dust and prall samples. Two samples with distilled water and two filters prepared as reagent blanks that monitor background contamination. The reagent blank filters were spiked with 10 μL IS (1 ppm) before extraction, and the liquid reagent blanks were spiked with 10 μL IS (1 ppm) before SPE. The liquid samples were then stored in the refrigerator (4°C).

The filters were left to dry in the fume hood for 3 days, before weighing. After the filters were weighed, they were spiked with 10 μL of internal standard (BTR-d4) and left to dry overnight. The 50 mL liquid samples from filtering were acidified using HCl (1M) to pH 3, controlled with pH-paper, and transferred to a 50 mL VWR tube. Each liquid sample was spiked with 10 μL of internal standard (BTR-d4), and stored in the refrigerator (4°C).

3.3 Methods - Organic

3.3.1 Chemicals and materials

Standards of BTH ($\geq$ 97%), BTR ($\geq$ 98%), XTR ($\geq$ 99%), TTR ($\geq$ 90%), BTR-COOH (99%), 5-Cl-BTR (99%), 5-Amino-BTR (CPR), 2-S-BTH (97%), 2-OH-BTH (98%), 2-NH2-BTH (97%), 2-Me-S-BTH (97%), 2-M-BTH (CPR), 1-OH-BTR ($\geq$ 97%) and BTR-d4 ($10\mu g/mL$ in acetone) were purchased from Sigma-Aldrich (Steinheim, Germany).

SPE cartridges, Strata™-X RP 3 mL/200 mg (Phenomenex, Germany) had 29 μm average particle diameter, 85 Å average pore diameter, and 812 m^2/g specific surface area. A 12-fold Visiprep DL (Disposable Liners) SPE vacuum manifold was obtained from Supelco (Bellefonte, PA, USA). Disposable liners (from PTFE) were used to eliminate cross-contamination during SPE and solvent evaporation.

3.3.2 Internal Standards (IS)

For spiking, BTR-d4 was used. The stock solution was 10 ppm, so in order to make 1 ppm solution, 100 μL was transferred to a glass vial (LC-MS) using an Eppendorf pipette, and 900 μL of MeOH was added.

Standard stock solutions

For most of the standard stock solutions, they were prepared by weighing 10 mg of chemical in a 10 mL vial and dissolved in methanol (MeOH). The standard stock solution of 2-morpholin-4-yl-benzothiazole (2-M-BTH) was prepared by dissolving 5 mg in its original container with 2 mL of MeOH. Benzotriazole-5-carboxylic acid (BTR-COOH) did not dissolve in plain methanol, and consequently it was prepared with 5 mL MeOH, 5 mL Milli-Q water and 1 mL of ammoniumhydroxide (NH_4-OH).

From the standard stock solutions, 10 ppm working solutions were prepared. To make the 10 ppm solutions a calculated amount of standard stock solution was extracted to a 20 mL glass vial, with the use of an Eppendorf pipette before diluting up to 10 mL with MeOH. 9 mL of the MeOH were added with the use of a measuring cylinder, and the remaining fraction of MeOH was added with an Eppendorf pipette. Amounts of stock solutions extracted and MeOH added with the Eppendorf pipette are given in **Table A**. The amounts of extracted standard stock solution were calculated based on the ppm of the stock solution (**Table A.1**). The 1 ppm solutions were made by extracting 0.5 mL of the 10 ppm solution to a 20 mL glass vial, before adding 4.5 mL of Me-OH, with the use of an Eppendorf pipette.

3.3.3 Solid-liquid extraction (SLE)

SLE was used to extract the particulate matter that were collected from the prall, road dust, air filters, and background soil sample. The dried filters (prall, road dust and air filters) were inserted in a plastic tube (15 mL), before adding 5 mL of 50/50 ”Milli-Q”-water:MeOH mixture acidified to pH <3 with HCl (1 M). The filters were pushed down in the tube so that the filters were set below the liquid surface. For the background soil sample, approximately 0.1 g was weighed in a plastic tube and added 5 mL of 50/50 ”Milli-Q”-water:MeOH mixture acidified to pH <3 with HCl (1 M). The particulate matter samples were sonicated for 45 minutes. After sonication the filters were pushed down (compressed) down to the bottom of the tube, using a

glass pipette. The filters were then centrifuged in a Hettich EBA III, using setting 10 (15 G) for 10 min. After centrifuging, the supernatant liquid was transferred to a 50 mL VWR tube, and diluted up to 50 mL with acidified Milli-Q water (pH 3, HCl 1M).

For the air filters, the supernatant liquid was split into two equal fractions of 2.5 mL with one fraction used for elemental analysis and the other for organic analysis. The fractions used for organic analysis were transferred to a 50 mL VWR tube, an diluted up to 25 mL with acidified Milli-Q water (pH 3, HCl 1M), and spiked with 10 μL IS (1 ppm).

Four spike samples (filters; pre-extraction) were prepared by spiking the filters with 10 μL of IS (1 ppm), 10 μL mixture of all the BTHs (1ppm) and 10 μL mixture of BTRs (1 ppm). The filters were dried overnight before extraction with sonication.

Four aqueous spike samples (pre- extraction) were prepared using 50 mL acidified Milli-Q water. Each sample was spiked with 10 μL IS (1 ppm), 10 μL mixture of the BTHs (1ppm) and 10 μL mixture of the BTRs (1 ppm). The samples were then stored in the refrigerator (4°).

3.3.4 Solid phase extraction (SPE)

SPE was used of extraction/sample pre-treatment of the aqueous matrices and for the clean-up of the extracts that were obtained for the particulates with SLE. The SPE was performed using Strata-X 33 μm Polymeric Reversed Phase (200 mg/3mL) tubes. The cartridges were conditioned by passing through them 10 mL of MeOH, before equilibrating with acidified Milli-Q water (pH $<$3, using HCl). Then the acidified samples were passed through the cartridges, and rinsed with 10 mL of acidified Milli-Q water (pH $<$3, using HCl) to remove interfering endogenous matrix components. The sample was then dried under vacuum for 11 min, before eluted with 10 mL of MeOH/ACN solution (50/50).

The samples from the SPE were run in a Turbovap (TurboVap® LV automated evaporation system) system to evaporate the solvent. Evaporation was performed to near dryness (50-55 min) in a water bath with a temperature set at 45 °C under a N_2 gas stream (2.5 psi). After evaporation, the samples were diluted with Milli-Q/ACN solution (80/20) up to a final volume of 1 mL and transferred for LC-MS/MS analysis.

3.3.5 Liquid-liquid extraction (LLE)

The samples of the asphalt binding agent and tires were weighed to approximately 0.1 g, and dichloromethane (DCM) was added. It must be noted that every tire-sample was cut down to grinds, and thereafter 1 mL of DCM was added. The tire-samples were then sonicated for 45 min, and 5 mL of acidified MilliQ/MeOH solution (50/50, pH 3) were added before sonicated again for 45 min. For the binding-agent 5 mL of DCM were added and were dissolved. 100 μL were transferred to a new tube and 5 mL of acidified MilliQ/MeOH solution (50/50, pH 3) were added. Thereafter, sonication followed for 45 min. After sonication, both the tire samples and the binding agent were centrifuged in a Hettich EBA III, using setting 10 (15G) for 10 min. After centrifugation, the supernatant liquid was transferred to a new vial, ensuring that all particulates were removed. The tire samples and binding agent samples where thereafter spiked with 10 μL IS (1 ppm), and 1 mL of each sample was taken for analysis.

3.3.6 LC-MS/MS

The chromatographic separation was carried out using an Acquity UHPLC Thermo system with a column manager, a flow through needle sample manager, and binary solvent manager (Waters, Milford, USA). The tandem mass spectrometric system was a Xevo TQ-S, triple quadrupole mass analyser, with ZSpray ESI (Waters, Milford, USA). The LC column used was an Atlantis C18 T3 (150 mm × 2.1 mm, 3 μm) connected to a Phenomenex C18 guard column (4.0 mm × 2.0 mm, 5 μm). Determination of the mass spectrometry parameters were done by direct infusion and the IntelliStart software (Waters, Milford, USA) (see **Appendix E**). The parent and fragment ions of every chemical included in the method are demonstrated in **Table 3.1**.

Table 3.1: Analyte specific MS/MS parameters

Component	Quantification transition (CE[a] [eV])	Confirmation transition (CE [eV])	CV[b] (V)
BTH	135 > 109 (28)	135 > 65 (22)	44
2-S-BTH	168 > 135 (20)	168 > 92 (20)	2
2-OH-BTH	152 > 124 (16)	152 > 92 (16)	2
		152 > 80 (22)	2
2-NH2-BTH	151 > 124 (18)	151 > 109 (20)	28
2-Me-S-BTH	182 > 167 (22)	182 > 109 (32)	26
2-M-S-BTH	221 > 177 (18)	221 > 109 (30)	2
BTR	120 > 65 (16)	120 > 92 (14)	28
TTR	134 > 77 (18)	134 > 79 (22)	40
XTR	148 > 93 (16)	148 > 77 (24)	16
BTR COOH	164 > 80 (18)	164 > 108 (18)	2
5-Cl-BTR	154 > 99 (22)	154 > 73 (24)	24
5-Amino-BTR	135 > 80 (16)	135 > 107 (16)	42
1-OH-BTR	136 > 119 (18)	136 > 91 (14)	24
BTR-d4 (IS)	124 > 69 (18)	124 > 96 (16)	38

a: Collision energy b: Cone voltage

Chromatographic separation was performed by Atlantis® T3 C18 and the column temperature was set at 40°C. Chromatographic analyses were carried out using a gradient elution program with ACN and Milli-Q water (both acidified with 0.1% v/v formic acid) as binary mobile phase mixture at a flow rate of 250 μL/min. The gradient elution started with 2% (v/v) ACN and increased linearly to 40% ACN in 4.5 min, and then to 100% ACN in 12.0 min which was held for 3.5 min (until 15.50 min), reverted to 50% ACN at 18 min and re-equilibrated for 4.0 min (from 18.0 to 22.0 min) at 2% ACN for a total run time of 22.0 min. The electrospray ionization voltage was applied at +2.5 kV. The cone gas (N2) flow rate was set at 150 (L/Hr). The desolvation gas (N2) flow rate was set at 800 (L/Hr). The source temperature was set at 150°C, and the desolvation temperature was set at 500°C. The final in-vial composition of all samples and standard solutions were in MeOH/MilliQ water (2:8 v/v), and were injected on column with loop injection (2 μL). Data were acquired with the MassLynx and TargetLynx software packages (version 4.1 SCN871, Waters, Milford, USA). Data treatment was performed with Excel (Microsoft Office, 2016).

3.4 Methods elemental analysis

3.4.1 Sample preparation

A total of 53 samples were analysed by ICP-MS, 22 filtered road dust samples, 8 air filters (see **section 3.3.3** for extraction), 22 turbid road dust samples and 1 background soil sample.

The filtered road dust samples were prepared using a syringe (Norm-Ject 10 mL) and a syringe filter (capsule type, 0.45 μm pores, diameter 25 mm, VWR). 6-10 g of turbid road dust sample was filtered into a VWR 15 mL tube and acidified with pure concentrated nitric acid HNO_3 (UltraPure grade, distilled with Milestone SubPur, 9 mL 50 % v/v) with one drop per 3 g sample (0.1 M) for conservation. The syringe and filters was rinsed with Milli-Q water for each sample. The samples from the air-filtering station (2.5 mL) was diluted to 16.5 mL (because of 50% MeOH content) and added HNO_3(0.1 M) for conservation.

The turbid road dust samples were prepared by weighing approximately 8 g of turbid road dust sample and transferring to PTFE-Teflon vials (18 mL) before adding 2 mL pure concentrated HNO_3. Digestion of the samples was carried out in a high-pressure microwave system (Milestone UltraClave, EMLS, Leutkirch, Germany) according to a temperature profile which increases gradually from room temperature up to 250°C within 1 h. In addition, there was a cooling step which allowed temperature to return back to the initial value within approximately 1 h (**Table 3.2**). After cooling to room temperature, the digested samples were diluted with Milli-Q water up to 47 mL in polypropylene vials to achieve a final HNO_3concentration of approximately 0.6 M. For the background sample, approximately 230 mg of soil sample was weighed and transferred to PTFE-Teflon vial (18 mL)to added 9 mL HNO_3 (50% v/v) before decomposition with Ultraclave, and diluted to 108 mL with ultrapure water and transferred to a polypropylene vial.

Table 3.2: Steps in Ultraclave decomposition

Step	Time (min)	Temp 1 (°C)	Temp 2 (°C)	Press (bar)	Energy (Watt)
1	5	50	60	160	1000
2	10	50	60	160	1000
3	10	100	60	160	1000
4	8	110	60	160	1000
5	15	190	60	160	1000
6	5	210	60	160	1000
7	15	245	60	160	1000
8	10	245	60	160	1000

3.4.2 ICP-MS

High resolution inductively coupled plasma mass spectrometry (HR-ICP-MS) analyses were performed using a Thermo Finnigan model Element 2 instrument (Bremen, Germany). The radio frequency power was set to 1350 W. The samples were introduced using a combination of SC2 DX autosampler (with ULPA filter dust cover) and PrepFAST flow injection analysis system (ESI, Elemental Scientific, Inc. Omaha, NE) with a total flow of 200 μL/min. The instrument was equipped with a PFA-ST nebulizer, spray chamber (PFA Barrel 35 mm), demountable torch, quarts standard injector as well as Al sample skimmer and X-skimmer cones. Methane gas was added to the sample gas to achieve lower levels of oxides and to provide enhanced sensitivity, especially for Se and As. More details on instrumentation and instrumentation can be found in **Appendix G**.

The accuracy of the ICP-MS instrument was verified against certified calibration solutions. For this analysis, two sets of calibration solutions (CS) were used, delivered by ESI from two independent producers. One of the sets is used as a CS and the other for accuracy ascertainment. There are two different solutions in each set to cover all the elements, PS-ClBrI and PS-70. PS-70 is the primary solution containing 70 elements. PS-ClBrI contains chlorine, bromine and iodine, because these elements cannot be mixed into the PS-70 due to the HCl matrix. There was not used any reference materials in this study, but the reproducibility of the ICP-MS instrument is ensured by continuously repeating analyses of reference materials. The precision was calculated by RSD% values, calculated from three consecutive scans of each individual sample. Detection limits were calculated by taking the concentration which approximately gives a RSD of 25%, uncorrected of baseline. The quantification limit (QL) is then calculated from the detection limit (DL), with correction from baseline and total measurement uncertainty (MU). The total MU is calculated by this equation:

$$MU = \sqrt{DL^2 + DL'^2} \tag{3.1}$$

Where DL' is the DL with baseline correction.

3.5 Data treatment

Statistical analysis and correlations were done using SPSS Statistics (IBM, version 25). Principal component analysis (PCA) was done using the statistical software R.

4 Results and discussion

4.1 Quality assurance and method validation

4.1.1 Organics

Table 4.1 shows the precision of the tandem LC-MS/MS method. All the ion ratios (IR%, **Table 4.1**) meets the criteria of tolerance stated in Commission Decision 2002/657/EC (European Commission, 2002).

Table 4.1: Ion ratios (IR%), Retention times (RT) and Relative retention times (RRT) (RSD%, N=6 highest calibration points)

	IR%	*RT*	*RRT*
BTH	29.5 (21.2)*	5.38 (0.14)	1.39 (0.10)
2-S-BTH	51.4 (3.62)	7.48 (0.07)	1.39 (0.07)
2-OH-BTH	1.02 (5.90)	6.85 (0.11)	1.27 (0.11)
2-NH2-BTH	79.2 (0.90)	4.19 (0.10)	0.78 (0.10)
2-Me-S-BTH	8.44 (6.63)	8.98 (0.06)	1.67 (0.06)
2-M-BTH	74.1 (2.37)	7.48 (0.00)	1.39 (0.00)
BTR	46.0 (2.61)	5.41 (0.10)	1.00 (0.10)
TTR	76.0 (3.04)	6.12 (0.00)	1.14 (0.00)
XTR	86.2 (2.79)	6.66 (0.00)	1.24 (0.00)
BTR COOH	71.1 (3.41)	4.67 (0.00)	0.87 (0.00)
5-Cl-BTR	18.0 (1.36)	6.69 (0.06)	1.24 (0.06)
1-OH-BTR	25.1 (3.75)	4.48 (0.00)	0.83 (0.00)
5-Amino-BTR	22.1 (9.31)	2.93 (0.00)	0.54 (0.00)

*: N = 5

Table 4.2 shows the recoveries for the method. The absolute recoveries in particulate and liquid phase are >70 for the majority of target analytes. The recoveries of the target analytes are similar to previous studies (Maceira et al., 2018; Wang et al., 2016; Zhang et al., 2018).

Table 4.2: Recoveries% (RSD%, N = 3; [10 ng/mL]) of target analytes.

	Absolute recovery		Relative recovery	
	Filter	*Particulate phase*	*Filter*	*Particulate phase*
BTH	118	109	165	111
2-S-BTH	29.2	20.7	37.6	18.8
2-OH-BTH	105	80.2	125	75.0
2-NH2-BTH	61.3	67.0	70.4	63.4
2-Me-S-BTH	49.7	40.0	53.4	33.1
2-M-BTH	77.2	72.2	88.3	68.2
BTR	94.1	107	107	108
TTR	76.8	106	86.2	107
XTR	92.6	105	105	106
BTR COOH	86.2	101	97.5	102
5-Cl-BTR	93.4	102	105	103
1-OH-BTR	67.4	66.7	74.8	65.8
5-Amino-BTR	4.05	14.0	4.55	14.0
BTR-d4	87.7	99.8	-	-

This is the first work that demonstrates a method for the analysis of BTR COOH. In this method, BTR COOH demonstrated excellent recoveries with 86% (± 18.3) for particulate samples and 101% (± 11.5) for liquid samples. To my far knowledge, 5-Amino-BTR was also analysed for the first time. However, the developed method demonstrated low recoveries. Thus, this compound was semiquantified. This low recovery is attributed to the strong retention on the SPE-cartridges due to interactions between the NH_2 group and the sorbent, previously stated by Asimakopoulos et al. (2014).

Table 4.3 shows the repeatability/reproducibility of the method.

Table 4.3: Reproducibility (RSD%, N = 3; [10 ng/mL]) of target analytes

	Particulates	*Liquid phase*
BTH	7.84	24.0
2-S-BTH	16.5	34.2
2-OH-BTH	8.82	12.0
2-NH2-BTH	5.88	17.2
2-Me-S-BTH	4.70	13.9
2-M-BTH	5.44	14.8
BTR	15.9	11.0
TTR	19.4	12.4
XTR	22.9	8.03
BTR COOH	18.3	11.5
5-Cl-BTR	18.7	10.9
1-OH-BTR	15.7	15.4
5-Amino-BTR	32.7	7.87
BTR-d4	2.71	24.9

The limit of quantification and detection for the BTHs and BTRs is presented in **Table 4.4** (see section 2.8.1 for calculations). From the instrumental LOD and LLOQ, method LLOQ and LOD was calculated to account for the 50-fold pre-concentration from (see **section 3.3.4**). Concentrations detected below method LOD were removed from the data set.

Table 4.4: Lower limits of quantification and limits of detection (ng/mL)

	Instrumental		**Method (preconcentrated 50-fold)**	
	LLOQ	*LOD*	*LLOQ*	*LOD*
BTH	1.00	0.33	0.02	6.67×10^{-3}
2-S-BTH	0.10	0.03	2.00×10^{-3}	6.67×10^{-4}
2-OH-BTH	0.50	0.17	0.01	3.33×10^{-3}
2-NH2-BTH	0.10	0.03	2.00×10^{-3}	6.67×10^{-4}
2-Me-S-BTH	0.10	0.03	2.00×10^{-3}	6.67×10^{-4}
2-M-BTH	0.10	0.03	2.00×10^{-3}	6.67×10^{-4}
BTR	0.50	0.17	0.01	3.33×10^{-3}
TTR	0.10	0.03	2.00×10^{-3}	6.67×10^{-4}
XTR	0.10	0.03	2.00×10^{-3}	6.67×10^{-4}
BTR COOH	0.10	0.03	2.00×10^{-3}	6.67×10^{-4}
5-Cl-BTR	0.10	0.03	2.00×10^{-3}	6.67×10^{-4}
1-OH-BTR	0.10	0.03	2.00×10^{-3}	6.67×10^{-4}
5-Amino-BTR	0.10	0.03	2.00×10^{-3}	6.67×10^{-4}

Table 4.5 shows the matrix factors and matrix effects for the BTHs and BTRs analysed by LC-MS/MS. Compared to previously published methods, the target analytes did not suffer from strong matrix effects, except from 2-S-BTH, where the ME% was -95.6%. The high matrix effects for this chemical are expected since the free thio-group is highly reactive. Overall, BTRs demonstrates higher ME% (-41.5 to -29.5) than most of the BTHs (-12.4 to -3.30); this is due to the fact that BTRs elute chromatographically earlier, alongside with the more polar endogenous interferences of the matrices.

Table 4.5: Matrix factors (MF) and matrix effects (ME%)

	MF	*ME%*
BTH	0.53	-47.1
2-S-BTH	0.04	-95.6
2-OH-BTH	0.91	-8.51
2-NH2-BTH	0.97	-3.30
2-Me-S-BTH	0.96	-4.06
2-M-BTH	0.88	-12.4
BTR	0.68	-32.0
TTR	0.65	-34.7
XTR	0.66	-34.1
BTR COOH	0.64	-36.3
5-Cl-BTR	0.70	-29.5
1-OH-BTR	0.68	-31.9
5-Amino-BTR	0.58	-41.5

4.1.2 Element analysis by ICP-MS

The precision of the element analysis was very good (RSD% < 5) for most of the elements. Only Ag, Au, Ir, Pt and Se had RSD% above 25% in the turbid samples. The RSD% and quantification limit for all elements are given in **Table B.9**. All of the selected elements in turbid samples used for discussion (**Table 4.10**) have detected concentrations above the quantification limit. The calculations of detection limits for ICP-MS is described in **section 3.4.2**.

4.2 Occurrence of benzothiazoles, benzotriazoles and elements in analysed matrices

Table 4.6 shows the weight of particles collected from filtering of the turbid road dust samples (**section 3.2.1**). **Figure 4.1** shows a box plot of the weight data of the filters.

The weight/amount of particles from filtering is approximately the same for the summer season and the prall. In the winter season, the weight of particles is approximately 3.5 times higher than in the summer season and prall. This indicates that more road dust is generated during the winter season than in the summer season, as stated by Pant and Harrison (2013). The weather in the different seasons also affect the amounts of road dust on the road surface. Longer periods of dry weather and wind will contribute to less particles on the road surface,

while rain contributes to settle the particulates on the road surface. Heavy rain can contribute to ”washing” off the road surface and eliminate precipitated particulates into the drainage system. The time of sampling since the last sweeping/cleaning of road will also affect the amount of particles collected.

Table 4.6: Statistics for particles weight from filtering of turbid road dust samples (50 mL)

	N	Mean (mg)	Median (mg)	Stdev (mg)	RSD (%)
Summer	32	26.9	23.2	10.4	38.6
Winter	16	101	80.3	47.4	46.7
Prall	8	23.3	23.6	3.26	14.0

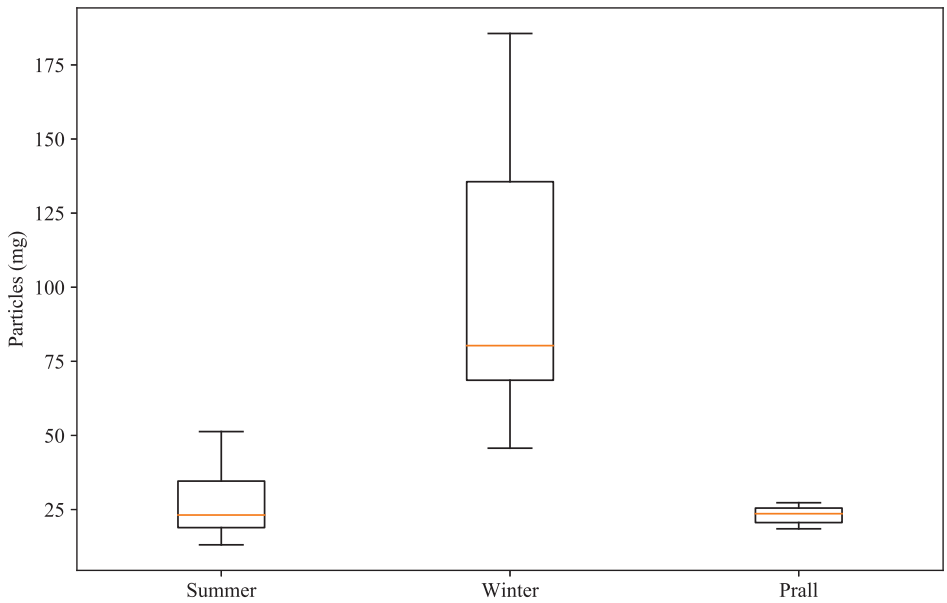

Figure 4.1: Box plot of particle weight collected from filtering of turbid road dust samples (50 mL)

The box plot of weight of particles shows that the amount of particles in the filtered samples differs more in the winter than the summer. As stated by Forsberg et al. (2005), the use of studded tires increases the wear of the pavement and the emission of coarse particles. This will lead to a more heterogeneous matrix with a dispersion of coarse particles, resulting in a dispersion of weight of the particles filtered based on the partition of coarse particles in the sample transferred for filtering.

4.2.1 Benzothiazoles and benzotriazoles

The total concentrations (sum of liquid and particulate matter) of BTHs and BTRs (Table 4.7) are used for the comparison of the different seasons and matrices, because of the variation in distribution coefficient for BTHs and BTRs in different matrices (described in text below). The concentrations of BTHs and BTRs in particulate (**Table B.1**) and liquid phase (**Figure B.2**) is given in **Appendix B**.

The concentrations of BTHs and BTRs detected in particulate matter of road dust and tires in this study (**Table B.1**) is low, compared to previous studies, and significantly lower than concentrations found in the most recent study on road dust by Zhang et al. (2018) in China (**Table 2.1**). The concentration of BTH and 2-S-BTH detected in this study is also lower than reported in Sweden, by (Avagyan et al., 2014). But to my far knowledge, this is the first study to analyse BTRs in road dust, and detected/reported 2-OH-BTH, 2-NH2-BTH, XTR and 1-OH-BTR in tires.

The total concentrations (particulate and liquid) of road dust and prall are given in **Table 4.7**. The total concentration of BTHs and BTRs was higher in the winter season, and lower in the prall-samples. The total concentrations of BTHs in the winter season (939 ng/L) is approximately three times higher than in the summer season (303 ng/L), and the concentration in the dust from the prall test (242 ng/L) is lower than the summer samples. The total concentration of BTRs in the winter season (977 ng/L) is almost two times higher than in the summer season (529 ng/L), and the concentration in the dust from the prall test (40.7 ng/L) is significantly lower than in summer.

Table 4.7: Total concentrations of BTHs and BTRs (sum of particulate and liquid phase) in the turbid road dust and prall samples (ng/L)

	Summer				**Winter**				**Prall**			
	Median	*Min*	*Max*	*n/N**	*Median*	*Min*	*Max*	*n/N**	*Median*	*Min*	*Max*	*n/N**
BTH	23.7	9.74	66.4	10/17	127	40.5	203.2	9/16	-	-	-	-
2-S-BTH	12.7	6.79	19.0	17/17	8.83	1.74	19.4	16/16	3.17	1.51	3.96	3/4
2-OH-BTH	197	26.6	521	17/17	692	246	1404	16/16	141	55.9	405	4/4
2-NH2-BTH	42.4	27.0	162	17/17	52.8	26.9	134	16/16	2.8	2.52	5.54	3/4
2-Me-S-BTH	35.3	16.8	116	17/17	125	77.4	195	16/16	77.2	16.8	91.0	4/4
2-M-BTH	1.33	0.06	9.19	16/17	3.54	1.74	6.61	16/16	9.4	5.40	12.3	4/4
∑ BTHs	303	93.4	801	17/17	939	360	1903	16/16	242	82.0	495	4/4
BTR	38.0	20.8	70.8	17/17	80.1	43.4	135	16/16	7.96	3.40	14.2	3/4
TTR	277	157	1240	17/17	759	386	1260	16/16	23.6	9.12	27.2	4/4
XTR	4.14	4.14	4.14	1/17	1.88	1.15	86.3	7/16	-	-	-	-
BTR COOH	23.4	8.95	52.9	17/17	10.4	4.11	29.2	16/16	1.72	1.72	1.72	1/4
5-Cl-BTR	4.36	1.11	37.9	17/17	7.19	3.41	19.8	16/16	1.01	0.96	2.02	4/4
1-OH-BTR	4.43	0.77	22.2	10/17	51.1	14.5	213	16/16	4.54	2.82	6.26	2/4
5-Amino-BTR	256	92.5	471	9/17	78.8	40.2	2251	5/16	37.7	37.7	37.7	1/4
∑ BTRs	529	191	1308	17/17	977	473	3054	16/16	40.7	33.3	47.8	4/4

*: n is number of detected samples and N is total samples in the set

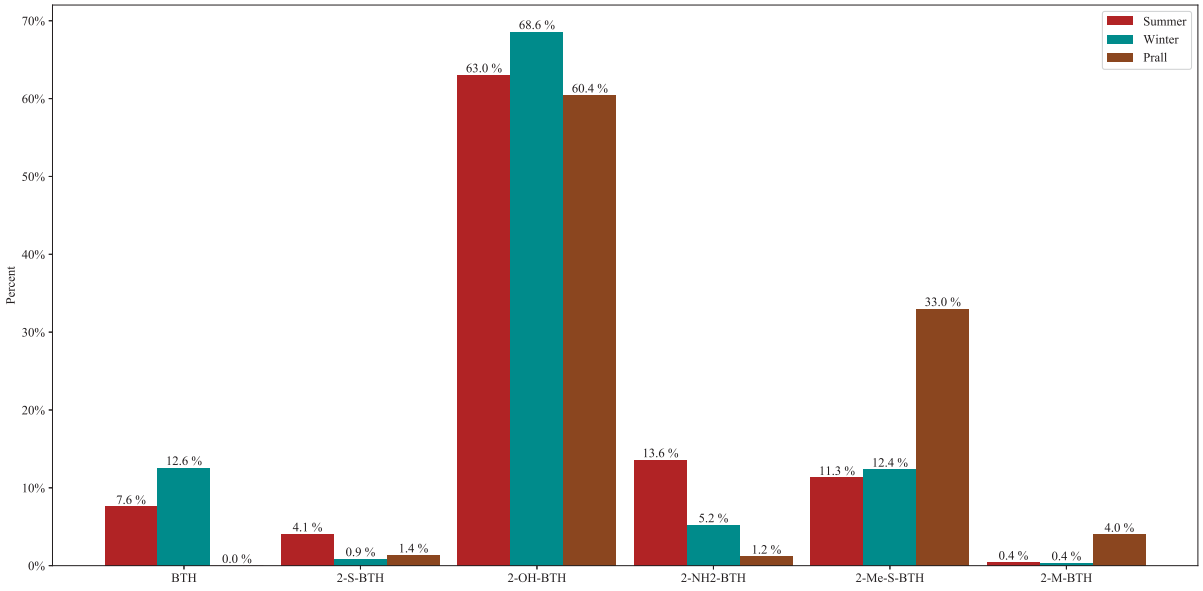

Figure 4.2: Distribution of benzothiazole derivatives in road dust, compared to ∑BTHs

The distribution of the individual BTHs in the road dust samples (**Figure 4.2**) shows that 2-OH-BTH, 2-NH2-BTH and 2-Me-S-BTH are the major components in the summer season. In the winter season, the major components are 2-OH-BTH, BTH and 2-Me-S-BTH. BTH was not detected in the dust from the prall test, and the major components of the BTHs were 2-OH-BTH and 2-Me-S-BTH. For the partition of BTRs in the road dust samples (**Figure 4.3**), TTR and 5-Amino BTR are the major components in the road dust from the summer season. In the winter season is TTR the major component, accounting for 76.6% of the total concentrations of BTRs. From the BTRs in the dust from the prall test, 5-Amino-BTR, TTR and BTR are the major components. 5-Amino-BTR was only detected in one of the four prall samples (**Table 4.7**).

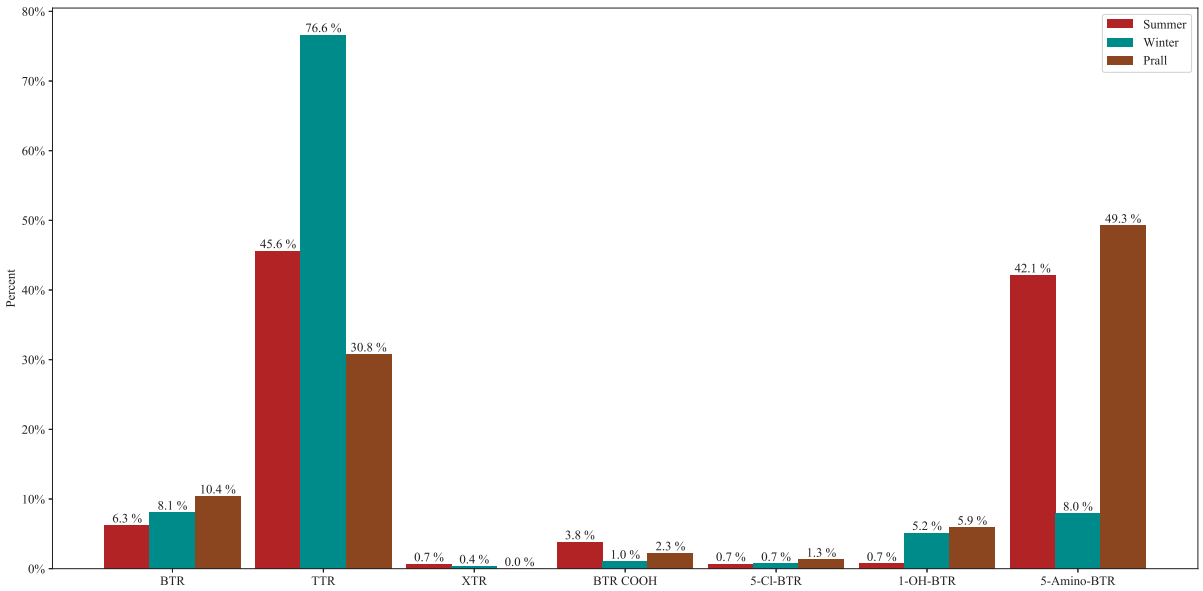

Figure 4.3: Distribution of benzotriazoles derivatives in road dust, compared to ∑BTRs

TTR increases considerably in the winter season. BTR and TTR are known anti-icing/de-icing agents (Breedveld et al., 2003), and are mainly used as corrosion inhibitors for steel, copper and brass (Cantwell et al., 2015). BTR was used as a corrosion inhibitor for copper in windshield fluid, patented by Shell Oil Co (1976) and as an additive in windshield fluid from Trico Products (Trico Products, 2016). It is unknown if BTRs are used in anti-icing/de-icing and windshield fluids in Norway, but a strong correlation (0.99, ref **Table C.1**) indicates that they are applied for the same purposes.

All BTHs were detected in the tires analysed in this study (**Table B.1**). 2-M-BTH was only detected in summer and studded tires for heavy duty vehicles. XTR and 1-OH-BTR were the only BTRs detected in tires. XTR was detected in summer and studded tires for personal vehicles, and 1-OH-BTR was detected in summer tires for heavy duty vehicles and studded and stud free winter tires for personal vehicles. The total concentration of BTHs in the tires ranked: stud free winter tires (37 644 ng/g) > summer tires (16 678 ng/g) > studded tires (10 265 ng/g). The total concentration of BTRs in tires was ranked: stud free winter tires (4304 ng/g) > studded tires (2170 ng/g) > summer tires (128 ng/g). The major components of BTHs in summer tires are 2-S-BTH and BTH. The distribution of BTHs is approximately the same for all types of tire (**Figure 4.4**). This matches the literature reports stating that 2-S-BTH is the BTH derivative most widely used in car tires (Herrero et al., 2014; Leng and Gries, 2017). In studded tires, the increase in the partition of 2-OH-BTH is approximately the same as the decrease of 2-S-BTH (∼7%), which can indicate that part of the 2-S-BTH, which is used in summer and stud-free tires, are substituted by 2-OH-BTH in studded tires. The partition of BTRs in tires is mainly 1-OH-BTR (99.6-100%), with 0.4% XTR detected in summer tires. The ratio between 2-S-BTH and BTH, the major partitions in summer and stud free tires, is 1.55 for both tire types. The ratio between 2-S-BTH and 2-OH-BTH is almost the same for both tire types; 0.09 for summer tires and 0.10 for stud free tires. Since the tires in this study are unused, this supports that BTH and 2-OH-BTH are major break down products of 2-S-BTH during manufacturing, as proposed by Reddy and Quinn (1997), since they are present before possible wearing of the tires occurs.

Contribution from tires Zhang et al. (2018) stated that tire wear was the main source of BTHs in road dust. This is also indicated by the high concentrations of BTHs found in the tires analysed in this study. All BTHs except 2-S-BTH increases in the winter season.

To estimate the amount of BTHs leached from tires in the different season, two simple equations were used. Leach summer (**Equation 4.1**) and leach winter (**Equation 4.2**):

$$\text{Leach summer} = \frac{[\sum BTHs(\text{summer})]}{[\sum BTHs(\text{summer tires})]} \times 100 \tag{4.1}$$

$$\text{Leach winter} = \frac{[\sum BTHs(\text{winter})]}{0.28 \times [\sum BTHs(\text{studded tires})] + 0.72 \times [\sum BTHs(\text{stud free tires})]} \times 100 \tag{4.2}$$

By using the sum of BTHs, it takes in account possible transformations in between the BTHs. The 0.28 and 0.72 that were used in the winter leach equation is to account for the fraction of tire types used in Trondheim in the studded tire season 2017-2018, as Statens Vegvesen (2018) reported that 72% of the cars used stud free tires and 28% of the cars used studded tires in this period.

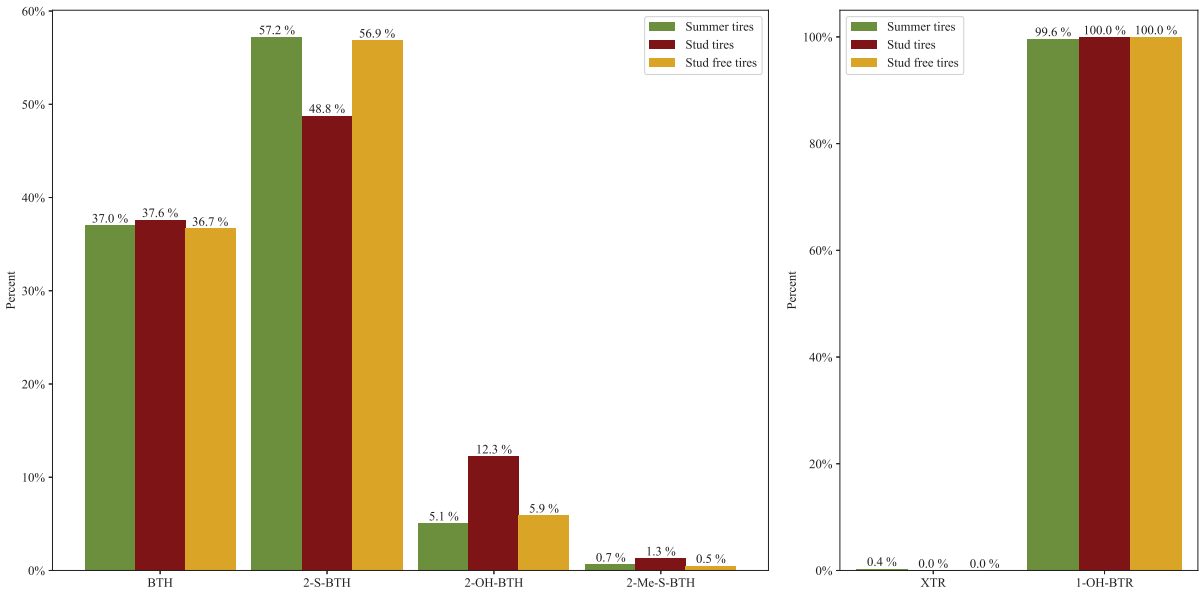

Figure 4.4: Distribution of benzothiazoles and benzotriazoles in tires, compared to ∑BTHs and ∑BTRs

From the equations above, the leaching of BTHs from the tires were calculated to 0.087 in the summer season and 0.136 in the winter season. This indicates that more BTHs are leached from the tires in the winter, than in the summer season. The data in this study is not sufficient to determine if the increase in BTHs from tires come from the properties of the different tires, or the different conditions of the seasons (road salt, weather, etc.). But it is reasonable to assume that more BTHs could leach from stud free tires, as the concentrations are twice as high as in summer tires.

Contribution from asphalt pavement It is difficult to draw conclusions on the contribution of BTHs from the road surface due to the fact that steel balls are hammering a rubber packing in the interior of the ”prall-test” instrumentation (**Figure 3.3**). Therefore, there is a possibility that the prall-machine itself contribute to the BTHs content in the asphalt dust.

Based on the possible transformations of BTHs reported in the literature (**Figure 2.3**), and the distribution of BTHs (**Figure 4.2**), different rates of transformation in the summer and winter season are indicated. By assuming the same contribution from tires in the winter and the summer, it is indicated, by the distribution of BTHs in the winter, that more of the 2-S-BTH gets methylated or transformed to BTH/2-OH-BTH in the winter season than the summer season. The increase in the portion of 2-OH-BTH in the winter can come from oxidation of BTH, or transformation of 2-S-BTH. It is also a possibility that 2-OH-BTH is leached from studded tires, which have a higher portion of 2-OH-BTH than summer and stud free tires. The partition of 2-NH2-BTH in winter is over to times less than in the summer, which can be explained by the rapid degradation of 2-NH2-BTH in solutions with chloride (Nika et al., 2017), caused by the road salt. The partition of 5-Amino-BTR is more than 5 times less in the winter, than the summer, suggesting the same degradation pattern as 2-NH2-BTH.

From the airborne dust collected by the air filters, five of the six analysed BTHs and two of the seven analysed BTRs were detected (**Figure 4.5**). All BTHs except 2-M-BTH were detected in

the air filters. The highest concentration of the BTHs in the air filters was 2-OH-BTH detected in the one of the PM_{coarse} filter (60.4 ng/L), while the highest concentration of the BTRs was BTR detected in the volatile $PM_{2.5}$ filters (813 ng/L) (**Table 4.8**). Detected concentrations are all lower than previously reported concentrations (Maceira et al., 2018), that are measured in ng/m^3 (**Table 2.1**). This study found BTR to be the biggest partition of the BTRs, and 2-OH-BTH to be the biggest partition of the BTHs in air filters, matching the findings of Maceira et al. (2018)

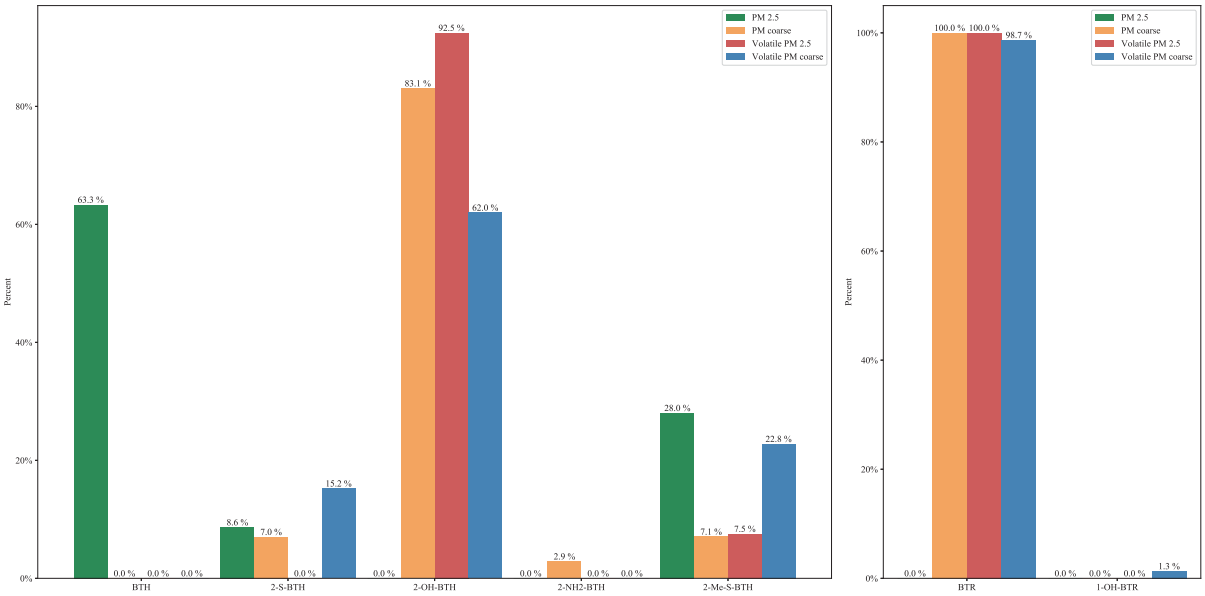

Figure 4.5: Distribution of benzothiazoles and benzotriazoles in air filters, compared to ∑BTHs and ∑BTRs

The highest concentrations of BTHs were detected in the non-volatile filters (**section 3.1.4**), with most of the BTHs detected in the PM_{coarse}. BTH was only detected in the non-volatile $PM_{2.5}$, and 2-S-BTH had higher concentration in the non-volatile $PM_{2.5}$ rather than the non-volatile PM_{coarse}. 2-S-BTH was also detected in the volatile PM_{coarse} with approximately half the concentration as in the non-volatile PM_{coarse}. 2-OH-BTH was not detected in the non-volatile $PM_{2.5}$. However, it is the major partition (92.5%; 34.8 ng/L) of the BTHs in the volatile $PM_{2.5}$. None of the BTRs were detected in the non-volatile $PM_{2.5}$, but BTR was detected in non-volatile PM_{coarse}. The concentration of BTR detected in the volatile $PM_{2.5}$ (813 ng/L) and volatile PM_{coarse} (223 ng/L) is significantly higher than the detected in the road dust during the same season (23.4 ng/L; summer). The highest concentration of the BTHs in the volatile particulate is 2-OH-BTH in $PM_{2.5}$ (34.8 ng/L), which is much lower than the concentration detected in the road dust during the same season (197 ng/L; summer). This indicates that the BTHs is less volatile, and is adsorbed/bound to the road dust, while the BTR is more volatile and less bound to the road dust. BTH and 2-Me-S-BTH are most abundant in the $PM_{2.5}$, while 2-S-BTH, 2-OH-BTH and 2-NH2-BTH are most abundant in the PM_{coarse}.

Table 4.8: Concentrations of BTHs and BTRs in total (particulate and liquid phase) (ng/L) in the different air filters

	$PM_{2.5}$	n/N*	PM^{a}_{coarse}	n/N*	Volatile $PM_{2.5}$	n/N*	Volatile PM_{coarse}	n/N*
BTH	18.1	1/2	-	-	-	-	-	-
2-S-BTH	2.47	1/2	5.10	1/2	-	-	2.20	1/2
2-OH-BTH	-	-	60.4	1/2	34.8	2/2	8.95	1/2
2-NH2-BTH	-	-	2.08	2/2	-	-	-	-
2-Me-S-BTH	8.02	2/2	5.14	2/2	2.83	2/2	3.29	1/2
∑ BTHs	18.3	2/2	40.0	2/2	37.6	2/2	7.22	2/2
BTR	-	-	10.0	2/2	813	2/2	223	2/2
1-OH-BTR	-	-	-	-	-	-	3.0	1/2
∑ BTRs	-	-	10.0	2/2	813	2/2	225	2/2

*: n is number of detected samples and N is total samples in the set
a: particles between $PM_{2.5}$ and PM_{10}

According to the calculations (**Table 4.9**), the distribution coefficient values, K_d vary greatly between the different matrices. There is also high variation within the same matrices as well, as shown by the standard deviations. The K_d is calculated by dividing the concentration in particulate matter (ng/g) by the corresponding amount in the liquid (ng/mL) phase (see **Table B.1** and **B.2**), and higher K_d means higher affinity to the particulate phase.

Table 4.9: Distribution coefficient values, K_d, for BTHs and BTR in road dust

	Summer	**Winter**	**Prall**
	K_d (L/kg) (± SD*)	K_d (L/kg) (± SD)	K_d (L/kg) (± SD)
BTH	-	93.9 (± -)	-
2-S-BTH	1953 (± 1178)	635 (± 753)	4114 (± 2689)
2-OH-BTH	23724 (± 23231)	450 (± 4782)	1077 (± 1789)
2-NH2-BTH	642 (± 286)	174 (± 80.1)	931 (± 409)
2-Me-S-BTH	1355 (± 2449)	3005 (± 3078)	30122 (± 24055)
2-M-BTH	-	567 (± 398.4)	528 (± 178)
BTR	2608 (± 895)	368 (± 174)	929 (-)
TTR	1682 (± 610)	295 (± 118)	4383 (± 2183)
XTR	-	523 (± 442)	-
BTR COOH	5033 (± 3653)	417 (± 253)	-
5-Cl-BTR	2728 (± 7598)	2219 (-)	-
1-OH-BTR	-	524 (± 366)	-
5-Amino-BTR	-	-	-

*: Standard Deviation
- : Not calculated
(-): Only one calculation

4.2.2 Elements

Table 4.10 shows the concentrations of a selection of elements detected in the turbid road dust samples. Full table of concentrations of all elements detected in the turbid road dust samples can be found in **Table: B.4** and **B.5** in **Appendix B**.

Based on the report of Erichsen et al. (2004), the minerals in the coarse aggregate in Elgeseter street mainly consists of plagioclase ($Na(AlSi_3O_8)$, $Ca(Al_2Si_2O_8)$), quartz (SiO_2) and amphibole (Mg-Fe silicate). This is consistent with the concentrations of elements from the prall-test detected in this study, which support this, where the major elements are Si, Al, Ca, Na, Fe and Mg. These elements are the major components in the turbid road dust samples (**Table 4.10**), which supports the statement of Pant and Harrison (2013), that the crustal dust is a key component in road dust. By comparing the concentration elements in road dust from the summer season and the prall-test, it is evident that the amount of Fe has more sources than only the road surface. The concentrations of the crustal elements are more than doubled in the winter season, supporting the statement of Forsberg et al. (2005), that sanding of the road and use of studded tires substantially increase the wear of the road surface. By comparing with the concentration in the filtered samples (particles < 0.45 μm) in **Table B.8** it also supports the statement of Forsberg et al. (2005), that this is mainly coarse particles, since the concentration in fine particles severely lower.

All of the ”selected” elements (**Table 4.10**) demonstrated higher concentrations in the winter season than the summer season. Some of these elements, especially crustal elements are potentially coming from the increased wear of the road surface in the winter season. The concentration of Cl in the winter is approximately 80 times higher in the winter (81 490 ng/mL) than in summer (1146 ng/mL); this 80-fold increase can be explained by the addition of salt to the road surface. The increase of Na, Mg, and Ca in the winter can also partly be explained by the addition of salt, since NaCl is added to prevent/remove ice and $CaCl_2$ and $MgCl_2$ is used as de-icing and dust binding chemicals.

The concentration of Sb, a major component in brake dust/wear particles (Thorpe and Harrison, 2008; Schauer et al., 2006), is approximately the same for the summer (10.6 ng/mL) and winter (11.3 ng/mL) season. This indicates that Sb has the same source, and its concentration is independent of season. Ni and V, previously reported in exhaust due to oil combustion (Pant and Harrison, 2013), is 4-5 times higher in the winter season compared to the summer season. Both elements reported in gasoline (Br, Ba, Cu, Mn and Sr) and diesel (Ba, Cd, Pb, V, Zn) (Cheng et al., 2010; Lin et al., 2005) have higher concentrations in winter compared to summer. This is attributed to the increase in fuel consumption in colder temperatures, and also from the increase in exhaust particle emissions due to cold engines. Sb has been previously reported in both gasoline (Cheng et al., 2010) and diesel (Lin et al., 2005), but since concentrations detected are approximately the same for winter and summer, it can be suggested that brake wear is the main source of road pollution.

Table 4.10: Concentrations of elements in turbid road dust samples (ng/mL)

	Total				Summer				Winter				Prall			
	Median	*min*	*max*	*n/N**	*Median*	*min*	*max*	*n/N**	*Median*	*min*	*max*	*n/N**	*Median*	*min*	*max*	*n/N**
Si	186,995	64,922	330,623	22/22	96,378	64,922	190,789	10/10	267,979	183,201	330,623	10/10	97,833	66,586	129,080	2/2
Fe	85,161	26,309	287,388	22/22	37,926	26,309	91,898	10/10	184,785	78,423	287,388	10/10	22,571	15,474	29,668	2/2
Al	82,052	27,179	223,320	22/22	39,707	27,179	82,903	10/10	145,219	81,201	223,320	10/10	43,208	30,076	56,340	2/2
Ca	75,876	23,519	248,288	22/22	34,282	23,519	79,987	10/10	155,541	71,766	248,288	10/10	41,276	33,510	49,042	2/2
Mg	38,742	10,028	148,694	22/22	15,178	10,028	33,962	10/10	97,234	43,523	148,694	10/10	10,452	7,470	13,434	2/2
Cl	20,583	858	123,265	22/22	1,134	858	1,364	10/10	81,490	39,802	123,265	10/10	8,157	8,157	8,157	2/2
Na	19,163	7,072	36,372	22/22	9,891	7,072	15,466	10/10	28,486	22,861	36,372	10/10	16,906	12,808	21,005	2/2
K	11,452	3,325	30,018	22/22	5,172	3,325	10,892	10/10	20,471	12,011	30,018	10/10	8,819	6,091	11,547	2/2
Ti	8,382	2,552	26,312	22/22	3,753	2,552	9,566	10/10	16,092	7,199	26,312	10/10	2,065	1,404	2,725	2/2
S	3,071	997	11,304	22/22	1,437	997	2,811	10/10	7,339	3,331	11,304	10/10	1,437	1,320	1,554	2/2
Mn	1,359	499	4,244	22/22	657	499	1,433	10/10	2,843	1,285	4,244	10/10	420	285	555	2/2
P	895	345	3,305	22/22	555	345	968	10/10	1,914	823	3,305	10/10	323	217	430	2/2
Zn	421	189	1,246	22/22	295	189	441	10/10	900	401	1,246	10/10	93.5	64.8	122	2/2
V	342	95.1	1,126	22/22	146	95.1	375	10/10	687	309	1,126	10/10	69.5	46.9	92.1	2/2
Ba	340	106	927	22/22	161	106	342	10/10	641	338	927	10/10	251	165	337	2/2
Sr	309	86.9	1,012	22/22	132	86.9	313	10/10	595	305	1,012	10/10	228	164	292	2/2
Cu	216	96.9	516	22/22	135	96.9	238	10/10	358	195	516	10/10	100	76.8	124	2/2
Br	199	17.3	1,209	22/22	22.5	17.3	31.0	10/10	802	367	1,209	10/10	34.6	33.3	35.9	2/2
Cr	189	63.8	586	22/22	96.5	63.8	215	10/10	374	164	586	10/10	149	126	172	2/2
Ni	76.5	26.2	224	22/22	38.8	26.2	79.7	10/10	156	73.2	224	10/10	33.7	28.5	38.9	2/2
Ce	56.6	16.4	206	22/22	24.0	16.4	60.4	10/10	116	52.9	206	10/10	24.9	17.3	32.6	2/2
Sc	42.6	12.5	117	22/22	19.2	12.5	47.7	10/10	75.0	37.5	117	10/10	8.34	5.61	11.1	2/2
Co	40.4	11.6	117	22/22	18.3	11.6	40.3	10/10	88.3	40.5	117	10/10	9.58	6.95	12.2	2/2
Pb	30.5	13.8	242	22/22	20.7	13.8	242	10/10	50.6	26.2	74.6	10/10	6.22	4.73	7.72	2/2
Li	18.7	6.23	79.9	22/22	9.13	6.23	16.7	10/10	47.6	20.6	79.9	10/10	8.52	6.24	10.8	2/2
Sn	18.4	9.13	29.2	22/22	13.6	9.13	26.6	10/10	25.2	14.7	29.2	10/10	1.82	1.16	2.49	2/2
W	15.8	2.80	34.6	22/22	6.32	2.80	9.57	10/10	30.5	21.9	34.6	10/10	1.15	1.02	1.28	2/2
Sb	11.3	8.02	39.7	22/22	10.6	8.02	39.7	10/10	11.3	8.69	14.0	10/10	0.76	0.74	0.79	2/2
As	9.37	2.99	40.1	22/22	4.55	2.99	10.8	10/10	19.5	7.59	40.1	10/10	1.52	1.38	1.66	2/2
Mo	6.70	3.37	17.7	22/22	4.52	3.37	7.51	10/10	10.8	4.54	17.7	10/10	1.53	1.21	1.85	2/2
Cs	1.29	0.43	4.81	22/22	0.68	0.43	1.21	10/10	2.95	1.36	4.81	10/10	0.34	0.29	0.39	2/2
Be	1.07	0.36	2.94	22/22	0.51	0.36	1.06	10/10	1.66	1.08	2.94	10/10	0.47	0.37	0.58	2/2
Hg	0.05	0.02	0.29	21/22	0.03	0.02	0.05	9/10	0.18	0.04	0.29	10/10	0.01	0.01	0.02	2/2

*: n is number of detected samples and N is total samples in the set

Because some of the elements, have both minerals in the road pavement and vehicle parts as sources, an attempt was made to distinguish the concentration explained by surface wear. To do this an equation was purposed:

$$RW\% = \frac{[Summer] \times k_{RW}}{[Winter]} \times 100\% \tag{4.3}$$

Where $RW\%$ is the percentage explained by road wear, $[Summer]$ is concentration detected in summer, $[Winter]$ is the concentration detected in winter and k_{RW} is the road wear correction factor. The correction factor was calculated based on Si because of mineral, by my knowledge, as the only source. The correction factor is calculated so that the $RW\%$ of Si becomes 100, and was calculated to be 2.78 in this study.

Table 4.11: Amount of detected concentration explained by road wear, using road wear factor 2.78 (based on Si)

Element	RW%
Si	100
Fe	57.1
Al	76.1
Ca	61.3
Mg	43.4
Na	96.5
Ti	64.8
Ba	69.7
Cr	71.6

Table 4.11 shows the calculations using **equation 4.3**. This equation calculates the amount of concentration in winter that is explained by road wear. This equation can only be used on elements having a higher increase than Si in the winter season compared to the summer season (concentration in winter is higher than 2.78 times concentration in summer). From the calculation, only 57.1% of the Fe concentration is explained by road wear and other sources must contribute to the concentration detected. The same applies for Al, Ca and Mg. Almost all of the Na concentration is explained by road wear, using this calculation, suggesting that most of the salt added to the road surface at sampling was for dust binding purposes (using $CaCl_2$ and $MgCl_2$) and not for ice removal. These calculations have a high degree of uncertainty, and are meant as an attempt to broadly distinguish sources and not for quantitative calculations.

Some of the elements found in the dust generated from the prall-test can originate from other sources than the road itself, as it is possible that these elements incorporate into the road surface from other sources, as stated by Thorpe and Harrison (2008). A possible source of Fe is brake wear, as brake pads contain 13-45% Fe (Amato et al., 2014). The increased concentrations of Al, Fe, Ba, Zn, Cu could also come from corrosion of vehicle parts, as Fe, Al and Ti is used in car chassis, wheels and shocks (Cole, 2017), and road salt contributes to the corrosion of vehicles (Kogel et al., 2006). Ba, Cu and Zn are components in brake systems (Schauer et al., 2006; Thorpe and Harrison, 2008), which are exposed to corrosion from road salt. The most evident contribution factor in the winter season is the increased road wear from studded tires and the additional corrosive properties of road salt. The increase in elements in the winter,

which is not explained by the road wear (**Table 4.11**), and the corrosive properties of the road salt, indicates that a major source is corrosion of vehicle parts, or increased wear induced by the addition of road salt. Barium is easily oxidized, and a high increase of Ba in winter can come from both brake wear, and corrosion of brake-components. Titanium alloys are known to be very corrosion resistant, but low in wear resistance (Fuji et al., 2003), hence the increase in titanium comes from abrasion of vehicle parts instead of corrosion.

The Cu:Sb (used in literature for brake wear) ratio found in this study, was 12.7 (summer season) and 31.6 (winter season), indicating that the brake wear is much higher in the winter season than in the summer season. It is evident that the ratio itself cannot be used as a sole indicator for brake wear, as proposed by previous studies (Sternbeck et al., 2002; Hjortenkrans et al., 2007), as the ratio differs between geographical areas (**section 2.2.3**). A more stable ratio, independent of geographical area is deemed necessary.

4.3 Correlations between BTHs, BTRs and elements

The goal of finding correlations between the elements and the organic is to propose possible markers for different sources. The different transformations of BTHs and BTRs during seasons, and the different possible sources of elements makes it difficult to solely using elements or organics as key tracers.

Zn demonstrate a strong correlation with 2-Me-S-BTH and 1-OH-BTR, which the latter are both found in the tires analysed, alongside with other BTHs. Zn with 2-Me-S-BTH could be used as a possible marker, as 2-Me-S-BTH is a major transformation product of 2-S-BTH (Brownlee et al., 1992). **Table 4.12** shows all significant correlations between elements and organics.

Table 4.12: Correlations between log conc. (ng/mL) of BTHs/BTRs and metals in summer and winter samples ($p < 0.01$)

	Si	Fe	Al	Ca	Mg	Cl	Na	K	Ti	S	Mn	P
BTH	0.74	0.77	0.77	0.76	0.77	0.70*	0.71*	0.76	0.78	0.75	0.77	0.76
2-OH-BTH	0.82	0.83	0.82	0.84	0.82	0.78	0.77	0.82	0.83	0.84	0.84	0.81
2-NH2-BTH	0.52*	0.54*	0.53*	0.50*	0.52*			0.52*	0.55*		0.52*	0.53*
2-Me-S-BTH	0.90	0.90	0.89	0.90	0.90	0.83	0.88	0.90	0.90	0.91	0.90	0.87
2-M-BTH	0.73	0.71	0.71	0.68	0.70	0.55*	0.71	0.71	0.72	0.67	0.70	0.65
BTR	0.92	0.95	0.95	0.94	0.94	0.80	0.89	0.93	0.95	0.93	0.95	0.93
TTR	0.60*	0.66	0.65	0.67	0.68	0.71	0.62*	0.64	0.65	0.67	0.68	0.63
BTR COOH						-0.58*						
5-Cl-BTR	0.50*		0.50*						0.53*			
1-OH-BTR	0.78	0.82	0.82	0.82	0.87	0.94	0.87	0.83	0.78	0.88	0.84	0.81

	Zn	V	Ba	Sr	Cu	Br	Cr	Ni	Ce	Sc	Co	Pb
BTH	0.78	0.77	0.76	0.75	0.78	0.72*	0.78	0.77	0.77	0.76	0.76	
2-OH-BTH	0.76	0.83	0.82	0.84	0.80	0.80	0.81	0.82	0.84	0.84	0.83	
2-NH2-BTH	0.63	0.53*	0.53*		0.59*		0.56*	0.54*	0.53*	0.53*	0.51*	
2-Me-S-BTH	0.85	0.90	0.90	0.90	0.88	0.87	0.88	0.90	0.89	0.90	0.90	
2-M-BTH	0.72	0.71	0.72	0.69	0.71	0.61*	0.71	0.72	0.73	0.70	0.71	
BTR	0.96	0.94	0.94	0.93	0.96	0.84	0.95	0.94	0.94	0.94	0.93	
TTR	0.70	0.65	0.64	0.65	0.66	0.72	0.67	0.66	0.66	0.63	0.65	
BTR COOH						-0.54*						
5-Cl-BTR		0.50*			0.54*		0.50*		0.52*	0.52*		
1-OH-BTR	0.84	0.80	0.82	0.81	0.80	0.94	0.79	0.84	0.80	0.77	0.83	0.86

	Li	Sn	W	As	Mo	Cs	Be	Se	Cd	Hg	Pt
BTH	0.79	0.71*	0.63*	0.80	0.80	0.79	0.79		0.76		0.65*
2-OH-BTH	0.80	0.52*	0.82	0.84	0.65	0.79	0.79	0.73	0.80	0.60*	
2-NH2-BTH	0.54*	0.64		0.55*	0.64	0.54*	0.53*		0.65		0.63*
2-Me-S-BTH	0.88	0.63	0.89	0.86	0.77	0.87	0.87	0.81	0.87	0.63	0.52*
2-M-BTH	0.68		0.69	0.68	0.70	0.68	0.70		0.77	0.42	0.56*
BTR	0.94	0.73	0.82	0.93	0.93	0.95	0.94	0.61*	0.97	0.73	0.65
TTR	0.69		0.57*	0.69	0.61*	0.67	0.67		0.72	0.66	0.57*
BTR COOH			-0.56*								
5-Cl-BTR		0.52*		0.51*				0.67*	0.60*		0.57*
1-OH-BTR	0.88	0.67*	0.83	0.78	0.73	0.86	0.80		0.80	0.90	

*. $p < 0.05$

4.3.1 Corrosion, TTR and road salt

To distinguish a relationship between road salt and corrosion of car parts, chloride was plotted against some of the elements commonly used in car parts (**Figure 4.6**). In this figure it is evident that there is a relationship in the winter season (when road salt is used), which is not found in the summer season. As the concentration of chloride increases, the concentration of selected metals also increases. Zn has the most linear relationship, from these figures. Both Fe and Al have coarse aggregate in the road surface as a source, which can lead to a lesser linear relationship with chloride.

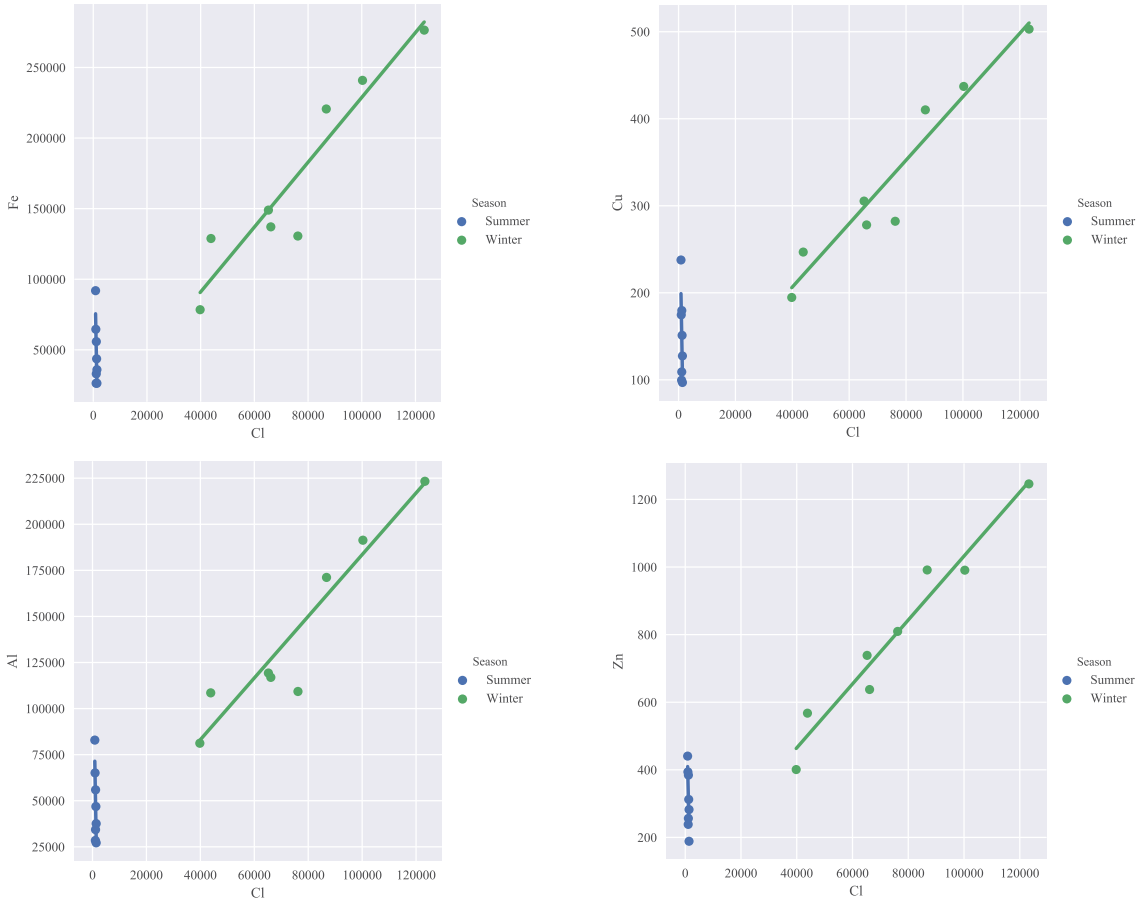

Figure 4.6: Scatter plot of chloride versus selected elements in car parts

By comparing the amount of tolyltriazole (TTR) with the chloride and the same elements as in **Figure 4.6**, more assumptions about corrosion can be made. By comparing the relationship between TTR and chloride (**Figure 4.7**) is it evident that there is a relationship between chloride and TTR, as chloride increases so does TTR. By plotting TTR concentrations against the metals with possible corrosion, it is evident that as there is an increase in TTR, other metals also increase. The increase in TTR in the winter season follows the increase of the metals, which indicates that TTR may come from corrosion of car parts, and not added as de-icing/anti-icing in road salt. If they were found in de-icing/anti-icing in road salt, then there should be a more negative relationship between the TTR and the metals, as TTR inhibits corrosion.

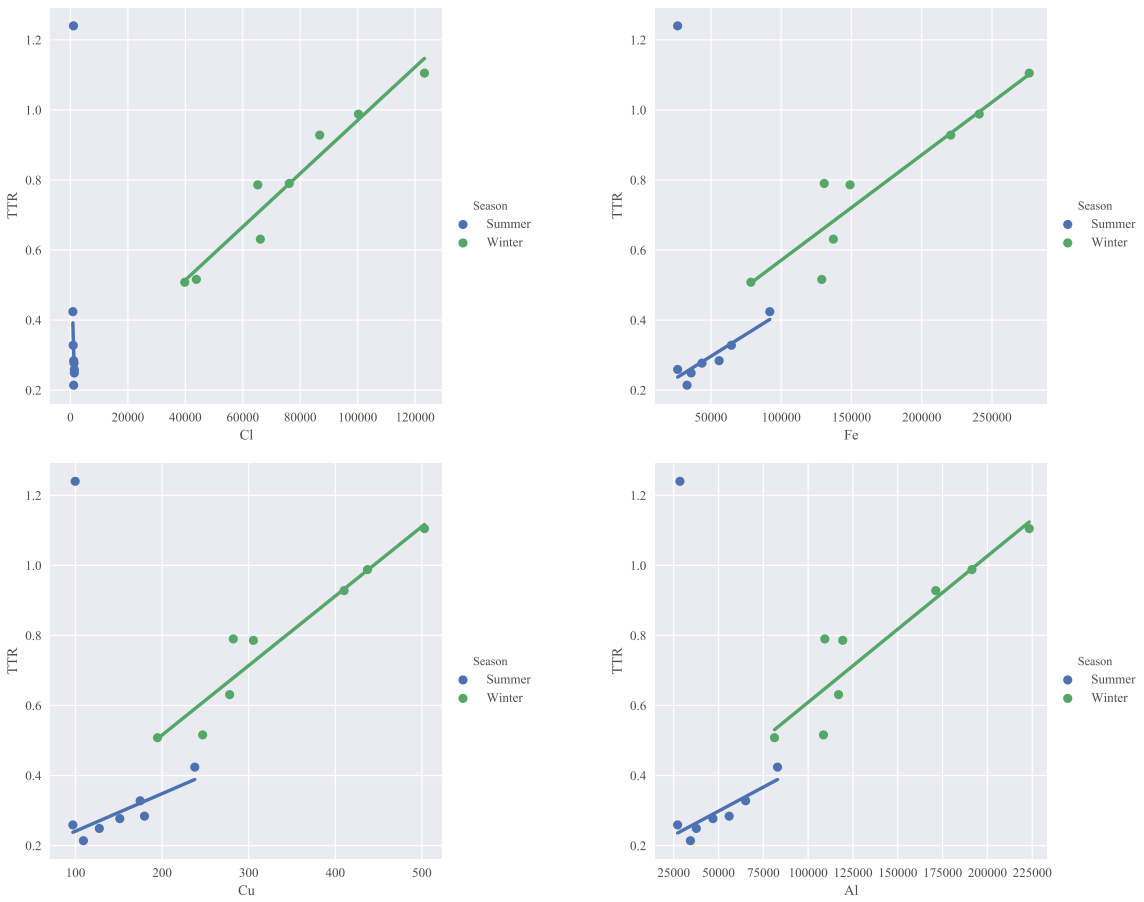

Figure 4.7: Scatter plot of tolyltriazole (TTR) versus some selected elements in car parts

4.3.2 PCA

The PCA analysis demonstrates a ”fingerprint” of the sample matrices. The samples get grouped or separated based on the variation in the samples. It groups the samples together on the basis of the same relationships between the components analysed. This can be used to analyse an unknown sample matrix for the same components, and distinguish the matrix based on the placement in the PCA score plot. Simplified loading plots are presented in this section, and the more detailed loading plots can be found in **Appendix H**.

Figure 4.8: PCA of BTHs and BTRs in road dust samples

With PCA analysis of the total concentrations of BTHs and BTRs (**Figure 4.8**) it was possible to separate the tire samples, prall samples and road dust samples. The road dust from summer and winter is partially separated, but not completely. From the loadings plot it can be stated that the BTHs and the BTRs are used in different applications, as they are clearly separated in the loading plot (**Figure 4.9**).

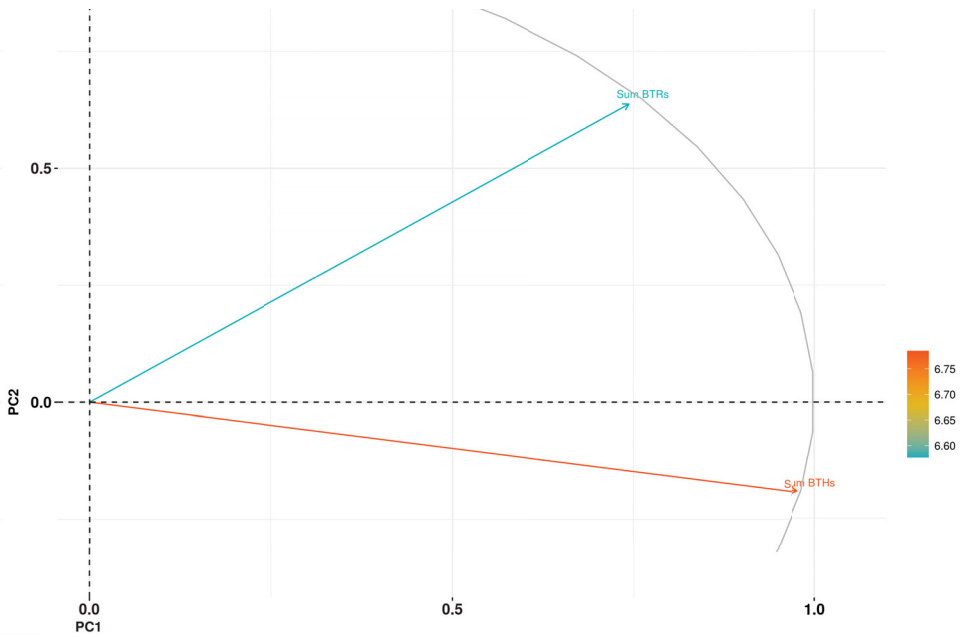

Figure 4.9: Loading plot for PCA of organics (demonstrating only total BTHs and total BTRs)

Figure 4.10: PCA of elements in turbid road dust samples

In the PCA of elements (**Figure 4.10**), there is a clear separation of road dust from summer and winter season. There is also a clear separation of the air filters and the road dust. However, the prall samples are in the same group as the road dust collected in summer. From this it can be concluded that the dust from prall and the road dust collected in summer have a very similar composition, making them hard to separate using PCA. This also support that metals from road dust, or other sources, can be incorporated into the asphalt (road surface), as previously stated by Thorpe and Harrison (2008).

In the loading plot for elements (**Figure 4.11**), the biggest group is described as background level. Elements closer to each other are more correlated to each other. Ba and Sn, are close to each other since both are found in components of brake systems. Sb is relatively close to Ba and Sn, because it is also a brake component. Zn that are reported in tires are lesser correlated to other elements, suggesting multiple sources or a source that produces solely Zn.

The PCA of both organics (BTHs and BTRs) and elements (**Figure 4.12**) clearly separates the dust from the prall from the road dust from summer and winter season.

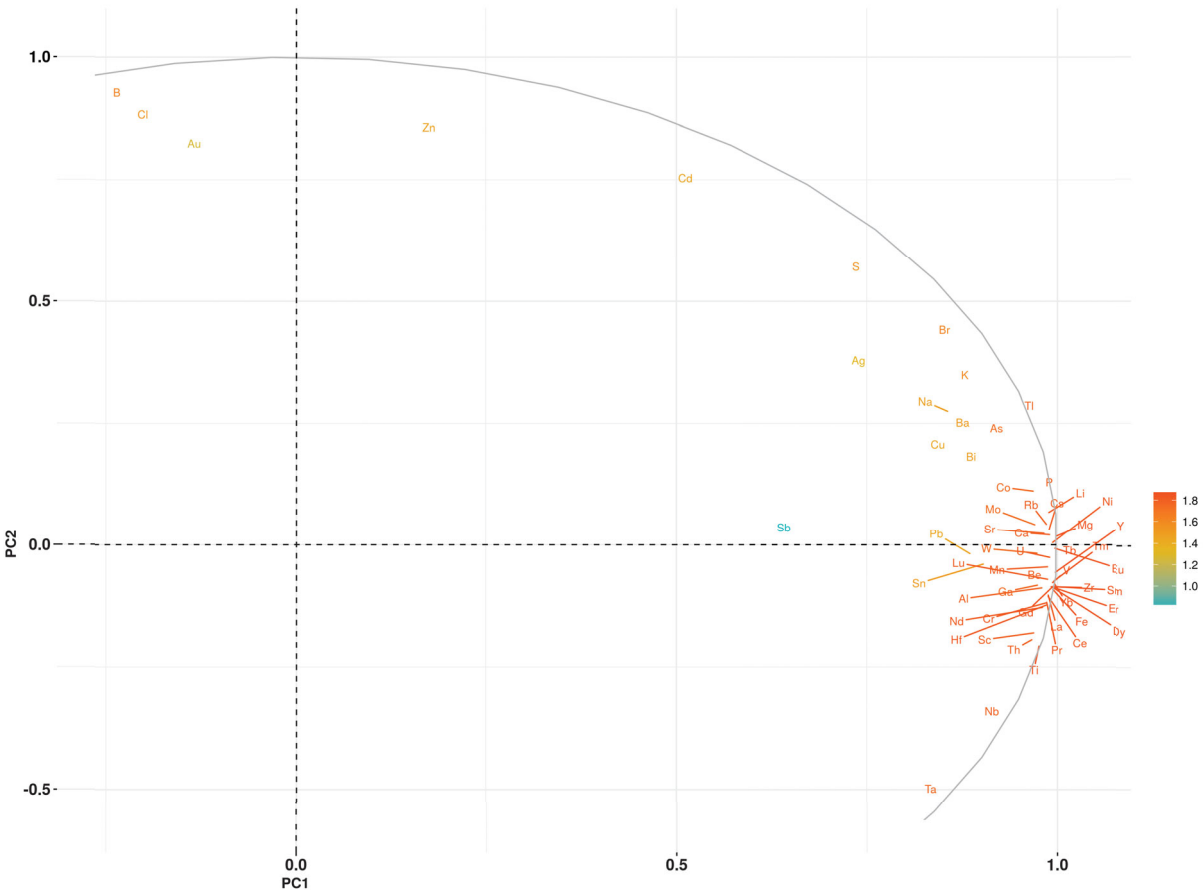

Figure 4.11: Loading plot for PCA of elements

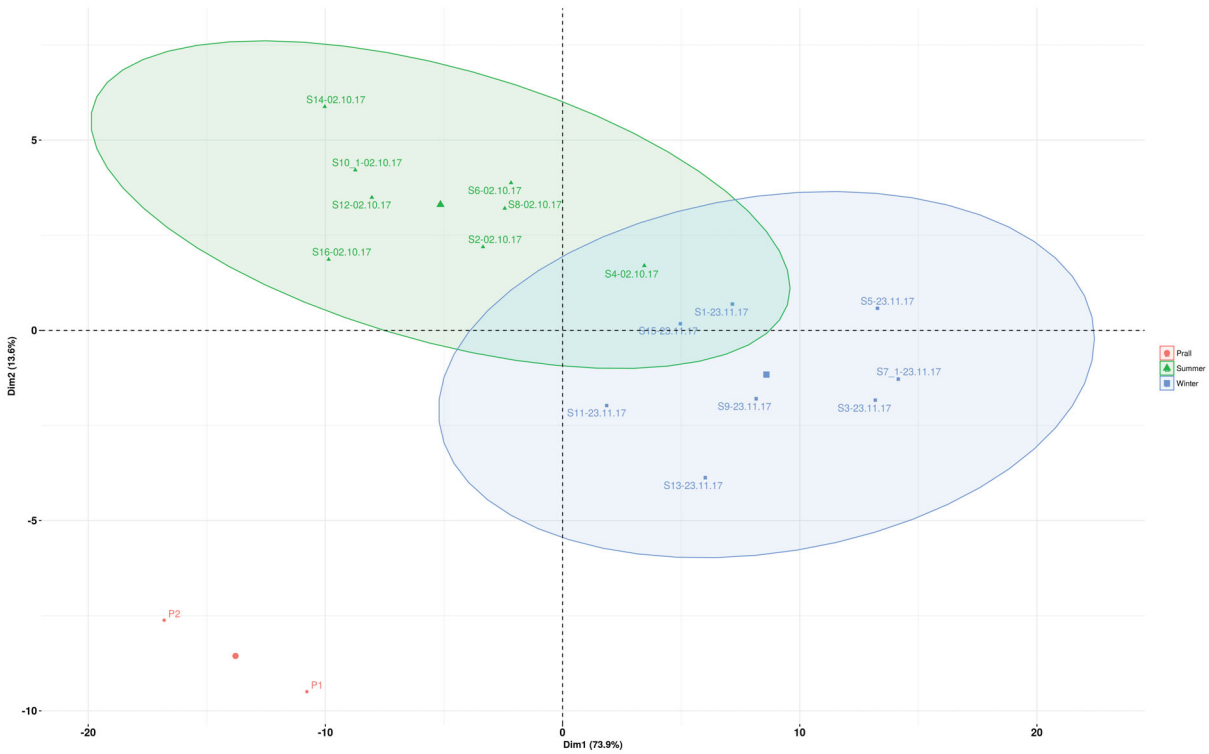

Figure 4.12: PCA of metals, BTHs and BTRs in turbid road dust samples

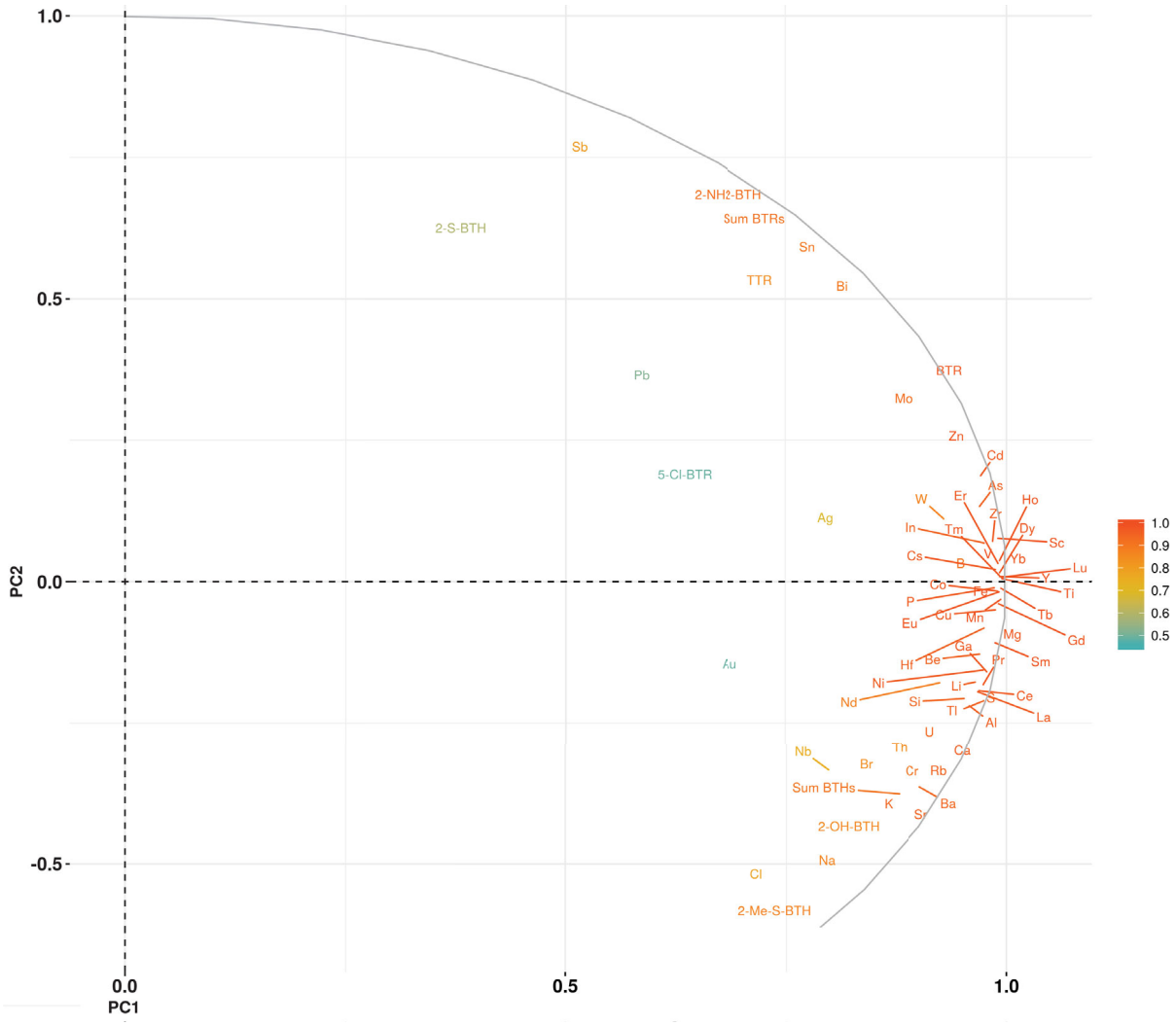

Figure 4.13: Loading plot for PCA metals, BTHs and BTRs

There is a correlation between the components close to each other (grouped together) in the loading plot of the PCA. From **figure 4.13** indications on possible tracers can be made. Sb and 2-S-BTH are correlated since Sb is coming from brake wear and 2-S-BTH is coming from wear (physical) of tires (as braking leads to physical tear/wear of the tires). The transformation product of 2-S-BTH, 2-S-Me-BTH is more correlated to the components in road salt. The road salt is also correlated with 2-OH-BTH, a major component in tires and break down/transformation product of BTH. This suggests that the road salt has an impact on the transformation/break down of BTHs like 2-S-BTH and BTH, and/or increased wear of tires.

The association between braking (Sb) and tire wear (2-S-BTH) also indicate that 2-S-BTH mainly is in rubber particles torn from tires, and not free in the environment. Since 2-S-BTH is highly reactive, it is rapidly methylated into its transformation product 2-Me-S-BTH (**Figure 2.3**). This suggests 2-S-BTH together with Sb to be a possible marker for rubber particles from tires, and 2-Me-S-BTH and 2-OH-BTH together with Cl to be a possible marker for chemical wear/leaching from tires due to road salt.

The correlation between $MgCl_2$ as road salt and corrosion of steel (Fe) and aluminium with TTR as corrosion inhibitor, is difficult to distinguish due to high concentrations from other sources (background).

5 Conclusions

The wet dust sampler (WDS) worked well for sample collecting road dust for both inorganic and organic analysis. The use of distilled water ensures that the contamination is low, and the design of the apparatus ensures that all of the dust on the surface gets collected. This leads to a better characterization of the road dust, than collecting the dust by hand. The automated sampling provided by the WDS also ensures good reproducibility.

The uncertainty of using the prall-test for producing ”clean” road dust from the asphalt, contamination wise, is too high for both analysis of BTHs and elements. The use of steel balls to hammer the sample can contribute to the dust produced by both wear of the balls and also from wear of the prall-test instrument. The fact that the ”hammering chamber” has a rubber seal introduces the risk of BTHs contamination to leach into the ”clean” dust sample.

The BTR COOH, for which no analytical method has been previously reported, showed good reproducibility and had high recovery. The 5-Amino-BTR demonstrated low recoveries, rendering more appropriate to have semiquantification for this component. All BTHs and BTRs analysed were found in the road dust in both summer and winter season. For the elements, 61 of the 66 analysed had detected concentrations above the quantification limit in the turbid road dust samples.

The concentration of BTHs and BTRs are higher in the winter season than in the summer season. High concentrations of BTHs in tires tested in the study, together with previous studies, indicates that tire wear is the major source of BTHs in road dust. 2-OH-BTH is the BTH derivative with the highest concentrations in both summer, winter and prall sample. This can indicate that 2-OH-BTH is the major transformation products from BTHs, as both BTH and 2-S-BTH is known to biotransform to 2-OH-BTH. The increase in the partition of 2-OH-BTH and 2-Me-S-BTH in the winter indicates that the rate of transformation is higher in the winter season, than the summer season. The road salt increases the concentration of chlorine on the road surface, which contribute to the breakdown/transformation of several BTHs and BTRs, with the most significant effect on 2-NH2-BTH which is decreased two-fold in the winter season. Based on the increase in concentration of BTHs in the winter, together with higher concentration of BTHs in stud free tires (most common tire), this study shows that more BTHs are leached from tires in the winter season.

TTR was the major BTR derivative in the road dust, with the highest concentration detected for all BTHs and BTRs analysed. TTR is used as corrosion inhibitor in steel and copper. It is a reason to believe that most of the TTR comes from wear of vehicle parts treated with corrosion inhibitors. The increase in TTR in the winter season, together with the relationship with elements used in vehicle chassis and chloride, suggest that TTR derives from wear of the vehicle and not from the road salt solution. The increase in TTR also supports that the road salt increase wear of the vehicle parts.

The major inorganic components in the road salt is the crustal elements (Si, Fe, Mg, Al, Ca), indicating that most of the road dust comes from wear of the road surface. This wear increases in the winter season, mostly due to the use of studded tires and salting of the road (wet conditions). However, the concentrations of the crustal elements, in winter season, cannot solely be explained by the road wear. With a simple equation made in this study, an estimate on the contribution from road wear can be made. Using this equation, it was indicated that the road wear only explains about half of the concentration of iron, meaning that the remaining must come from other sources. Increase of elements known to be present in the car exteriors (chassis, wheels, shock, brake pads, etc.) were all increased in the winter season. This is believed to come from the wear and vehicle parts, with an increase in the winter because of the road salt.

Elements previously reported in exhaust (Ba, Br, Cu, Cd, Mn, Ni, Pb, Sr and V) had increased concentrations in the winter season, attributed to the increase in fuel consumption in colder temperatures, as well as from increase in exhaust particle emissions due to cold engines. Sb, previously reported in exhaust and brake dust, had approximately the same concentrations for summer and winter season, suggesting that brake wear is the main source of Sb in road dust.

With the use of PCA, it was possible to separate the different samples analysed (summer, winter, prall) only when combining the elements with the BTHs and BTRs. By combining the concentrations of the inorganic analytes with the organic analytes a clearer picture of sources can be made, comparing organic components and elements with the same, or similar, source. An example of this is comparing 2-S-BTH from rubber particles and Sb from tires to distinguish rubber particles worn from tires, and comparing 2-OH-BTH and 2-Me-S-BTH with Cl to distinguish the wear/leach of tires affected by road salt. Many of the elements cannot be used as a sole key indicator for wear of specific parts of a vehicle, but by correlation with organic components known to have the same source a more reliable assumption can be made. Tolyltriazole (TTR) together with Fe, Al, Ti, Cu can be a possible marker for wear of car parts, and together with Cl it can be a possible marker for corrosion of car parts. These relationships emphasise the importance of simultaneously analysing both inorganic and organic parts of the road dust sample to be able to distinguish pollution sources and to determine better markers for contributors to road dust (e.g. tire wear and brake wear).

Bibliography

Alves, C.A., Evtyugina, M., Vicente, A.M.P., Vicente, E.D., Nunes, T.V., Silva, P.M.A., Duarte, M.A.C., Pio, C.A., Amato, F., and Querol, X. (2018). Chemical profiling of pm10 from urban road dust. *Science of the Total Environment*, 634:41–51.

Alvey, J.K., Hagedorn, B., and Dotson, A. (2016). Benzotriazole enrichment in snowmelt discharge emanating from engineered snow storage facilities. *Water Environment Research*, 88(6):510–520.

Amato, F., Alastuey, A., de la Rosa, J., de la Campa, A.M.S., Pandolfi, M., Lozano, A., González, J.C., and Querol, X. (2014). Trends of road dust emissions contributions on ambient air particulate levels at rural, urban and industrial sites in southern spain. *Atmospheric Chemistry and Physics*, 14(7):3533–3544.

Apeagyei, E., Bank, M.S., and Spengler, J.D. (2011). Distribution of heavy metals in road dust along an urban-rural gradient in massachusetts. *Atmospheric Environment*, 45(13):2310–2323.

Asimakopoulos, A. (2014). Development of methods for the determination of xenobiotic compounds in biological matrices by lc-ms/ms-phd thesis.

Asimakopoulos, A.G., Wang, L., Thomaidis, N.S., and Kannan, K. (2013a). Benzotriazoles and benzothiazoles in human urine from several countries: A perspective on occurrence, biotransformation, and human exposure. *Environment International*, 59:274–281. URL `http://www.sciencedirect.com/science/article/pii/S0160412013001256`.

Asimakopoulos, A.G., Bletsou, A.A., Wu, Q., Thomaidis, N.S., and Kannan, K. (2013b). Determination of benzotriazoles and benzothiazoles in human urine by liquid chromatography-tandem mass spectrometry. *Anal. Chem.*, 85(1):441–448. URL `https://doi.org/10.1021/ac303266m`.

Asimakopoulos, A.G., Wang, L., Thomaidis, N.S., and Kannan, K. (2014). A multi-class bioanalytical methodology for the determination of bisphenol a diglycidyl ethers, p-hydroxybenzoic acid esters, benzophenone-type ultraviolet filters, triclosan, and triclocarban in human urine by liquid chromatography-tandem mass spectrometry. *Journal of Chromatography A*, 1324:141–148. URL `http://www.sciencedirect.com/science/article/pii/S0021967313018025`.

Asimakopoulos, A.G., Elangovan, M., and Kannan, K. (2016). Migration of parabens, bisphenols, benzophenone-type UV filters, triclosan, and triclocarban from teethers and its implications for infant exposure. *Environmental Science & Technology*, 50(24):13539–13547.

Asuero, A.G., Sayago, A., and González, A.G. (2006). The correlation coefficient: An overview. *Critical Reviews in Analytical Chemistry*, 36(1):41–59. URL `https://doi.org/10.1080/10408340500526766`.

Avagyan, R., Sadiktsis, I., Thorsén, G., Östman, C., and Westerholm, R. (2013). Determination of benzothiazole and benzotriazole derivates in tire and clothing textile samples by high performance liquid chromatography-electrospray ionization tandem mass spectrometry. *Journal of Chromatography A*, 1307:119–125. URL http://www.sciencedirect.com/science/article/pii/S0021967313011667.

Avagyan, R., Sadiktsis, I., Bergvall, C., and Westerholm, R. (2014). Tire tread wear particles in ambient air—a previously unknown source of human exposure to the biocide 2-mercaptobenzothiazole. *Environmental Science and Pollution Research*, 21(19):11580–11586.

Bakus, G.J. (2007). *Quantitative Analysis of Marine Biological Communities: Field Biology and Environment*. Wiley. URL https://books.google.no/books?id=2AFarAtWTP0C.

Ballesteros, L.F., Teixeira, J.A., and Mussatto, S.I. (2013). Selection of the solvent and extraction conditions for maximum recovery of antioxidant phenolic compounds from coffee silverskin. *Food and Bioprocess Technology*, 7(5):1322–1332.

Baranowska, I., editor (2016). *Handbook of Trace Analysis*. Springer International Publishing.

Bartlett, J.W. and Frost, C. (2008). Reliability, repeatability and reproducibility: analysis of measurement errors in continuous variables. URL http:https://doi.org/10.1002/uog.5256.

Breedveld, G.D., Roseth, R., Sparrevik, M., Hartnik, T., and Hem, L.J. (2003). Persistence of the de-icing additive benzotriazole at an abandoned airport. *Water, Air and Soil Pollution: Focus*, 3(3):91–101. URL https://doi.org/10.1023/A:1023961213839.

Brownlee, B.G., Carey, J.H., MacInnis, G.A., and Pellizzari, I.T. (1992). Aquatic environmental chemistry of 2-(thiocyanomethylthio)benzothiazole and related benzothiazoles. *Environmental Toxicology and Chemistry*, 11(8):1153–1168.

Cantwell, M.G., Sullivan, J.C., and Burgess, R.M. (2015). *Benzotriazoles: History, Environmental Distribution, and Potential Ecological Effects*, chapter 16, pages 513–545. Elsevier.

Cheng, Y., Lee, S.C., Ho, K.F., Chow, J.C., Watson, J.G., Louie, P.K.K., Cao, J.J., and Hai, X. (2010). Chemically-speciated on-road pm2.5 motor vehicle emission factors in hong kong. *Science of the Total Environment*, 408(7):1621–1627. URL http://www.sciencedirect.com/science/article/pii/S0048969709011760.

Cole, G. (2017). Automotive chassis/suspension materials. In *Reference Module in Materials Science and Materials Engineering*. Elsevier. URL https://www.sciencedirect.com/science/article/pii/B9780128035818019457.

Crosby, C.J., Fullen, M.A., Booth, C.A., and Searle, D.E. (2014). A dynamic approach to urban road deposited sediment pollution monitoring (marylebone road, london, uk). *Journal of Applied Geophysics*, 105:10–20. URL http://www.sciencedirect.com/science/article/pii/S0926985114000755.

Downs, W.R. (1968). Chemically induced ignition in aircraft and spacecraft electrical circuitry by glycol/water solutions. *NASA technical note TN D-4327*. URL https://ntrs.nasa.gov/archive/nasa/casi.ntrs.nasa.gov/19680012744.pdf.

Encyclopædia Britannica (2018). URL https://www.britannica.com/.

Erichsen, E., Schiellerup, H., Gautneb, H., Ottesen, R.T., and Broekmans, M. (2004). Vegstøv i trondheim - en analyse av mineralinnholdet i svevestøvet. resreport 2004.037, NGU. URL http://www.ngu.no/FileArchive/208/2004_037.pdf.

European Commission (2002). Commission decision of 12 august 2002 implementing council directive 96/23/ec concerning the performance of analytical methods and the interpretation of results (2002/657/ec). URL https://publications.europa.eu/en/publication-detail/-/publication/ed928116-a955-4a84-b10a-cf7a82bad858. Retrieved (14.05.2018).

Felis, E., Sochacki, A., and Magiera, S. (2016). Degradation of benzotriazole and benzothiazole in treatment wetlands and by artificial sunlight. *Water Research*, 104:441–448. URL http://www.sciencedirect.com/science/article/pii/S0043135416306376.

Fent, K., Chew, G., Li, J., and Gomez, E. (2014). Benzotriazole uv-stabilizers and benzotriazole: Antiandrogenic activity in vitro and activation of aryl hydrocarbon receptor pathway in zebrafish eleuthero-embryos. *Science of the Total Environment*, 482-483:125–136. URL http://www.sciencedirect.com/science/article/pii/S0048969714002927.

Forsberg, B., Hansson, H.C., Johansson, C., Areskoug, H., Persson, K., and Järvholm, B. (2005). Comparative health impact assessment of local and regional particulate air pollutants in scandinavia. *AMBIO: A Journal of the Human Environment*, 34(1):11–19.

Fuji, H., Yamashita, Y., and Takahashi, K. (2003). Application of titanium and its alloys for automobile parts. Technical Report 88, Nippon steel. URL http://www.nssmc.com/en/tech/report/nsc/pdf/n8815.pdf.

Gunawardana, C., Goonetilleke, A., Egodawatta, P., Dawes, L., and Kokot, S. (2012). Source characterisation of road dust based on chemical and mineralogical composition. *Chemosphere*, 87(2):163–170. URL http://www.sciencedirect.com/science/article/pii/S0045653511013804.

Harris, D.C. (2006). *Quantitative Chemical Analysis*. W. H. Freeman. URL https://www.amazon.com/Quantitative-Chemical-Analysis-Daniel-Harris/dp/0716770415?SubscriptionId=0JYN1NVW651KCA56C102&tag=techkie-20&linkCode=xm2&camp=2025&creative=165953&creativeASIN=0716770415.

Hassan, N.M., Rasmussen, P.E., Dabek-Zlotorzynska, E., Celo, V., and Chen, H. (2007). Analysis of environmental samples using microwave-assisted acid digestion and inductively coupled plasma mass spectrometry: Maximizing total element recoveries. *Water, Air, and Soil Pollution*, 178(1):323–334. URL https://doi.org/10.1007/s11270-006-9201-3.

Herrero, P., Borrull, F., Pocurull, E., and Marcé, R.M. (2014). An overview of analytical methods and occurrence of benzotriazoles, benzothiazoles and benzenesulfonamides in the environment. *TrAC Trends in Analytical Chemistry*, 62:46–55. URL http://www.sciencedirect.com/science/article/pii/S0165993614001630.

Hervé, A. and Williams Lynne, J. (2010). Principal component analysis. *WIREs Comp Stat*, 2(4):433–459. URL https://doi.org/10.1002/wics.101.

Hjortenkrans, D.S.T., Bergbäck, B.G., and Häggerud, A.V. (2007). Metal emissions from brake linings and tires: Case studies of stockholm, sweden 1995/1998 and 2005. *Environ. Sci. Technol.*, 41(15):5224–5230. URL https://doi.org/10.1021/es070198o.

HSDB (2018). Hazardous substances data bank. URL https://toxnet.nlm.nih.gov/newtoxnet/hsdb.htm.

Huntscha, S., Hofstetter, T.B., Schymanski, E.L., Spahr, S., and Hollender, J. (2014). Biotransformation of benzotriazoles: Insights from transformation product identification and compound-specific isotope analysis. *Environ. Sci. Technol.*, 48(8):4435–4443. URL https://doi.org/10.1021/es405694z.

Jafari, H., Akbarzade, K., and Danaee, I. (2014). Corrosion inhibition of carbon steel immersed in a 1m hcl solution using benzothiazole derivatives. *Arabian Journal of Chemistry*. URL http://www.sciencedirect.com/science/article/pii/S1878535214002664.

Kogel, J.E., Trivedi, N.C., Barker, J.M., and Krukowski, S.T. (2006). 59.3.6.1 government deicing. In *Industrial Minerals and Rocks - Commodities, Markets, and Uses (7th Edition)*. Society for Mining, Metallurgy, and Exploration (SME). URL https://app.knovel.com/hotlink/pdf/id:kt008MG3M2/industrial-minerals-rocks/government-deicing.

Kuster, M., López de Alda, M., and Barceló, D. (2009). Liquid chromatography-tandem mass spectrometric analysis and regulatory issues of polar pesticides in natural and treated waters. *Journal of Chromatography A*, 1216(3):520–529. URL http://www.sciencedirect.com/science/article/pii/S0021967308013654.

LaboratoryInfo.com (2018). High performance liquid chromatography (hplc) : Principle, types, instrumentation and applications. URL https://laboratoryinfo.com/hplc/. (Retrieved 08.05.2018).

Leng, G. and Gries, W. (2017). New specific and sensitive biomonitoring methods for chemicals of emerging health relevance. *International Journal of Hygiene and Environmental Health*, 220(2, Part A):113–122. URL http://www.sciencedirect.com/science/article/pii/S1438463916301067.

Li, H., Andrews, G., Zhu, G., Daham, B., Bell, M., Tate, J., Ropkins, K., and Engineers, S. (2005). Impact of ambient temperatures on exhaust thermal characteristics during cold start for real world si car urban driving tests.

Liao, C., Kim, U.J., and Kannan, K. (2018). A review of environmental occurrence, fate, exposure, and toxicity of benzothiazoles. *Environ. Sci. Technol.*, 52(9):5007–5026. URL https://doi.org/10.1021/acs.est.7b05493.

Lin, C.C., Chen, S.J., Huang, K.L., Hwang, W.I., Chang-Chien, G.P., and Lin, W.Y. (2005). Characteristics of metals in nano/ultrafine/fine/coarse particles collected beside a heavily trafficked road. *Environ. Sci. Technol.*, 39(21):8113–8122. URL https://doi.org/10.1021/es048182a.

Liu, W., Xue, J., and Kannan, K. (2017). Occurrence of and exposure to benzothiazoles and benzotriazoles from textiles and infant clothing. *Science of the Total Environment*, 592:91–96. URL http://www.sciencedirect.com/science/article/pii/S0048969717306022.

Llompart, M., Sanchez-Prado, L., Pablo Lamas, J., Garcia-Jares, C., Roca, E., and Dagnac, T. (2013). Hazardous organic chemicals in rubber recycled tire playgrounds and pavers. *Chemosphere*, 90:423–31.

Loi, C.H., Busetti, F., Linge, K.L., and Joll, C.A. (2013). Development of a solid-phase extraction liquid chromatography tandem mass spectrometry method for benzotriazoles and benzothiazoles in wastewater and recycled water. *Journal of Chromatography A*, 1299:48–57. URL http://www.sciencedirect.com/science/article/pii/S0021967313007012.

Lu, J., Mao, H., Li, H., Wang, Q., and Yang, Z. (2017). Occurrence of and human exposure to parabens, benzophenones, benzotriazoles, triclosan and triclocarban in outdoor swimming pool water in changsha, china. *Science of the Total Environment*, 605-606:1064–1069. URL http://www.sciencedirect.com/science/article/pii/S0048969717315395.

Lundanes, E., Reubsaet, L., and Greibrokk, T. (2014). *Chromatography : basic principles, sample preparations and related methods*. Wiley-VCH, Weinheim, Germany.

Lundberg, J. (2018). Non-exhaust pm10 and road dust.

Maceira, A., Marcé, R.M., and Borrull, F. (2018). Occurrence of benzothiazole, benzotriazole and benzenesulfonamide derivates in outdoor air particulate matter samples and human exposure assessment. *Chemosphere*, 193:557–566. URL http://www.sciencedirect.com/science/article/pii/S0045653517318507.

Matti Maricq, M. (2007). Chemical characterization of particulate emissions from diesel engines: A review. *Journal of Aerosol Science*, 38(11):1079–1118. URL http://www.sciencedirect.com/science/article/pii/S0021850207001231.

Matuszewski, B.K., Constanzer, M.L., and Chavez-Eng, C.M. (2003). Strategies for the assessment of matrix effect in quantitative bioanalytical methods based on hplc-ms/ms. *Analytical chemistry*, 75:3019–30.

McMaster, M.C. (2005). *LC/MS : a practical user's guide*. Wiley-Interscience, Hoboken, NJ.

Meier, P.C. and Zünd, R.E. (2005). *Statistical Methods in Analytical Chemistry*. Chemical Analysis: A Series of Monographs on Analytical Chemistry and Its Applications. Wiley. URL https://books.google.no/books?id=Pfnb8fZE6QgC.

Miguel, E.d., Llamas, J.F., Chacón, E., Berg, T., Larssen, S., Røyset, O., and Vadset, M. (1997). Origin and patterns of distribution of trace elements in street dust: Unleaded petrol and urban lead. *Atmospheric Environment*, 31(17):2733–2740. URL http://www.sciencedirect.com/science/article/pii/S1352231097001015.

Mitra, S., editor (2003). *Sample Preparation Techniques in Analytical Chemistry*. John Wiley & Sons. URL https://www.ebook.de/de/product/3606159/mitra_sample_prep_in_analytical_chemistry.html.

Niessen, W.M.A. (2006). *Liquid Chromatography-Mass Spectrometry*. Taylor & Francis Ltd., 3 edition.

Nika, M.C., Bletsou, A.A., Koumaki, E., Noutsopoulos, C., Mamais, D., Stasinakis, A.S., and Thomaidis, N.S. (2017). Chlorination of benzothiazoles and benzotriazoles and transformation products identification by lc-hr-ms/ms. *Journal of hazardous materials*, 323:400–413.

Norwegian Road Departement (2014). Tyres and snow chains. URL https://www.vegvesen.no/en/vehicles/own-and-maintain/tyres-and-snow-chains.

Omstedt, G., Bringfelt, B., and Johansson, C. (2005). A model for vehicle-induced non-tailpipe emissions of particles along swedish roads. *Atmospheric Environment*, 39(33):6088–6097.

Padrón, M., Afonso-Olivares, C., Sosa-Ferrera, Z., and Santana-Rodríguez, J. (2014). Microextraction techniques coupled to liquid chromatography with mass spectrometry for the determination of organic micropollutants in environmental water samples. *Molecules*, 19(7):10320–10349.

Pan, S., Sun, Y., Zhang, G., Li, J., Xie, Q., and Chakraborty, P. (2012). Assessment of 2-(4-morpholinyl) benzothiazole (24mobt) and n-cyclohexyl-2-benzothiazolamine (ncba) as traffic tracers in metropolitan cities of china and india. *Atmospheric Environment*, 56:246–249. URL http://www.sciencedirect.com/science/article/pii/S1352231012002701.

Pant, P. and Harrison, R.M. (2013). Estimation of the contribution of road traffic emissions to particulate matter concentrations from field measurements: A review. *Atmospheric Environment*, 77:78–97. URL http://www.sciencedirect.com/science/article/pii/S1352231013002732.

Per Jonsson, Göran Blomquist, M.G. (2008). Wet dust sampler: technological innovation for sampling particles and salt on road surface. *Transportation research circular.*

Pérez-Fernández, V., Mainero Rocca, L., Tomai, P., Fanali, S., and Gentili, A. (2017). Recent advancements and future trends in environmental analysis: Sample preparation, liquid chromatography and mass spectrometry. *Analytica Chimica Acta*, 983:9–41. URL http://www.sciencedirect.com/science/article/pii/S0003267017307353.

Prošek, T., Thierry, D., Taxén, C., and Maixner, J. (2007). *Effect of Cations on Corrosion of Zinc and Carbon Steel Covered with Chloride Deposits under Atmospheric Conditions*, volume 49.

Ramos, F. (2013). *Liquid Chromatography : Principles, Technology and Applications*. Nova Science Publishers, Inc, Hauppauge, New York. URL http://search.ebscohost.com/login.aspx?direct=true&db=nlebk&AN=591961&site=ehost-live.

Reddy, C.M. and Quinn, J.G. (1997). Environmental chemistry of benzothiazoles derived from rubber. *Environ. Sci. Technol.*, 31(10):2847–2853. URL https://doi.org/10.1021/es970078o.

Schauer, J.J., Lough, G.C., Shafer, M.M., Christensen, W.F., Arndt, M.F., DeMinter, J.T., and Park, J.S. (2006). Characterization of metals emitted from motor vehicles. *Research report (Health Effects Institute)*, pages 1–76; discussion 77–88.

Schmeltz, I. and Hoffmann, D. (1977). Nitrogen-containing compounds in tobacco and tobacco smoke. *Chem. Rev.*, 77(3):295–311. URL https://pubs.acs.org/doi/abs/10.1021/cr60307a001.

Seo, K.W., Park, M., Kim, J.G., Kim, T.W., and Kim, H.J. (2000). Effects of benzothiazole on the xenobiotic metabolizing enzymes and metabolism of acetaminophen. *Journal of Applied Toxicology*, 20(6):427–430.

Shell Oil Co (1976). Windshield cleaner formulation. Patent: US3988264A. URL https://patentimages.storage.googleapis.com/5b/a2/98/8d742fdf37725f/US3988264.pdf. (Retrieved 18.05.18).

Silvestro, L., Tarcomnicu, I., and Rizea, S. (2013). Matrix effects in mass spectrometry combined with separation methods — comparison HPLC, GC and discussion on methods to control these effects. In *Tandem Mass Spectrometry - Molecular Characterization*. InTech.

Skoog, D.A., West, D.M., Holler, F.J., and Crouch, S.R. (2003). *Fundamentals of Analytical Chemistry*. Brooks Cole. URL https://www.amazon.com/Fundamentals-Analytical-Chemistry-CD-ROM-InfoTrac/dp/0030355230?SubscriptionId=0JYN1NVW651KCA56C102&tag=techkie-20&linkCode=xm2&camp=2025&creative=165953&creativeASIN=0030355230.

Snilsberg, B., Uthus, N., Aurstad, J., and Myran, T. (2008). Evaluation of different laboratory methods for simulation of pavement wear and road dust generation. *Road Materials and Pavement Design*, 9:287–304.

Snilsberg, B., Gryteselv, D., and Veivåg, I.L.S. (2017). Road cleaning in tunnel and street, 2017. NPRA reports, Norwegian Public Roads Administration. URL https://www.vegvesen.no/fag/publikasjoner/Publikasjoner/Statens+vegvesens+rapporter/_attachment/2105462?_ts=16069741358&download=true&fast_title=Renholdsfors%C3%B8k+2017%3A+Uttesting+av+ny+spylebom+i+tunnel+og+gate+i+Kristiansund.

Statens Vegvesen (2018). Piggfriandelen høyere enn noensinne. URL https://www.vegvesen.no/om+statens+vegvesen/presse/nyheter/nasjonalt/piggfriandelen-hoyere-enn-noensinne. (Retrieved 21.05.18).

Steene, J.C. and Lambert, W.E. (2008). Comparison of matrix effects in HPLC-MS/MS and UPLC-MS/MS analysis of nine basic pharmaceuticals in surface waters. *Journal of the American Society for Mass Spectrometry*, 19(5):713–718.

Sternbeck, J., Sjödin, k., and Andréasson, K. (2002). Metal emissions from road traffic and the influence of resuspension–results from two tunnel studies. *Atmospheric Environment*, 36(30):4735–4744. URL http://www.sciencedirect.com/science/article/pii/S1352231002005617.

Suarez-Bertoa, R. and Astorga, C. (2018). Impact of cold temperature on euro 6 passenger car emissions. *Environmental Pollution*, 234:318–329. URL http://www.sciencedirect.com/science/article/pii/S0269749117318857.

Taylor, H.E. (2001). *Inductively Coupled Plasma-Mass Spectrometry : Practices and Techniques*. Academic Press, San Diego. URL http://search.ebscohost.com/login.aspx?direct=true&db=e230xww&AN=203246&site=ehost-live.

Technical Resources International Inc. (1997). Summary of data for chemical selection: benzothiazole. URL https://ntp.niehs.nih.gov/ntp/htdocs/chem_background/exsumpdf/benzothiazole_508.pdf. (Retrived 27.05.18).

Thermo Fisher Scientific (2018). Icp-ms sample preparation. URL https://www.thermofisher.com/no/en/home/industrial/spectroscopy-elemental-isotope-analysis/spectroscopy-elemental-isotope-analysis-learning-center/trace-elemental-analysis-tea-information/inductively-coupled-plasma-mass-spectrometry-icp-ms-information/icp-ms-sample-preparation.html. (Retrieved 21.05.18).

Thorpe, A. and Harrison, R.M. (2008). Sources and properties of non-exhaust particulate matter from road traffic: A review. *Science of The Total Environment*, 400(1):270–282. URL http://www.sciencedirect.com/science/article/pii/S004896970800658X.

Trico Products (2016). Windscreen washer additive - safety data sheet, version no: 3.1.1.1. URL http://tricoproducts.com.au/Files/SDS/A.%20Trico%20Additive%20SDS.pdf. (Retrieved 18.05.18).

Umamaheswari, B. and Rajaram, R. (2017). Microaerobic degradation of 2-mercaptobenzothiazole present in industrial wastewater. *Journal of Hazardous Materials*, 321:773–781. URL http://www.sciencedirect.com/science/article/pii/S0304389416308834.

Valotto, G., Zannoni, D., Rampazzo, G., Visin, F., Formenton, G., and Gasparello, A. (2018). Characterization and preliminary risk assessment of road dust collected in venice airport (italy). *Journal of Geochemical Exploration*. URL https://www.sciencedirect.com/science/article/pii/S0375674218301365.

Wang, L., Asimakopoulos, A.G., Moon, H.B., Nakata, H., and Kannan, K. (2013). Benzotriazole, benzothiazole, and benzophenone compounds in indoor dust from the united states and east asian countries. *Environ. Sci. Technol.*, 47(9):4752–4759. URL https://doi.org/10.1021/es305000d.

Wang, L., Zhang, J., Sun, H., and Zhou, Q. (2016). Widespread occurrence of benzotriazoles and benzothiazoles in tap water: Influencing factors and contribution to human exposure. *Environ. Sci. Technol.*, 50(5):2709–2717. URL https://doi.org/10.1021/acs.est.5b06093.

West, D.M., Holler, F.J., Crouch, S.R., and Skoog, D.A. (2014). *Fundamentals of analytical chemistry*. Brooks/Cole Cengage Learning, Boston, 9th ed. edition.

Zdravkovic, S.A. (2017). Solid-phase extraction for the preparation of aqueous sample matrices for gas chromatographic analysis in extractable/leachable studies: Solid-phase extraction has several advantages over liquid/liquid extraction for extractables and leachables studies. *Pharmaceutical Technology*, 41(5):54–60. URL http://search.ebscohost.com/login.aspx?direct=true&db=bth&AN=122877373&site=ehost-live.

Zeng, E.Y., Tran, K., and Young, D. (2004). Evaluation of potential molecular markers for urban stormwater runoff. *Environmental monitoring and assessment*, 90:23–43.

Zhang, J., Zhang, X., Wu, L., Wang, T., Zhao, J., Zhang, Y., Men, Z., and Mao, H. (2018). Occurrence of benzothiazole and its derivates in tire wear, road dust, and roadside soil. *Chemosphere*. URL https://www.sciencedirect.com/science/article/pii/S0045653518304119.

Appendices

Appendix A

Experimental calculations for organic analysis

Table A.1: Weight of chemical used for stock solutions and ppm per standard stock solution.

Chemical	Weight (grams)	ppm
BTR	0.0115	1150
BTH	0.0185	1850
TTR	0.0101	1010
XTR	0.0125	1250
2-NH2-BTH	0.0103	1030
2-S-BTH	0.0105	1050
1-OH-BTR	0.0105	1050
2-Me-S-BTH	0.0203	2030
BTR COOH	0.0101	1010
2-OH-BTH	0.0105	1050
5-Amino-BTR	0.0105	1050
2-M-BTH	0.005	2500
5-Cl-BTR	0.0108	1080

Table A.2: Calculated amount of extracted chemical for making the 10 ppm working solutions, and Me-OH added with pipette

Chemical	μL **extracted**	μL **Me-OH (added with pipette)**
BTR	87	913
BTH	54	946
TTR	99	901
XTR	80	920
2-NH2-BTH	97	903
2-S-BTH	95	905
1-OH-BTR	95	905
2-Me-S-BTH	49	951
BTR COOH	99	901
2-OH-BTH	95	905
5-Amino-BTR	95	905
2-M-BTH	40	960
5-Cl-BTR	93	907

Appendix B

Data tables

Table B.1: Concentrations of benzothiazoles and benzotriazoles in particulates filtered from 50 mL of turbid road dust sample (ng/g)

	Summer					Winter					Prall				
	Median	*Average*	*Min*	*Max*	*n/N**	*Median*	*Average*	*Min*	*Max*	*n/N**	*Median*	*Average*	*Min*	*Max*	*n/N**
BTH	160	160	151	170	2/16	9.45	9.45	9.45	9.45	1/16	-	-	-	-	-
2-S-BTH	13.7	14.3	5.98	35.5	16/16	3.10	2.98	0.82	5.23	15/16	4.82	4.46	3.03	5.54	3/4
2-OH-BTH	438	511	226	1137	16/16	175	181	99.5	262	16/16	106	105	80.3	129	4/4
2-NH2-BTH	21.9	22.7	12.9	40.2	16/16	6.60	6.75	5.01	10.1	16/16	1.84	1.91	1.64	2.25	3/4
2-Me-S-BTH	59.3	68.7	8.27	161	16/16	62.1	60.5	27.4	99.8	16/16	142	135	40.3	216	4/4
2-M-BTH	-	-	-	-	-	0.79	0.85	0.57	1.23	5/16	4.68	4.57	3.77	5.27	3/4
∑ BTHs	508	637	268	1265	16/16	251	252	140	384	16/16	249	249	138	358	4/4
BTR	46.7	49.7	30.1	80.6	16/16	16.3	16.6	11.8	22.7	16/16	9.02	12.0	7.43	19.6	3/4
TTR	268	335	164	1235	16/16	141	141	93.9	221	16/16	27.6	26.9	12.7	39.7	4/4
XTR	7.15	7.15	7.15	7.15	1/16	1.15	2.67	0.86	10.2	6/16	-	-	-	-	-
BTR COOH	37.9	44.2	13.7	128	16/16	3.83	3.72	0.58	6.42	10/16	-	-	-	-	-
5-Cl-BTR	7.91	14.0	3.70	97.1	16/16	4.72	4.31	2.13	6.63	16/16	2.37	2.96	2.10	4.99	4/4
1-OH-BTR	-	-	-	-	-	16.3	16.7	4.53	36.6	14/16	10.5	10.5	5.66	15.4	2/4
5-Amino-BTR	11.5	10.4	4.98	16.7	9/16	1.17	7.10	0.30	29.6	5/16	2.04	2.04	2.04	2.04	1/4
∑ BTRs	407	449	225	1315	16/16	176	181	132	273	16/16	31.7	35.6	20.5	58.7	4/4

	Summer tires		Studded tires		Stud free tires	
	Average	*n/N**	*Average*	*n/N**	*Average*	*n/N**
BTH	6173	2/2	3847	2/2	13807	2/2
2-S-BTH	9541	2/2	5038	2/2	21407	2/2
2-OH-BTH	847	2/2	1243	2/2	2229	2/2
2-NH2-BTH	4.49	2/2	2.50	2/2	3.93	2/2
2-Me-S-BTH	111	2/2	134	2/2	197	2/2
2-M-BTH	2.98	1/2	1.66	1/2	-	-
∑ BTHs	16678	2/2	10265	2/2	37644	2/2
BTR	-	-	-	-	-	-
TTR	-	-	-	-	-	-
XTR	0.90	1/2	0.42	1/2	-	-
BTR COOH	-	-	-	-	-	-
5-Cl-BTR	-	-	-	-	-	-
1-OH-BTR	256	1/2	2169	1/2	4304	1/2
5-Amino-BTR	-	-	-	-	-	-
∑ BTRs	128	2/2	2170	1/2	4304	1/2

*: n is number of detected samples and N is total samples in the set

Table B.2: Concentrations of BTHs and BTRs in liquid phases from filtering of 50 mL turbid road dust sample (ng/L)

	Summer					**Winter**					**Prall**				
	Median	*Average*	*Min*	*Max*	*n/N**	*Median*	*Average*	*Min*	*Max*	*n/N**	*Median*	*Average*	*Min*	*Max*	*n/N**
BTH	23.7	30.4	9.74	66.4	8/17	127	125	40.5	203	9/16	-	-	-	-	-
2-S-BTH	7.44	7.03	4.27	9.72	17/17	4.85	4.89	1.51	9.87	15/16	1.55	1.55	0.92	2.18	2/4
2-OH-BTH	16.3	41.0	4.63	224	8/17	436	398	13.0	885	16/16	96.7	140	21.4	346	4/4
2-NH2-BTH	34.6	42.3	19.5	151	17/17	41.1	45.6	21.4	113.3	16/16	1.88	2.75	1.77	4.62	3/4
2-Me-S-BTH	19.2	22.4	12.0	51.1	9/17	17.9	19.4	5.27	34.0	15/16	3.75	6.06	1.89	14.9	4/4
2-M-BTH	1.33	1.94	0.06	9.19	16/17	2.97	3.18	0.97	6.61	16/16	7.69	7.57	4.74	10.2	4/4
∑ BTHs	78.5	98.0	23.8	470	17/17	525	548	37.8	1194	16/16	113	157	30.9	370	4/4
BTR	19.2	19.9	12.9	36.6	17/17	51.3	50.1	26.0	82.6	16/16	9.70	9.70	9.70	9.70	1/4
TTR	156	195	123	800	17/17	507	485	263	713	16/16	8.89	9.29	2.86	16.5	4/4
XTR	-	-	-	-	-	1.46	13.02	0.68	48.5	4/16	-	-	-	-	-
BTR COOH	8.95	9.74	3.80	17.4	17/17	6.80	8.17	3.82	16.1	16/16	1.72	1.72	1.72	1.72	1/4
5-Cl-BTR	3.13	3.39	0.68	7.70	6/17	2.16	2.16	2.16	2.16	1/16	-	-	-	-	-
1-OH-BTR	4.43	6.68	0.77	22.2	10/17	29.6	33.1	9.28	87.1	16/16	-	-	-	-	-
5-Amino-BTR	-	-	-	-	-	-	-	-	-	-	-	-	-	-	-
∑ BTRs	184	229	148	840	17/17	601	580	307	875	16/16	9.75	12.1	2.86	26.2	4/4

*: n is number of detected samples and N is total samples in the set

Table B.3: Total concentrations of BTHs and BTRs in turbid road dust sample (both particulate and liquid phase) (ng/L)

	Summer					Winter					Prall				
	Median	*Average*	*Min*	*Max*	*n/N**	*Median*	*Average*	*Min*	*Max*	*n/N**	*Median*	*Average*	*Min*	*Max*	*n/N**
BTH	23.7	30.4	9.74	66.4	10/17	127	126	40.5	203	9/16	-	-	-	-	-
2-S-BTH	12.7	12.6	6.79	19.0	17/17	8.83	9.25	1.74	19.4	16/16	3.17	2.88	1.51	3.96	3/4
2-OH-BTH	197	232	26.6	521	17/17	692	729	246	1404	16/16	141	186	55.9	405	4/4
2-NH2-BTH	42.4	52.0	27.0	162	17/17	52.8	59.1	26.9	134	16/16	2.8	3.62	2.52	5.54	3/4
2-Me-S-BTH	35.3	41.2	16.8	116	17/17	125	126	77.4	195	16/16	77.2	65.5	16.8	91.0	4/4
2-M-BTH	1.33	1.94	0.06	9.19	16/17	3.54	3.47	1.74	6.61	16/16	9.4	9.11	5.40	12.3	4/4
∑ BTHs	303	361	93.4	801	17/17	939	1 005	360	1 903	16/16	242	265	82.0	495	4/4
BTR	38.0	41.72	20.8	70.8	17/17	80.1	82.1	43.4	135	16/16	7.96	8.52	3.40	14.2	3/4
TTR	277	335	157	1 240	17/17	759	761	386	1 260	16/16	23.6	20.9	9.12	27.2	4/4
XTR	4.14	4.14	4.14	4.14	1/17	1.88	14.1	1.15	86.3	7/16	-	-	-	-	-
BTR COOH	23.4	27.8	8.95	52.9	17/17	10.4	14.1	4.11	29.2	16/16	1.72	1.72	1.72	1.72	1/4
5-Cl-BTR	4.36	7.17	1.11	37.9	17/17	7.19	8.51	3.41	19.8	16/16	1.01	1.25	0.96	2.02	4/4
1-OH-BTR	4.43	6.7	0.77	22.2	10/17	51.1	67.3	14.5	213	16/16	4.54	4.54	2.82	6.26	2/4
5-Amino-BTR	256	266	92.5	471	9/17	78.8	535	40.2	2 251	5/16	37.7	37.7	37.7	37.7	1/4
∑ BTRs	529	557	191.0	1 308	17/17	977	1 106	473	3 054	16/16	40.7	40.6	33.3	47.8	4/4

	Air filters					Summer tires		Studded tires		Stud free tires		Background sample	Binding Agent
	Median	*Average*	*Min*	*Max*	*n/N**	*Average*	*n/N**	*Average*	*n/N**	*Average*	*n/N**	*Average*	*Average*
BTH	18.1	18.1	18.1	18.1	1/8	129 643	2/2	79 276	2/2	295 745	2/2	-	-
2-S-BTH	2.47	3.26	2.20	5.10	3/8	200 358	2/2	102 809	2/2	458 538	2/2	7.11	52.0
2-OH-BTH	34.7	34.7	7.45	62.1	4/8	17 780	2/2	25 837	2/2	47 749	2/2	-	-
2-NH2-BTH	2.08	2.08	1.78	2.39	2/8	94.2	2/2	51.6	2/2	84.3	2/2	-	-
2-Me-S-BTH	3.37	5.04	2.40	8.03	7/8	2 333	2/2	2 791	2/2	4 214	2/2	3.55	-
2-M-BTH	-	-	-	-	-	62.6	1/2[a]	35.1	1/2[a]	-	-	-	-
∑ BTHs	12.3	25.8	5.49	66.1	8/8	350 239	2/2	210 782	2/2	806 331	2/2	10.7	-
BTR	52.0	349	7.87	1 544	6/8	-	-	-	-	-	-	-	-
TTR	-	-	-	-	-	-	-	-	-	-	-	-	-
XTR	-	-	-	-	-	18.9	1/2[b]	8.51	1/2[b]	-	-	-	-
BTR COOH	-	-	-	-	-	-	-	-	-	-	-	-	-
5-Cl-BTR	-	-	-	-	-	-	-	-	-	-	-	-	-
1-OH-BTR	2.97	2.97	2.97	2.97	1/8	5 369	1/2[a]	44 251	1/2[b]	92 183	1/2[b]	-	-
5-Amino-BTR	-	-	-	-	-	-	-	-	-	-	-	56.4	-
∑ BTRs	53.5	349	7.87	1 544	6/8	2 694	2/2	44 259	1/2	92 183	1/2	56.4	-

*: n is number of detected samples and N is total samples in the set
a: only detected in tires for heavy vehicles
b: only detected in tires for personal vehicles

Table B.4: Concentrations of elements in turbid road dust samples (ng/mL)

	Total					Summer					Winter					Prall				
	Median	*Average*	*min*	*max*	*n/N**	*Median*	*Average*	*min*	*max*	*n/N**	*Median*	*Average*	*min*	*max*	*n/N**	*Median*	*Average*	*min*	*max*	*n/N**
Si	186,995	188,422	64,922	330,623	22/22	96,378	108,131	64,922	190,789	10/10	267,979	268,714	183201	330623	10/10	97,833	97,833	66,586	129,080	2/2
Fe	85,161	117,749	26,309	287,388	22/22	37,926	45,085	26,309	91,898	10/10	184,785	190,413	78,423	287388	10/10	22,571	22,571	15,474	29,668	2/2
Al	82,052	99,781	27,179	223,320	22/22	39,707	45,528	27,179	82,903	10/10	145,219	154,033	81,201	223320	10/10	43,208	43,208	30,076	56,340	2/2
Ca	75,876	100,139	23,519	248,288	22/22	34,282	39,323	23,519	79,987	10/10	155,541	160,955	71,766	248288	10/10	41,276	41,276	33,510	49,042	2/2
Mg	38,742	58,377	10,028	148,694	22/22	15,178	17,647	10,028	33,962	10/10	97,234	99,107	43,523	148694	10/10	10,452	10,452	7,470	13,434	2/2
Cl	20,583	40,829	858	123,265	22/22	1,134	1,146	858	1,364	10/10	81490	80,513	39,802	123,265	10/10	8,157	8,157	8,157	8,157	2/2
Na	19,163	19,540	7,072	36,372	22/22	9,891	10,585	7,072	15,466	10/10	28,486	28,494	22,861	36372	10/10	16,906	16,906	12,808	21,005	2/2
K	11,452	13,482	3,325	30,018	22/22	5,172	5,857	3,325	10,892	10/10	20,471	21,107	12,011	30018	10/10	8,819	8,819	6,091	11,547	2/2
Ti	8,382	10,743	2,552	26,312	22/22	3,753	4,465	,2,552	9,566	10/10	16,092	17,022	7,199	26312	10/10	2,065	2,065	1,404	2,725	2/2
S	3,071	4,565	997	11,304	22/22	1,437	1,639	997	2,811	10/10	7,339	7,490	3,331	11,304	10/10	1,437	1,437	1,320	1,554	2/2
Mn	1,359	1,823	499	4,244	22/22	657	759	499	1,433	10/10	2,843	2,888	1,285	4,244	10/10	420	420	285	555	2/2
P	895	1,296	345	3,305	22/22	555	577	345	968	10/10	1,914	2,014	823	3,305	10/10	323	323	217	430	2/2
Zn	421	582	189	1,246	22/22	295	308	189	441	10/10	900	855	401	1,246	10/10	93.5	93.5	64.8	122	2/2
V	342	448	95.1	1,126	22/22	146	175	95.1	375	10/10	687	720	309	1,126	10/10	69.5	69.5	46.9	92.1	2/2
Ba	340	410	106	927	22/22	161	184	106	342	10/10	641	636	338	927	10/10	251	251	165	337	2/2
Sr	309	392	86.9	1,012	22/22	132	153	86.9	313	10/10	595	631	305	1,012	10/10	228	228	164	292	2/2
Cu	216	255	96.9	516	22/22	135	143	96.9	238	10/10	358	367	195	516	10/10	100	100	76.8	124	2/2
Br	199	404	17.3	1,209	22/22	22.5	23.5	17.3	31.0	10/10	802	785	367	1209	10/10	34.6	34.6	33.3	35.9	2/2
Cr	189	247	63.8	586	22/22	96.5	111.1	63.8	215	10/10	374	382	164	586	10/10	149	149	126	172	2/2
Ni	76.5	101	26.2	224	22/22	38.8	43.7	26.2	79.7	10/10	156	159	73.2	224	10/10	33.7	33.7	28.5	38.9	2/2
Ce	56.6	77.7	16.4	206	22/22	24.0	29.7	16.4	60.4	10/10	116	126	52.9	206	10/10	24.9	24.9	17.3	32.6	2/2
Sc	42.6	49.1	12.5	117	22/22	19.2	22.1	12.5	47.7	10/10	75.0	76.0	37.5	117	10/10	8.34	8.34	5.61	11.1	2/2
Co	40.4	53.0	11.6	117	22/22	18.3	20.6	11.6	40.3	10/10	88.3	85.4	40.5	117	10/10	9.58	9.58	6.95	12.2	2/2
Y	40.0	50.7	12.3	138	22/22	18.7	21.0	12.3	44.8	10/10	75.1	80.5	35.1	138	10/10	9.78	9.78	6.68	12.9	2/2
Rb	33.5	44.2	10.3	108	22/22	16.5	18.2	10.3	32.5	10/10	69.8	70.2	34.5	108	10/10	21.6	21.6	14.9	28.2	2/2
Pb	30.5	46.7	13.8	242	22/22	20.7	42.2	13.8	242	10/10	50.6	51.1	26.2	74.6	10/10	6.22	6.22	4.73	7.72	2/2
Zr	26.7	32.0	9.66	74.6	22/22	12.7	14.8	9.66	26.4	10/10	48.8	49.1	27.1	74.6	10/10	6.38	6.38	4.52	8.24	2/2
La	24.2	33.6	7.04	91.3	22/22	10.3	12.7	7.04	25.5	10/10	49.4	54.5	22.9	91.3	10/10	10.8	10.8	7.45	14.2	2/2
B	22.1	30.2	8.73	67.4	22/22	10.9	10.8	8.73	14.0	10/10	48.4	49.7	30.1	67.4	10/10	5.08	5.08	4.98	5.18	2/2
Ga	21.3	27.2	5.87	66.7	22/22	9.12	10.8	5.87	22.4	10/10	41.8	43.7	20.1	66.7	10/10	8.16	8.16	5.47	10.9	2/2
Nd	18.8	22.8	5.46	53.5	22/22	9.45	11.9	5.46	27.6	10/10	33.5	33.7	13.9	53.5	10/10	10.4	10.4	7.05	13.8	2/2
Li	18.7	30.1	6.23	79.9	22/22	9.13	10.0	6.23	16.7	10/10	47.6	50.1	20.6	79.9	10/10	8.52	8.52	6.24	10.8	2/2
Sn	18.4	19.4	9.13	29.2	22/22	13.6	15.5	9.13	26.6	10/10	25.2	23.4	14.7	29.2	10/10	1.82	1.82	1.16	2.49	2/2
W	15.8	17.8	2.80	34.6	22/22	6.32	6.11	2.80	9.57	10/10	30.5	29.5	21.9	34.6	10/10	1.15	1.15	1.02	1.28	2/2
Sb	11.3	12.6	8.02	39.7	22/22	10.6	13.8	8.02	39.7	10/10	11.3	11.4	8.69	14.0	10/10	0.76	0.76	0.74	0.79	2/2
As	9.37	13.1	2.99	40.1	22/22	4.55	5.54	2.99	10.8	10/10	19.5	20.6	7.59	40.1	10/10	1.52	1.52	1.38	1.66	2/2
Th	8.39	10.5	2.02	25.8	22/22	3.55	4.70	2.02	12.6	10/10	14.1	16.2	6.77	25.8	10/10	4.79	4.79	3.96	5.62	2/2
Dy	7.76	9.51	2.38	24.8	22/22	3.47	4.06	2.38	8.73	10/10	14.1	15.0	6.78	24.8	10/10	1.87	1.87	1.22	2.53	2/2
Sm	7.56	9.42	2.20	24.9	22/22	3.16	3.79	2.20	8.22	10/10	14.7	15.1	6.90	24.9	10/10	2.43	2.43	1.61	3.25	2/2
Gd	7.04	8.91	2.19	23.5	22/22	3.09	3.66	2.19	7.86	10/10	13.3	14.1	6.23	23.5	10/10	1.99	1.99	1.29	2.69	2/2
Pr	6.84	8.75	1.95	22.1	22/22	2.85	3.47	1.95	7.21	10/10	13.6	14.0	6.47	22.1	10/10	2.77	2.77	1.90	3.64	2/2
Mo	6.70	7.77	3.37	17.7	22/22	4.52	4.88	3.37	7.51	10/10	10.8	10.7	4.54	17.7	10/10	1.53	1.53	1.21	1.85	2/2

*: n is number of detected samples and N is total samples in the set

Table B.5: Concentrations of elements in turbid road dust samples (ng/mL) (continued)

	Total					Summer					Winter					Prall				
	Median	*Average*	*min*	*max*	*n/N**	*Median*	*Average*	*min*	*max*	*n/N**	*Median*	*Average*	*min*	*max*	*n/N**	*Median*	*Average*	*min*	*max*	*n/N**
Er	4.56	5.62	1.50	14.7	22/22	2.11	2.41	1.50	5.16	10/10	8.43	8.83	3.96	14.7	10/10	1.09	1.09	0.68	1.50	2/2
Nb	4.18	4.10	1.95	6.67	22/22	2.72	2.97	1.95	4.97	10/10	5.32	5.24	4.17	6.67	10/10	3.24	3.24	2.43	4.06	2/2
Yb	4.05	5.05	1.36	13.2	22/22	1.91	2.15	1.36	4.49	10/10	7.58	7.95	3.61	13.2	10/10	0.99	0.99	0.70	1.28	2/2
Eu	2.06	2.48	0.58	6.61	22/22	0.85	1.03	0.58	2.31	10/10	3.67	3.92	1.81	6.61	10/10	0.51	0.51	0.38	0.64	2/2
U	1.88	2.58	0.56	6.66	22/22	0.98	1.06	0.56	1.90	10/10	3.95	4.09	1.86	6.66	10/10	1.18	1.18	0.88	1.47	2/2
Ho	1.51	1.89	0.49	5.00	22/22	0.68	0.80	0.49	1.72	10/10	2.85	2.99	1.30	5.00	10/10	0.35	0.35	0.22	0.47	2/2
Cs	1.29	1.89	0.43	4.81	22/22	0.68	0.74	0.43	1.21	10/10	2.95	3.04	1.36	4.81	10/10	0.34	0.34	0.29	0.39	2/2
Tb	1.18	1.50	0.37	3.93	22/22	0.54	0.63	0.37	1.32	10/10	2.24	2.37	1.04	3.93	10/10	0.31	0.31	0.22	0.40	2/2
Bi	1.18	1.69	0.48	4.22	22/22	0.76	0.92	0.48	2.13	10/10	2.32	2.47	1.00	4.22	10/10	0.07	0.07	0.07	0.08	2/2
Ge	1.11	1.57	0.07	4.37	16/22	0.41	0.57	0.07	1.41	5/10	1.78	2.07	0.20	4.37	10/10	1.65	1.65	1.65	1.65	1/2
Be	1.07	1.24	0.36	2.94	22/22	0.51	0.60	0.36	1.06	10/10	1.66	1.87	1.08	2.94	10/10	0.47	0.47	0.37	0.58	2/2
Hf	0.98	1.07	0.26	2.25	22/22	0.39	0.50	0.26	0.99	10/10	1.71	1.64	0.96	2.25	10/10	0.31	0.31	0.19	0.43	2/2
Tm	0.64	0.80	0.20	2.06	22/22	0.29	0.34	0.20	0.73	10/10	1.20	1.26	0.56	2.06	10/10	0.15	0.15	0.10	0.21	2/2
Lu	0.58	0.71	0.19	1.84	22/22	0.27	0.30	0.19	0.65	10/10	1.06	1.12	0.50	1.84	10/10	0.14	0.14	0.11	0.18	2/2
Cd	0.24	0.31	0.09	0.75	22/22	0.13	0.15	0.09	0.27	10/10	0.45	0.47	0.22	0.75	10/10	0.05	0.05	0.03	0.07	2/2
Tl	0.24	0.32	0.08	0.73	22/22	0.12	0.13	0.08	0.22	10/10	0.50	0.50	0.26	0.73	10/10	0.14	0.14	0.10	0.18	2/2
Ta	0.13	0.13	0.05	0.19	22/22	0.13	0.13	0.11	0.17	10/10	0.13	0.12	0.05	0.19	10/10	0.19	0.19	0.18	0.20	2/2
In	0.08	0.12	0.02	0.34	22/22	0.04	0.05	0.02	0.11	10/10	0.18	0.19	0.08	0.34	10/10	0.02	0.02	0.01	0.02	2/2
Hg	0.05	0.11	0.02	0.29	21/22	0.03	0.03	0.02	0.05	9/10	0.18	0.17	0.04	0.29	10/10	0.01	0.01	0.01	0.02	2/2

Elements with RSD% above 25% - Concentration set as < QL

Ag	< 0.12
Au	< 0.0012
Ir	< 0.003
Pt	< 0.0.006
Se	< 0.3

*: n is number of detected samples and N is total samples in the set

Table B.6: Concentrations of selected elements with RSD% $< 25\%$, in air filters (ng/mL)

	$PM_{2.5}$	PM^{a}_{coarse}	Volatile $PM_{2.5}$	Volatile PM_{coarse}
Al	135	579	1,315	1,662
As	0.67	0.72	<QL	0.68
Ba	36.9	55.3	154	117
Ca	453	4 290	1,531	3,534
Cd	0.16	<QL	0.13	0.18
Ce	0.08	0.82	0.18	0.41
Co	0.11	1.51	1.94	2.46
Cr	0.97	3.01	1.51	3.25
Cs	0.02	0.02	0.02	0.03
Cu	17.1	222	15.6	155
Fe	69.5	863	144	744
Hg	0.50	0.29	0.36	0.35
K	807	1,070	3,719	3,945
Li	0.07	0.50	0.60	0.86
Mg	89.5	814	276	670
Mn	4.40	60.2	5.58	38.4
Na	1,953	3,971	7,381	9,023
Ni	1.36	3.75	1.30	3.60
P	42.9	131	29.4	103
Pb	1.90	6.08	1.07	1.94
S	1,511	1,385	970	1,152
Sb	1.34	2.34	2.49	3.22
Si	n.d	478*	252	651
Sn	1.17	1.88	0.35	1.35
Sr	2.60	14.3	9.25	15.9
Ti	1.33	8.91	<QL	3.28
V	0.76	2.04	0.85	1.60
W	0.06	0.10	0.06	0.06
Zn	169	340	1,107	1,223

a: particles between $PM_{2.5}$ and PM_{10}
*: Detected in 1 of 2 samples

Table B.7: Concentration of elements in the background soil sample (ng/g)

Al	23,860	**Zr**	15.7	**U**	0.98	**Sb**	0.02
Fe	20,216	**Pb**	14.9	**As**	0.97	**W**	0.01
Ca	7,646	**La**	13.1	**Ag**	0.59	**Ta**	0.002
Mg	7,322	**Li**	11.7	**Eu**	0.59	**Au**	0.001
K	4,573	**Y**	11.0	**Be**	0.45	**Ir**	0.0004
Si	2,757	**Cu**	10.1	**Ho**	0.42	**Pt**	n.d
Ti	1,068	**Sc**	10.1	**Hf**	0.40		
Na	435	**Ga**	7.71	**Se**	0.37		
P	358	**Co**	5.86	**Sn**	0.34		
S	329	**Br**	4.80	**Tb**	0.34		
Mn	267	**Nd**	4.50	**Tl**	0.19		
Ba	116	**B**	3.57	**Tm**	0.19		
Cr	82.8	**Th**	2.87	**Lu**	0.18		
Cl	80.4	**Pr**	2.82	**Bi**	0.16		
V	63.3	**Sm**	2.52	**Mo**	0.15		
Sr	40.9	**Gd**	2.10	**Ge**	0.14		
Rb	29.7	**Dy**	2.08	**Nb**	0.14		
Ce	29.4	**Cs**	1.85	**Cd**	0.08		
Zn	24.1	**Er**	1.27	**Hg**	0.05		
Ni	19.8	**Yb**	1.24	**In**	0.03		

Table B.8: Concentrations of elements in filtered road dust samples (ng/mL), all RSD% $< 25\%$

	Total (N = 23)			Summer (N = 12)			Winter (N = 11)			Prall (N = 2)		
	Median	*min*	*max*	*Median*	*min*	*max*	*Median*	*min*	*max*	*Median*	*min*	*max*
Ca	9,908	5,347	17,931	7,589	5,347	9,908	16,098	12,585	17,931	19,708	19,669	19,746
Cl	1,122	748	103,361	970	748	1,122	72,844	38,989	103,361	7,817	7,696	7,938
Mg	445	301	27,634	416	301	445	17,811	9,690	27,634	910	887	933
Si	445	229	916	382	229	445	833	559	916	969	923	1,015
K	341	184	1,956	272	184	341	1,352	792	1,956	678	638	719
Na	270	144	14,907	186	144	270	13,947	7,846	14,907	4,181	4,143	4,218
Br	208	1.07	1,189	2.82	1.07	4.79	787	412	1,189	30.7	27.8	33.7
S	152	81.1	994	97.7	81.1	152	789	483	994	785	777	793
Ba	19.0	15.1	38.5	17.6	15.1	19.8	26.9	15.8	38.5	3.88	3.69	4.07
Al	17.4	3.57	93.1	4.22	3.57	17.4	57.8	34.6	93.1	81.1	77.0	85.1
Sr	15.3	9.10	30.4	12.8	9.10	15.3	25.9	18.3	30.4	42.4	42.3	42.5
P	9.21	3.46	15.2	10.5	9.21	15.2	4.07	3.46	4.50	4.33	4.20	4.47
B	5.94	4.30	38.5	5.00	4.30	5.94	27.6	18.2	38.5	3.71	3.62	3.79
Mn	4.51	0.25	36.5	2.68	0.25	4.71	11.4	3.98	36.5	3.74	3.21	4.28
Zn	4.26	0.60	37.6	30.1	4.26	37.6	0.96	0.60	1.67	3.11	2.75	3.47
Fe	3.51	1.50	6.17	3.06	1.50	3.51	4.80	3.96	6.17	30.5	30.0	31.1
Sn	3.05	1.56	7.56	2.20	1.56	4.80	3.55	2.70	7.56	0.61	0.12	1.11
Cu	2.83	1.24	3.50	3.22	2.83	3.50	1.71	1.24	2.05	13.0	12.9	13.1
Rb	0.77	0.42	3.08	0.64	0.42	0.77	2.24	1.43	3.08	0.95	0.83	1.08
Sb	0.60	0.48	1.41	0.52	0.48	0.73	0.86	0.50	1.41	0.06	0.05	0.06
Li	0.45	0.23	1.71	0.33	0.23	0.45	1.28	0.72	1.71	0.33	0.32	0.34
W	0.42	0.09	6.68	0.20	0.09	0.42	4.35	3.50	6.68	0.05	0.04	0.06
Mo	0.38	0.28	1.45	0.34	0.28	0.39	0.73	0.38	1.45	0.12	0.12	0.13
Ni	0.34	0.09	1.23	0.93	0.31	1.23	0.25	0.09	0.35	1.46	1.31	1.62
V	0.19	0.12	0.34	0.17	0.13	0.34	0.19	0.12	0.23	0.14	0.14	0.15
As	0.15	0.07	0.29	0.13	0.07	0.29	0.16	0.13	0.20	0.12	0.11	0.13
Cr	0.11	0.02	0.50	0.13	0.07	0.50	0.10	0.02	0.31	1.52	1.43	1.62

Table B.9: Quantification levels (QL) and RSD% for elements analysed with ICP-MS in different matrices (ng/mL)

Element	QL (turbid)	RSD%	QL (filtered)	RSD%	QL (air filters)	RSD%
Ag	0.12	43.2	0.02	114	0.14	51.3
Al	1.2	2.18	0.2	1.93	1.4	2.64
As	0.15	11.8	0.025	18.4	0.175	22.7
Au	0.0012	26.9	0.0002	23.2	0.0014	12.7
B	0.3	2.75	0.05	2.49	0.35	3.23
Ba	0.078	1.90	0.013	2.60	0.091	3.31
Be	0.012	11.6	0.002	70.3	0.014	58.4
Bi	0.006	3.25	0.001	39.5	0.007	7.31
Br	18	13.7	3	13.4	21	28.1
Ca	12	1.91	2	2.42	14	4.29
Cd	0.012	13.2	0.002	35.6	0.014	18.9
Ce	0.0012	1.69	0.0002	18.4	0.0014	8.22
Cl	600	3.86	100	2.82	700	2.61
Co	0.024	2.44	0.004	15.9	0.028	12.1
Cr	0.03	1.90	0.005	16.8	0.035	9.36
Cs	0.003	3.09	0.0005	8.83	0.0035	10.0
Cu	0.18	2.02	0.03	3.65	0.21	3.25
Dy	0.012	2.28	0.002	59.7	0.014	35.2
Er	0.0018	3.00	0.0003	82.8	0.0021	34.7
Eu	0.012	3.82	0.002	44.7	0.014	24.0
Fe	0.12	1.44	0.02	3.61	0.14	3.53
Ga	0.042	3.40	0.007	27.6	0.049	38.6
Gd	0.3	3.08	0.05	30.3	0.35	27.0
Ge	0.12	22.5	0.02	26.2	0.14	30.1
Hf	0.006	6.29	0.001	110	0.007	58.7
Hg	0.006	5.83	0.001	12.5	0.007	3.71
Ho	0.0012	2.58	0.0002	42.7	0.0014	44.3
In	0.003	13.9	0.0005	1689	0.0035	67.0
Ir	0.003	62.9	0.0005	90.9	0.0035	92.0
K	30	4.07	5	3.39	35	3.67
La	0.012	1.67	0.002	17.8	0.014	11.9
Li	0.18	2.13	0.03	2.81	0.21	5.87
Lu	0.0012	4.18	0.0002	92.2	0.0014	75.4
Mg	0.6	2.19	0.1	2.43	0.7	3.11
Mn	0.036	1.57	0.006	2.68	0.042	4.26
Mo	0.12	7.36	0.02	11.0	0.14	27.3
Na	60	2.20	10	3.16	70	3.60
Nb	0.15	2.56	0.025	38.8	0.175	26.9
Nd	0.0012	2.69	0.0002	53.4	0.0014	27.2
Ni	0.09	2.53	0.015	12.3	0.105	11.4
P	2.4	2.02	0.4	3.14	2.8	3.59
Pb	0.012	1.98	0.002	9.88	0.014	3.27
Pr	0.0018	1.93	0.0003	40.3	0.0021	13.1
Pt	0.006	43.0	0.001	74.6	0.007	62.2
Rb	0.072	2.69	0.012	4.22	0.084	10.5
S	120	2.76	20	2.76	140	4.30
Sb	0.012	4.07	0.002	7.84	0.014	4.61
Sc	0.024	2.72	0.004	27.7	0.028	28.0
Se	0.3	389	0.05	458	0.35	265
Si	24	1.87	4	1.70	28	2.75
Sm	0.003	2.98	0.0005	77.3	0.0035	47.2
Sn	0.006	2.41	0.001	2.48	0.007	7.77
Sr	0.15	1.83	0.025	2.26	0.175	4.13
Ta	0.0012	14.9	0.0002	67.2	0.0014	93.3
Tb	0.0012	2.75	0.0002	81.2	0.0014	21.2
Th	0.003	1.84	0.0005	55.7	0.0035	26.2
Ti	0.12	1.58	0.02	34.1	0.14	17.3
Tl	0.0015	7.53	0.00025	21.3	0.00175	14.7
Tm	0.003	3.53	0.0005	104.9	0.0035	44.8
U	0.0015	2.43	0.00025	8.74	0.00175	12.7
V	0.018	1.92	0.003	8.37	0.021	10.1
W	0.006	4.01	0.001	4.03	0.007	16.6
Y	0.0024	1.94	0.0004	12.3	0.0028	6.86
Yb	0.0024	3.57	0.0004	94.8	0.0028	45.9
Zn	0.24	2.34	0.04	7.82	0.175	3.65
Zr	0.003	5.84	0.0005	25.5	0.28	20.5

Appendix C

Correlations

Table C.1: Correlations between log concentration (ng/mL) of benzothiazoles and benzotriazoles in summer, winter and total (sum of both seasons) samples ($p < 0.01$)

	BTH			2-S-BTH			2-OH-BTH			2-NH2-BTH			2-Me-S-BTH			2-M-BTH		
	Total	*Summer*	*Winter*	*Total*	*Summer*	*Winter*	*Total*	*Summer*	*Winter*	*Total*	*Summer*	*Winter*	*Total*	*Summer*	*Winter*	*Total*	*Summer*	*Winter*
2-OH-BTH	0.70				0.67													
2-NH2-BTH				0.41*	0.62	0.54*	0.42*	0.67										
2-Me-S-BTH	0.70						0.86	0.75	0.52*	0.44	0.57*	0.71						
2-M-BTH	0.54*						0.50			0.63	0.75	0.80	0.60		0.56*			
BTR	0.74				0.61		0.82	0.83		0.66	0.76	0.84	0.86	0.70	0.74	0.66	0.54*	0.7
TTR	0.78						0.71			0.43*		0.84	0.73		0.79	0.54		0.7
BTR COOH				0.56	0.68			0.87		0.55	0.70	0.88		0.62	0.55*			0.7
5-Cl-BTR	0.50*					0.54*	0.48			0.58	0.54*	0.68	0.54	0.52*		0.58	0.51*	0.6
1-OH-BTR	0.63						0.70			0.42*		0.79	0.71		0.72	0.40*		0.6
5-Amino-BTR	-0.72*																	

	BTR			TTR			BTR COOH			5-Cl-BTR		
	Total	*Summer*	*Winter*	*Total*	*Summer*	*Winter*	*Total*	*Summer*	*Winter*	*Total*	*Summer*	*Winter*
TTR	0.85		0.99									
BTR COOH		0.89	0.88		0.50*	0.85						
5-Cl-BTR	0.62	0.59*	0.61*	0.38*		0.59*			0.75			
1-OH-BTR	0.74		0.94	0.86		0.93			0.84			0.65

*. $p < 0.05$

Table C.2: Correlations between log concentration (ng/g) of BTHs and BTRs in particulate in summer, winter and total (sum of both seasons) samples ($p < 0.01$)

	2-S-BTH			2-OH-BTH			2-NH2-BTH			2-Me-S-BTH		
	Total	*Summer*	*Winter*	*Total*	*Summer*	*Winter*	*Total*	*Summer*	*Winter*	*Total*	*Summer*	*Winter*
2-OH-BTH	0.88	0.57*	0.75									
2-NH2-BTH	0.87		0.64*	0.94	0.93							
2-Me-S-BTH		0.55*	0.75		0.56*	0.91						
BTR	0.84			0.96	0.90	0.8	0.96	0.90				0.83
TTR	0.75		0.65*	0.76		0.75	0.72		0.72			0.77
BTR COOH	0.82	0.53*		0.83	0.86		0.90	0.80				
5-Cl-BTR	0.54			0.71	0.53*		0.71	0.65				
1-OH-BTR												
5-Amino-BTR	0.61*						0.55*					

	BTR			TTR			BTR COOH		
	Total	*Summer*	*Winter*	*Total*	*Summer*	*Winter*	*Total*	*Summer*	*Winter*
TTR	0.78		0.81						
BTR COOH	0.86	0.79		0.64					
5-Cl-BTR	0.70	0.61*		0.48			0.59		
5-Amino-BTR	0.56*						0.72*		

*. p ¡ 0.05

Table C.3: Correlations between log total concentration (ng/mL) of BTHs/BTRs (liquid and particulate phase) and all elements in summer and winter season ($p < 0.01$)

	Si	Fe	Al	Ca	Mg	Cl	Na	K	Ti	S	Mn	P	Zn	V	Ba	Sr	Cu	Br	Cr	Ni
BTH	0.74	0.77	0.77	0.76	0.77	0.70*	0.71*	0.76	0.78	0.75	0.77	0.76	0.78	0.77	0.76	0.75	0.78	0.72*	0.78	0.77
2-OH-BTH	0.82	0.83	0.82	0.84	0.82	0.78	0.77	0.82	0.83	0.84	0.84	0.81	0.76	0.83	0.82	0.84	0.80	0.80	0.81	0.82
2-NH2-BTH	0.52*	0.54*	0.53*	0.50*	0.52*			0.52*	0.55*		0.52*	0.53*	0.63	0.53*	0.53*		0.59*		0.56*	0.54*
2-Me-S-BTH	0.90	0.90	0.89	0.90	0.90	0.83	0.88	0.90	0.90	0.91	0.90	0.87	0.85	0.90	0.90	0.90	0.88	0.87	0.88	0.90
2-M-BTH	0.73	0.71	0.71	0.68	0.70	0.55*	0.71	0.71	0.72	0.67	0.70	0.65	0.72	0.71	0.72	0.69	0.71	0.61*	0.71	0.72
BTR	0.92	0.95	0.95	0.94	0.94	0.80	0.89	0.93	0.95	0.93	0.95	0.93	0.96	0.94	0.94	0.93	0.96	0.84	0.95	0.94
TTR	0.60*	0.66	0.65	0.67	0.68	0.71	0.62*	0.64	0.65	0.67	0.68	0.63	0.70	0.65	0.64	0.65	0.66	0.72	0.67	0.66
BTR COOH						-0.58*												-0.54*		
5-Cl-BTR	0.50*		0.50*						0.53*					0.50*			0.54*		0.50*	
1-OH-BTR	0.78	0.82	0.82	0.82	0.87	0.94	0.87	0.83	0.78	0.88	0.84	0.81	0.84	0.80	0.82	0.81	0.80	0.94	0.79	0.84

	Ce	Sc	Co	Y	Rb	Pb	Zr	La	B	Ga	Nd	Li	Sn	W	As	Th	Dy	Sm	Gd	Pr
BTH	0.77	0.76	0.76	0.77	0.77		0.72*	0.77	0.74	0.77	0.79	0.79	0.71*	0.63*	0.80	0.71*	0.77	0.76	0.77	0.76
2-OH-BTH	0.84	0.84	0.83	0.84	0.81		0.83	0.83	0.81	0.83	0.78	0.80	0.52*	0.82	0.84	0.81	0.84	0.85	0.84	0.85
2-NH2-BTH	0.53*	0.53*	0.51*	0.50*	0.54*			0.54*		0.52*	0.66	0.54*	0.64		0.55*	0.61*	0.52*	0.52*	0.52*	0.52*
2-Me-S-BTH	0.89	0.90	0.90	0.90	0.90		0.88	0.89	0.88	0.91	0.84	0.88	0.63	0.89	0.86	0.84	0.90	0.90	0.90	0.90
2-M-BTH	0.73	0.70	0.71	0.68	0.70		0.66	0.72	0.59*	0.71	0.75	0.68		0.69	0.68	0.71	0.69	0.71	0.70	0.72
BTR	0.94	0.94	0.93	0.94	0.94		0.93	0.95	0.89	0.94	0.94	0.94	0.73	0.82	0.93	0.87	0.94	0.94	0.94	0.94
TTR	0.66	0.63	0.65	0.65	0.64		0.67	0.66	0.72	0.64	0.57*	0.69		0.57*	0.69	0.56*	0.64	0.65	0.66	0.66
BTR COOH														-0.56*						
5-Cl-BTR	0.52*	0.52*						0.52*		0.50*	0.65		0.52*		0.51*	0.71	0.51*	0.52*	0.50*	0.51*
1-OH-BTR	0.80	0.77	0.83	0.79	0.84	0.86	0.82	0.81	0.92	0.81	0.65*	0.88	0.67*	0.83	0.78	0.84	0.78	0.79	0.79	0.80

	Mo	Er	Nb	Yb	Eu	U	Ho	Cs	Tb	Bi	Ge	Be	Hf	Se	Tm	Lu	Cd	Tl	Ag	Ta
BTH	0.80	0.77		0.77	0.76	0.77	0.77	0.79	0.77	0.74		0.79	0.69*		0.78	0.77	0.76	0.78		-0.75
2-OH-BTH	0.65	0.84	0.76	0.84	0.84	0.82	0.84	0.79	0.84			0.79	0.84	0.73	0.84	0.84	0.80	0.81	0.67	
2-NH2-BTH	0.64	0.50*		0.50*	0.51*	0.55*	0.51*	0.54*	0.51*			0.53*			0.50*	0.51*	0.65	0.52*		
2-Me-S-BTH	0.77	0.90	0.83	0.90	0.90	0.87	0.90	0.87	0.90	0.59*		0.87	0.88	0.81	0.91	0.91	0.87	0.89	0.63	
2-M-BTH	0.70	0.68	0.58*	0.68	0.70	0.64*	0.70	0.68	0.70	0.53*		0.70	0.69		0.69	0.69	0.77	0.69	0.63*	
BTR	0.93	0.94	0.71	0.94	0.94	0.93	0.94	0.95	0.94	0.76	0.62*	0.94	0.91	0.61*	0.94	0.95	0.97	0.93	0.65	-0.53*
TTR	0.61*	0.66		0.67	0.65	0.63	0.66	0.67	0.65	0.59*		0.67	0.63		0.65	0.66	0.72	0.66		
BTR COOH			-0.50*																	
5-Cl-BTR					0.50*	0.56*	0.50*		0.51*					0.67*		0.51*	0.60*		0.58*	
1-OH-BTR	0.73	0.79	0.58*	0.80	0.77	0.82	0.79	0.86	0.79	0.64*		0.80	0.77		0.79	0.79	0.80	0.86		

	In	Hg	Au	Pt	Ir
BTH	0.69*			0.65*	
2-OH-BTH	0.83	0.60*	0.61*		0.77
2-NH2-BTH				0.63*	
2-Me-S-BTH	0.84	0.63	0.63	0.52*	0.73
2-M-BTH	0.64	0.42		0.56*	
BTR	0.92	0.73	0.71	0.65	0.69
TTR	0.67	0.66	0.67	0.57*	0.60*
BTR COOH					
5-Cl-BTR				0.57*	
1-OH-BTR	0.71	0.90	0.77		0.67*

*. p ¡ 0.05

Appendix D

Boxplots

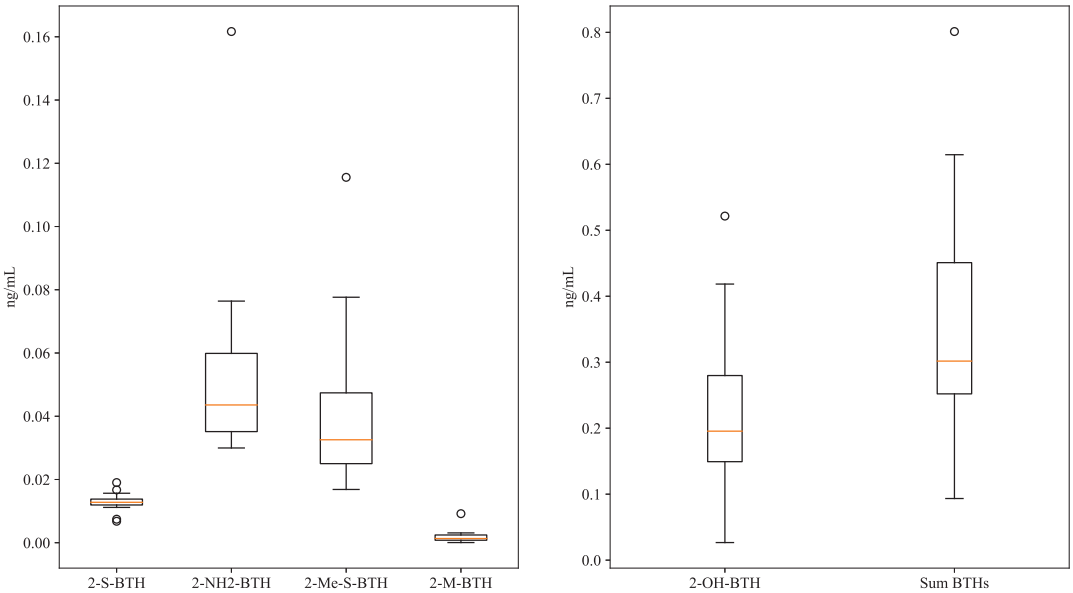

Figure D.1: Boxplot of concentrations of benzothiazoles in summer samples

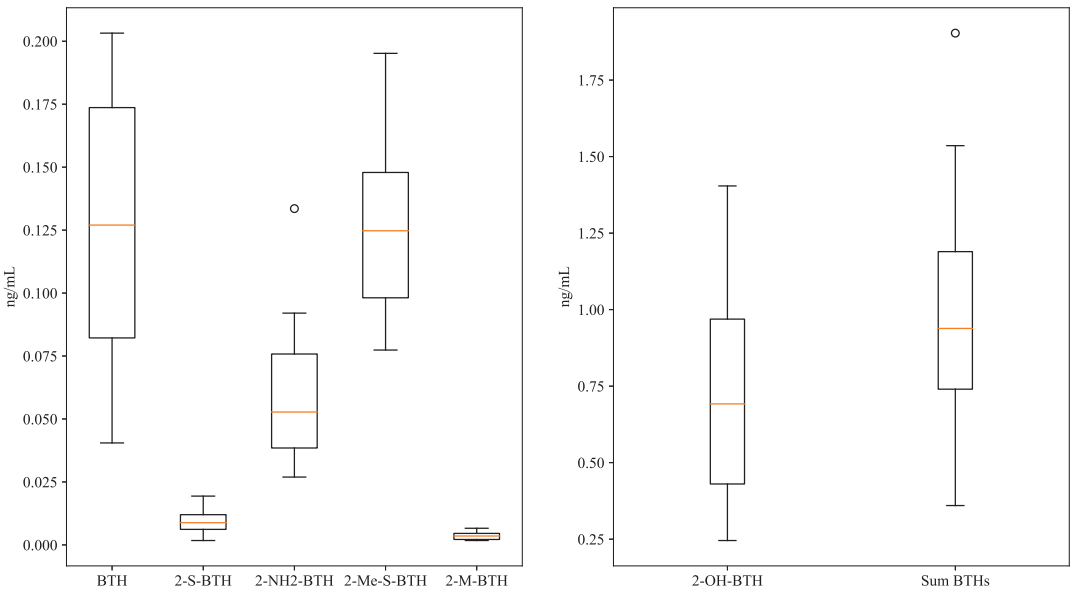

Figure D.2: Boxplot of concentrations of benzothiazoles in winter samples

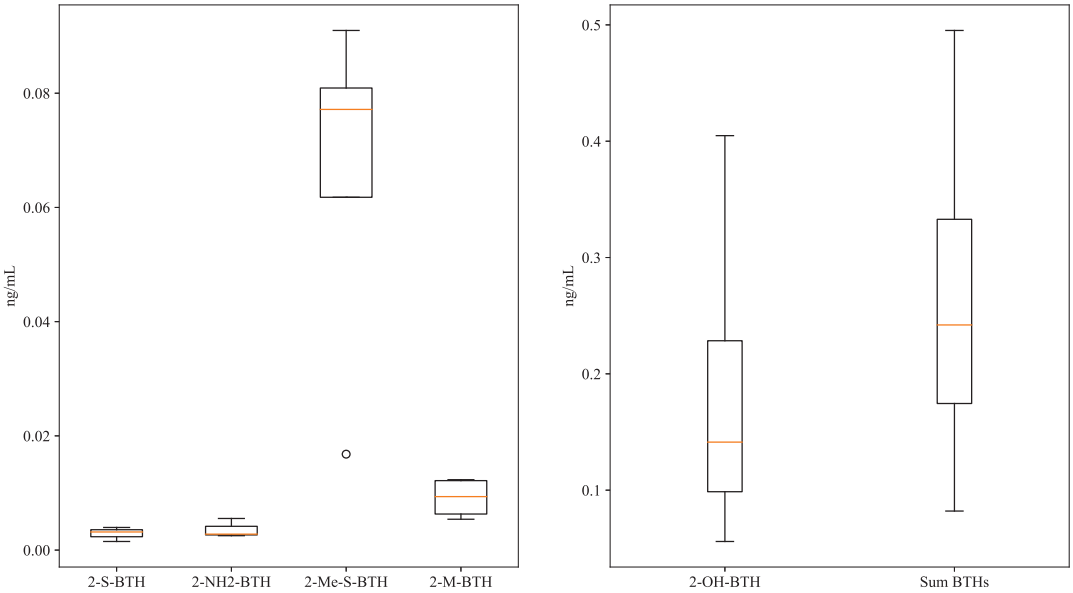

Figure D.3: Boxplot of concentrations of benzothiazoles in prall samples

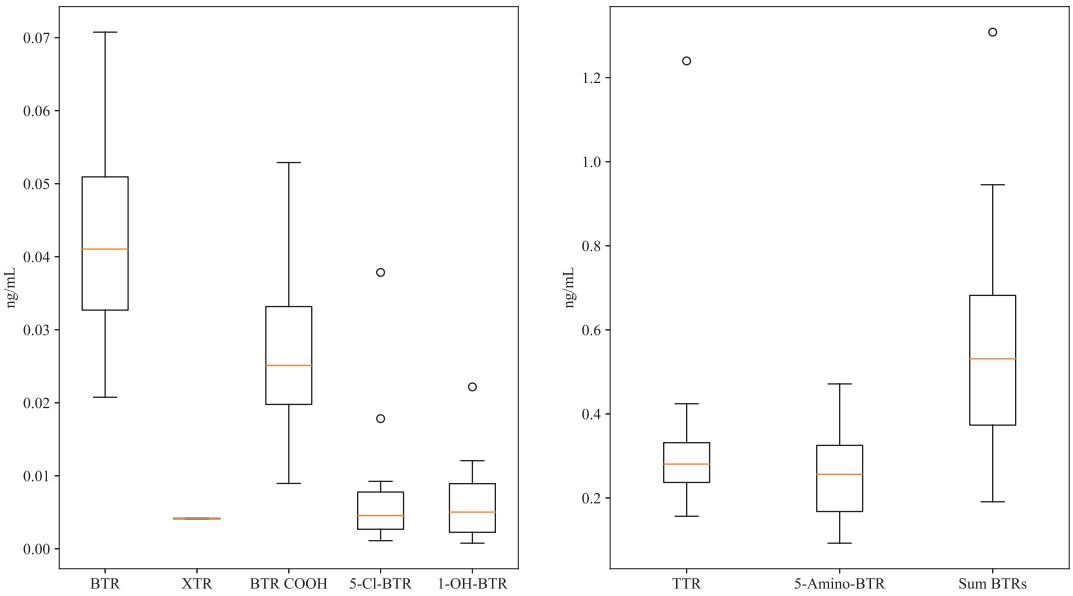

Figure D.4: Boxplot of concentrations of benzotriazoles in summer samples

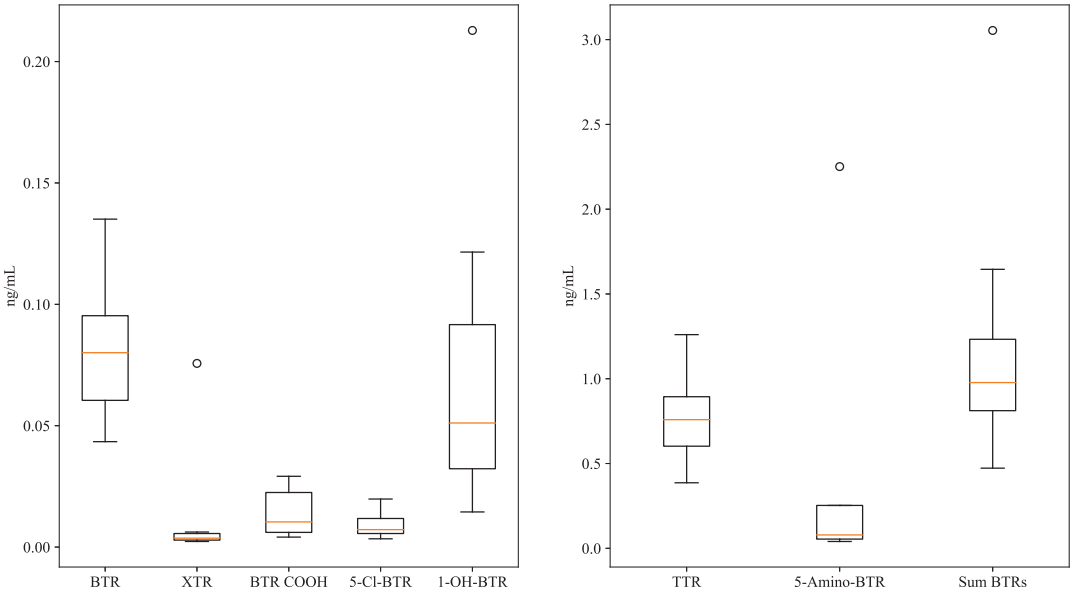

Figure D.5: Boxplot of concentrations of benzotriazoles in winter samples

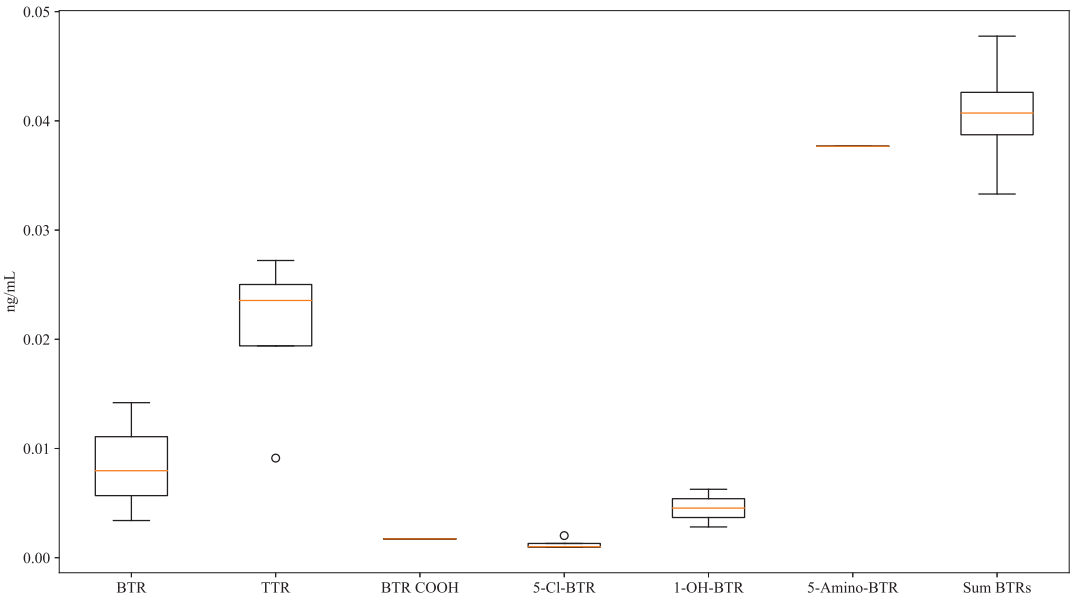

Figure D.6: Boxplot of concentrations of benzotriazoles in prall samples

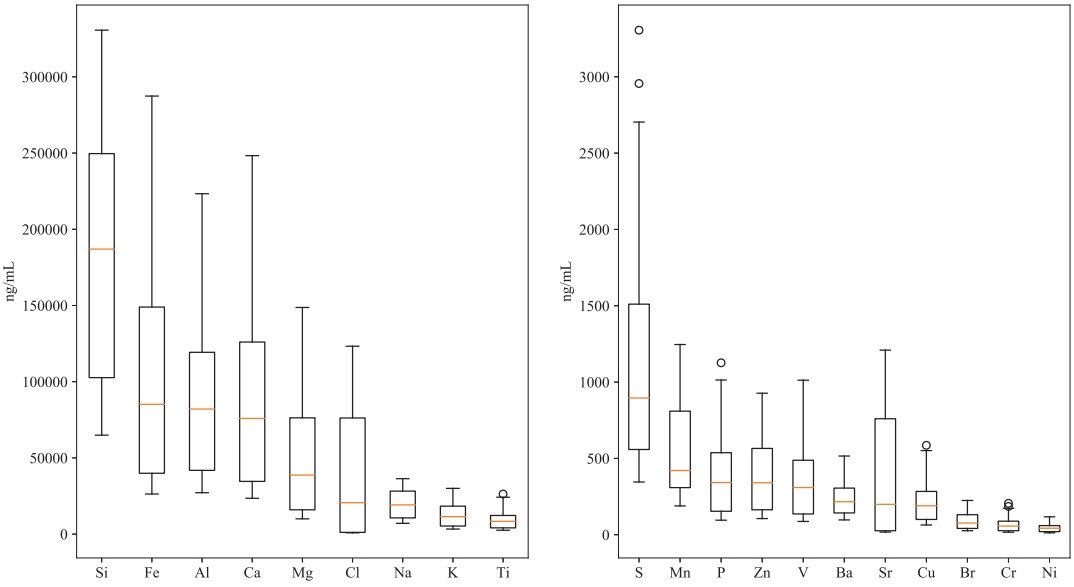

Figure D.7: Boxplot of concentrations of metals in summer and winter samples

Appendix E

MS/MS Fragmentation under Positive Ionization Mode

BTH – *Benzothiazole*

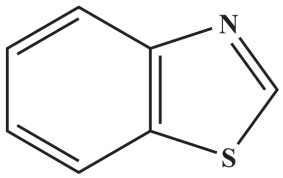

Benzothiazole

Compound	Formula/Mass		Parent m/z	Cone Voltage (V)	Daughters	Collision Energy (eV)	Ion Mode
BTH	C7H5NS	1	135.98	44	108.98	28	ES+
		4	135.98	44	64.98	22	ES+

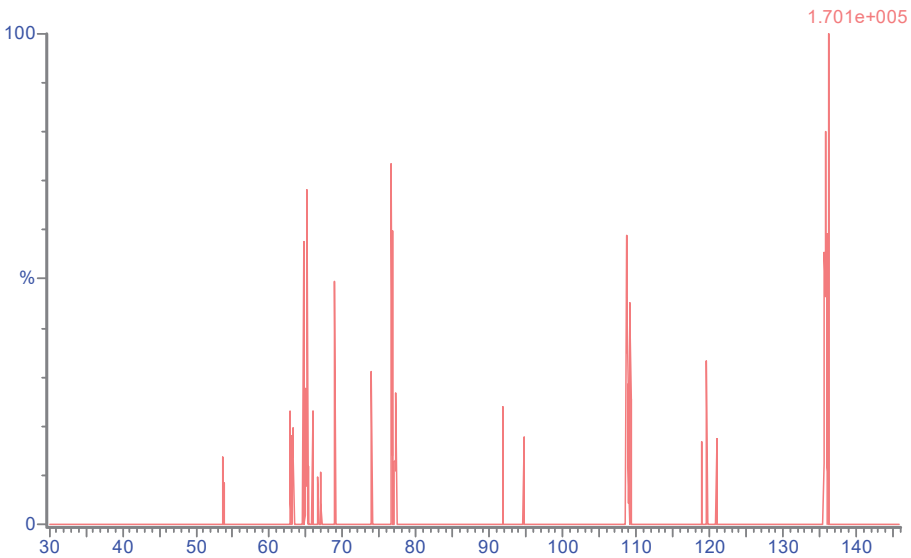

Optimized Daughter Spectrum (at Collision Energy 22eV)

2-S-BTH - *2-Mercaptobenzothiazole*

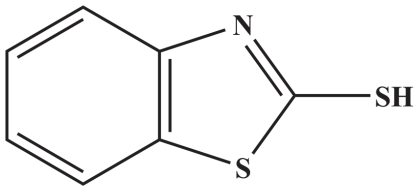

2-Mercaptobenzothiazole

Compound	Formula/Mass		Parent m/z	Cone Voltage (V)	Daughters	Collision Energy (eV)	Ion Mode
2-S-BTH	C7H5NS2	1	167.95	2	135.03	20	ES+
		3	167.95	2	92.00	20	ES+

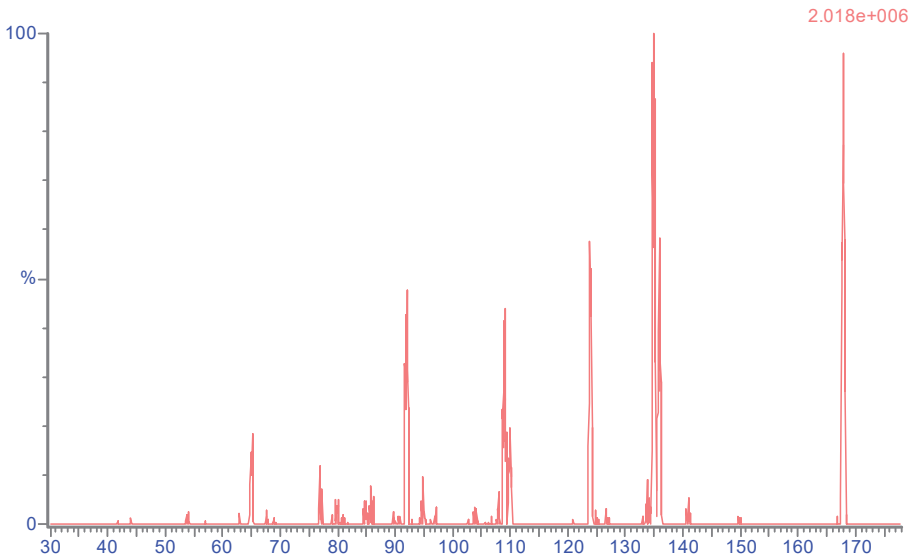

Optimized Daughter Spectrum (at Collision Energy 20eV)

2-OH-BTH - *2-Hydroxybenzothiazole*

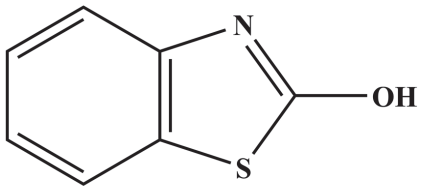

2-Hydroxybenzothiazole

Compound	Formula/Mass		Parent m/z	Cone Voltage (V)	Daughters	Collision Energy (eV)	Ion Mode
2-OH-BTH	C7H5NOS	1	151.98	2	92.01	16	ES+
		2	151.98	2	123.93	16	ES+
		3	151.98	2	79.99	22	ES+

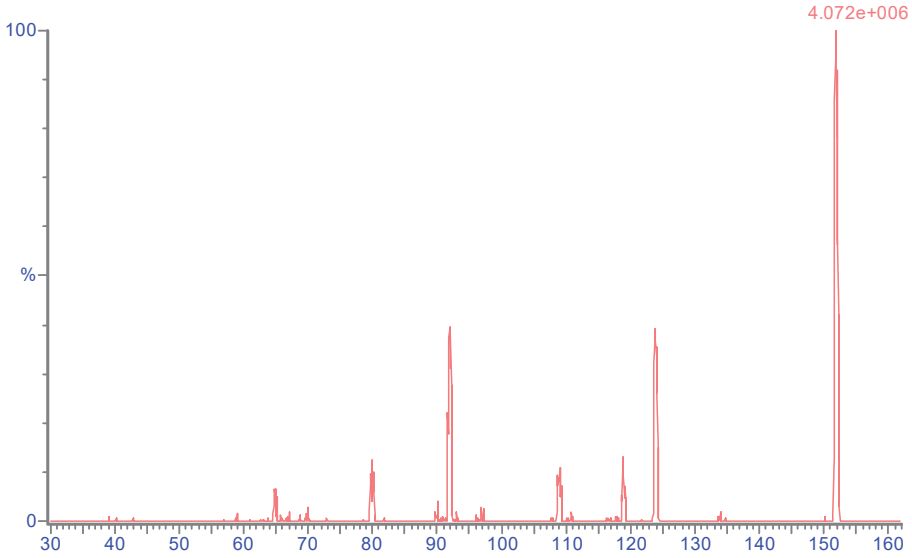

Optimized Daughter Spectrum (at Collision Energy 16eV)

2-NH2-BTH - *2-Aminobenzothiazole*

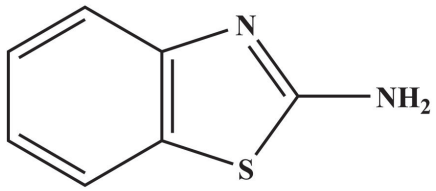

2-Aminobenzothiazole

Compound	Formula/Mass		Parent m/z	Cone Voltage (V)	Daughters	Collision Energy (eV)	Ion Mode
2-NH2-BTH	C7H6N2S	1	150.99	28	108.97	20	ES+
		2	150.99	28	123.99	18	ES+

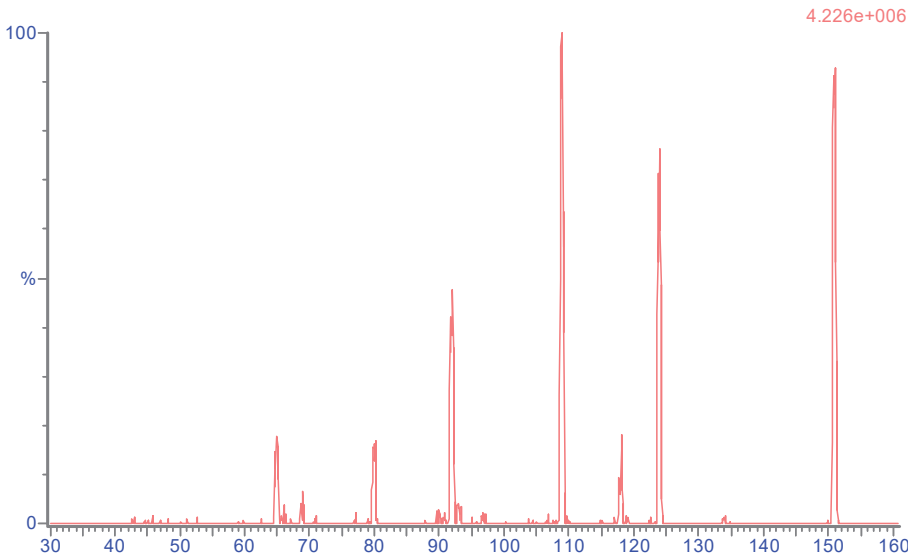

Optimized Daughter Spectrum (at Collision Energy 20eV)

2-Me-S-BTH - *2-(Methylthio)benzothiazole*

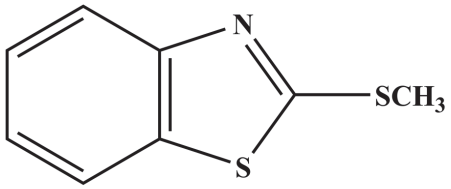

2-(Methylthio)benzothiazole

Compound	Formula/Mass		Parent m/z	Cone Voltage (V)	Daughters	Collision Energy (eV)	Ion Mode
2-Me-S-BTH	C8H7NS2	1	181.97	26	166.99	22	ES+
		2	181.97	26	108.95	32	ES+

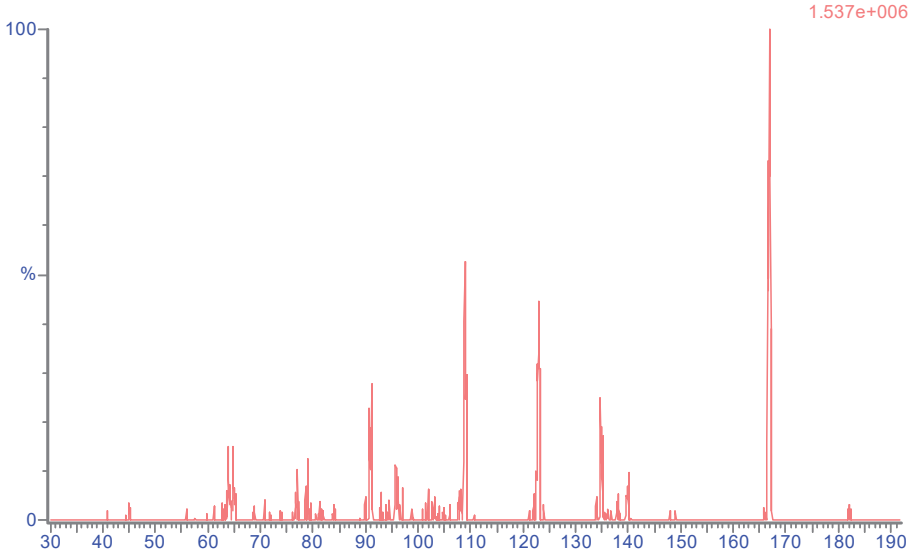

Optimized Daughter Spectrum (at Collision Energy 32eV)

2-M-BTH - *2-Morpholin-4-YL-benzothiazole*

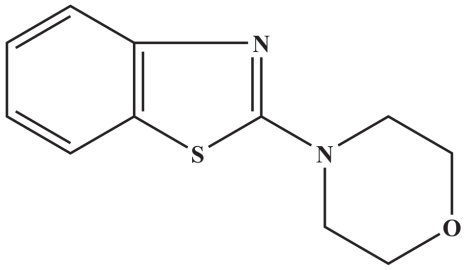

2-Morpholin-4-yl-benzothiazole

Compound	Formula/Mass		Parent m/z	Cone Voltage (V)	Daughters	Collision Energy (eV)	Ion Mode
2-M-BTH	C11H12N2OS	1	221.04	2	177.05	18	ES+
		2	221.04	2	108.95	30	ES+

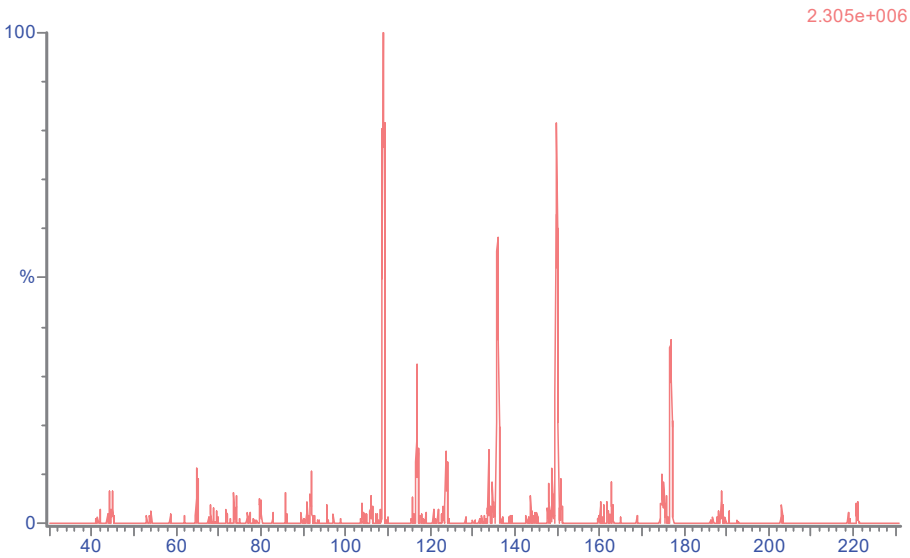

Optimized Daughter Spectrum (at Collision Energy 30eV)

BTR – *Benzotriazole*

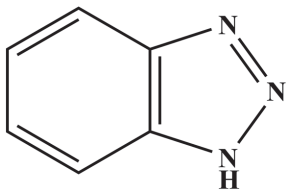

Benzotriazole

Compound	Formula/Mass		Parent m/z	Cone Voltage (V)	Daughters	Collision Energy (eV)	Ion Mode
BTR	C6H5N3	1	120.02	28	64.96	16	ES+
		3	120.02	28	92.00	14	ES+

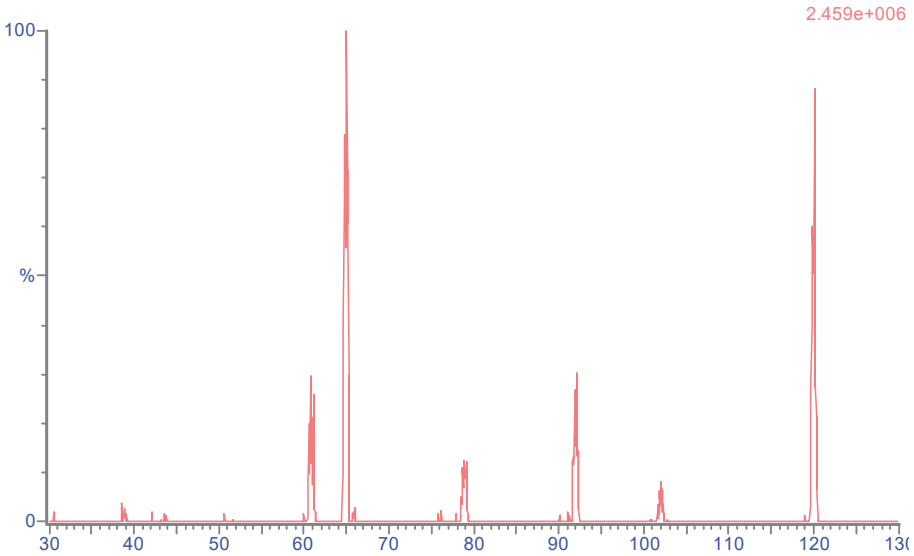

Optimized Daughter Spectrum (at Collision Energy 16eV)

TTR - *4-Methyl-1H-benzotriazole*

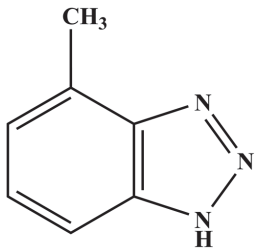

4-Methyl-1H-benzotriazole

Compound	Formula/Mass		Parent m/z	Cone Voltage (V)	Daughters	Collision Energy (eV)	Ion Mode
TTR	C7H7N3	1	133.97	40	78.95	18	ES+
		2	133.97	40	77.00	22	ES+

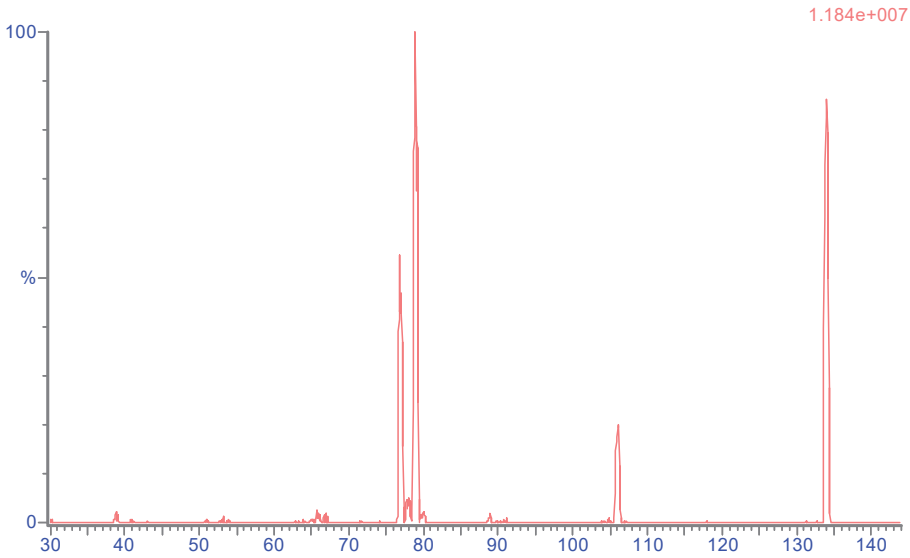

Optimized Daughter Spectrum (at Collision Energy 18eV)

XTR - *5,6-Dimethyl-1H-benzotriazole monohydrate*

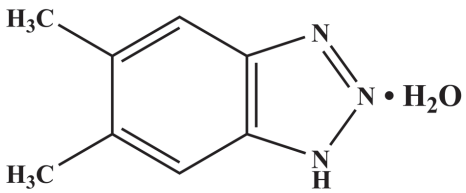

5,6-Dimethyl-1H-benzotriazole monohydrate

Compound	Formula/Mass		Parent m/z	Cone Voltage (V)	Daughters	Collision Energy (eV)	Ion Mode
XTR	C8H9N3	1	148.05	16	92.98	16	ES+
		2	148.05	16	76.98	24	ES+

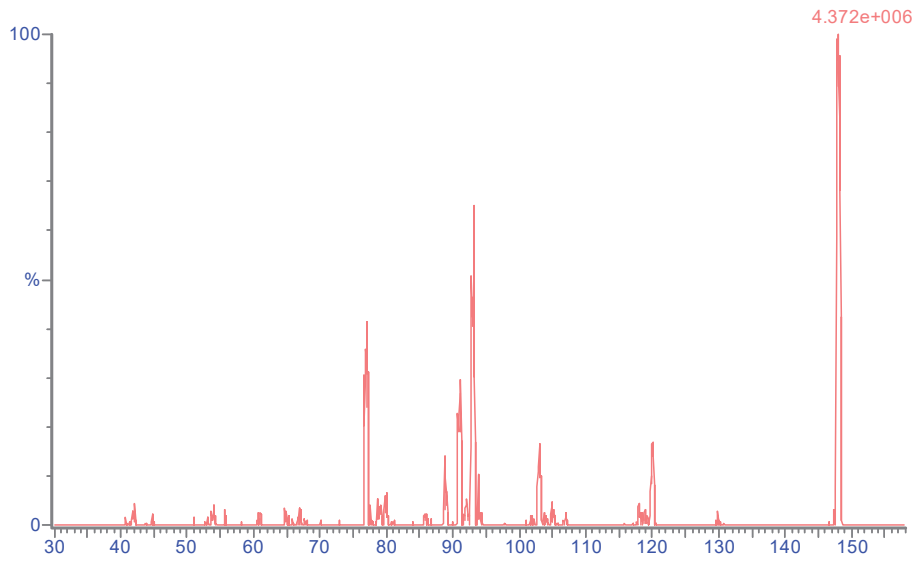

Optimized Daughter Spectrum (at Collision Energy 16eV)

BTR COOH - *Benzotriazole-5-carboxyl acid*

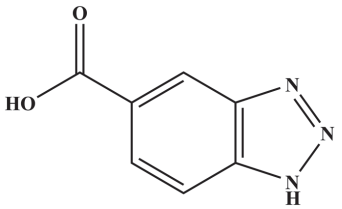

Benzotriazole-5-carboxylic acid

Compound	Formula/Mass		Parent m/z	Cone Voltage (V)	Daughters	Collision Energy (eV)	Ion Mode
BTR-COOH	C7H5N3O2	1	164.01	2	79.98	18	ES+
		2	164.01	2	108.00	18	ES+

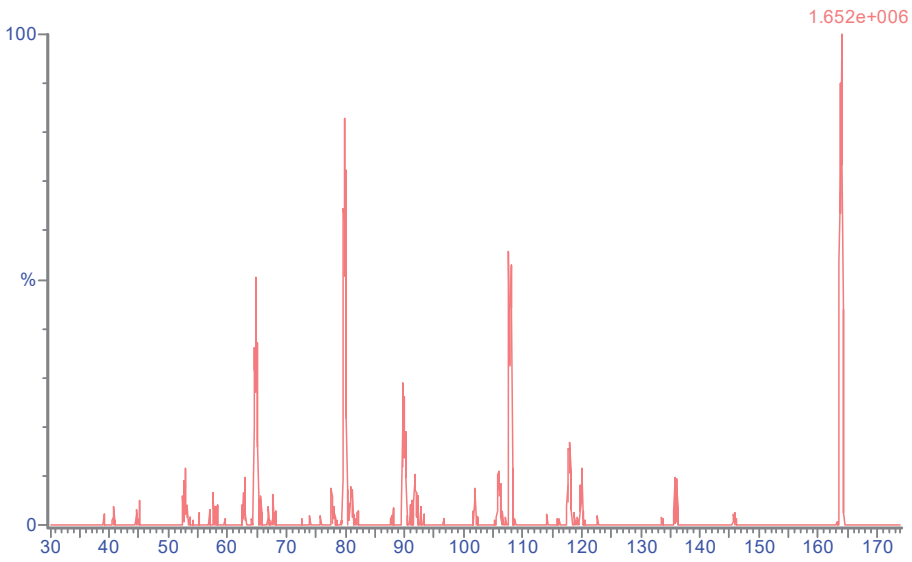

Optimized Daughter Spectrum (at Collision Energy 18eV)

5-Cl-BTR - *5-Chlorobenzotriazole*

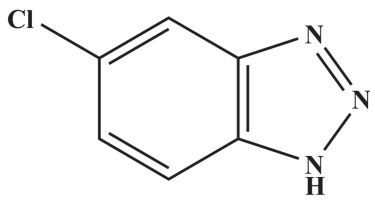

5-Chlorobenzotriazole

Compound	Formula/Mass		Parent m/z	Cone Voltage (V)	Daughters	Collision Energy (eV)	Ion Mode
5-Cl-BTR	C6H4ClN3	1	153.98	24	98.96	22	ES+
		3	153.98	24	72.89	24	ES+

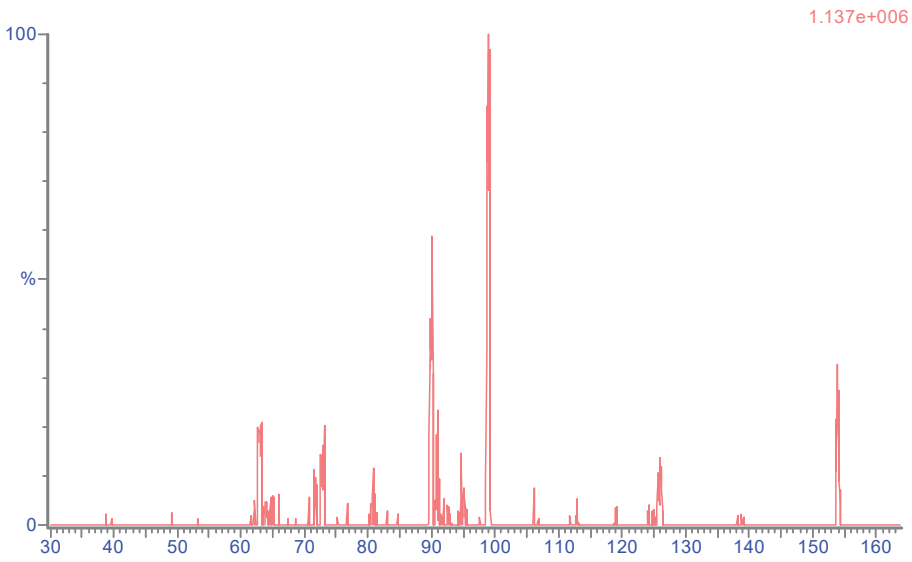

Optimized Daughter Spectrum (at Collision Energy 22eV)

1-OH-BTR - *1-Hydroxybenzotriazole hydrate*

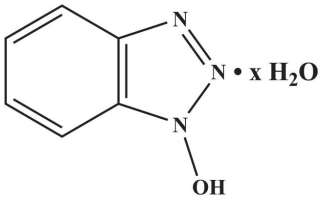

1-Hydroxybenzotriazole hydrate

Compound	Formula/Mass		Parent m/z	Cone Voltage (V)	Daughters	Collision Energy (eV)	Ion Mode
1-OH-BTR	C6H5N3O	1	136.01	24	90.96	18	ES+
		2	136.01	24	118.97	14	ES+

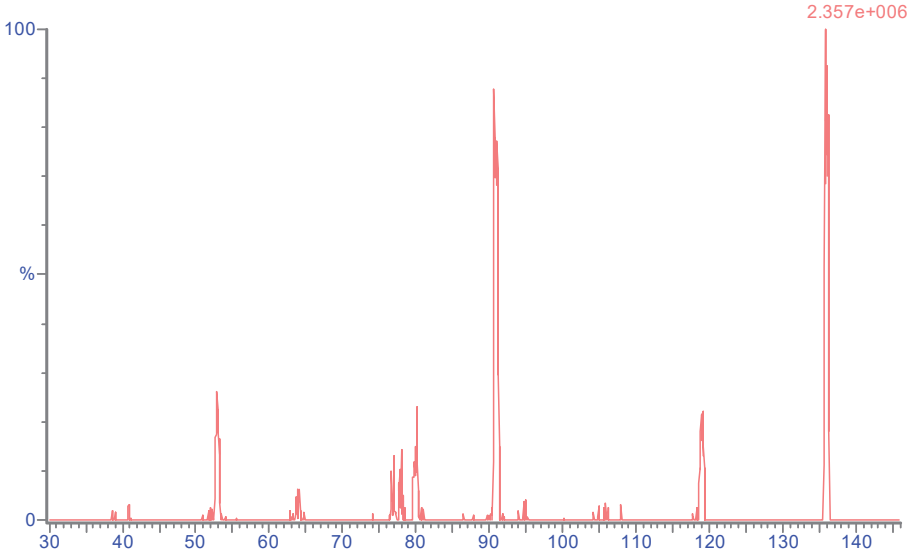

Optimized Daughter Spectrum (at Collision Energy 14eV)

5-Amino-BTR - *5-Amino-1H-benzotriazole*

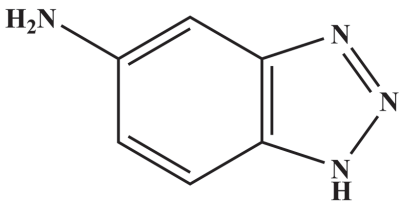

5-Amino-1H-benzotriazole

Compound	Formula/Mass		Parent m/z	Cone Voltage (V)	Daughters	Collision Energy (eV)	Ion Mode
5-Amino-BTR	C6H6N4	1	135.03	42	79.97	16	ES+
		2	135.03	42	107.00	16	ES+

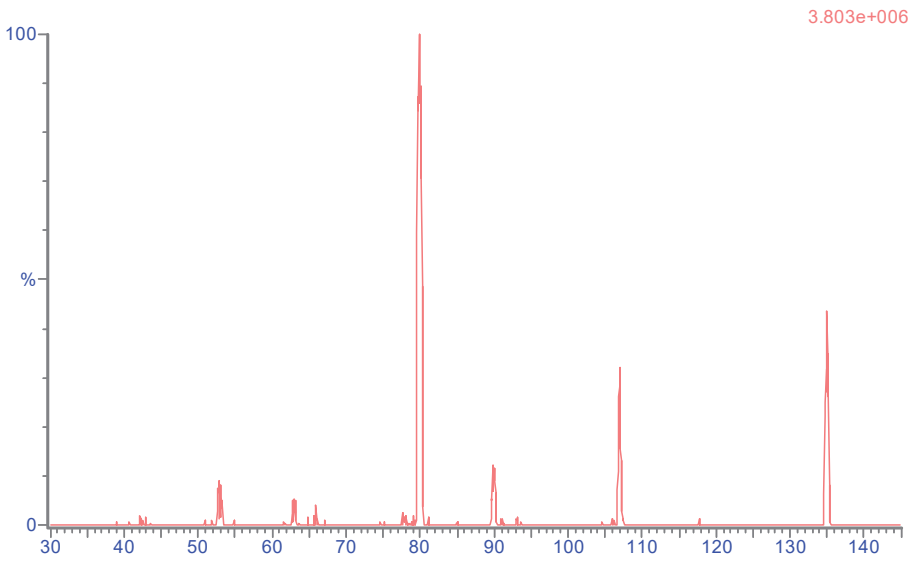

Optimized Daughter Spectrum (at Collision Energy 16eV)

BTR-d4 - *1H-Benzotriazole-(ring-d4) solution*

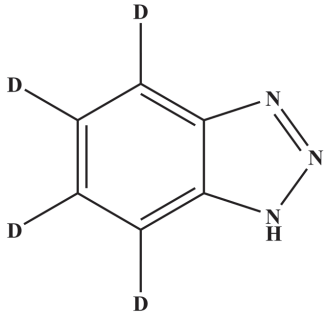

1H-Benzotriazole-(ring-d4) solution

Compound	Formula/Mass		Parent m/z	Cone Voltage (V)	Daughters	Collision Energy (eV)	Ion Mode
BTR D4	2H4C6HN3	1	123.98	38	68.68	18	ES+
		2	123.98	38	96.03	16	ES+

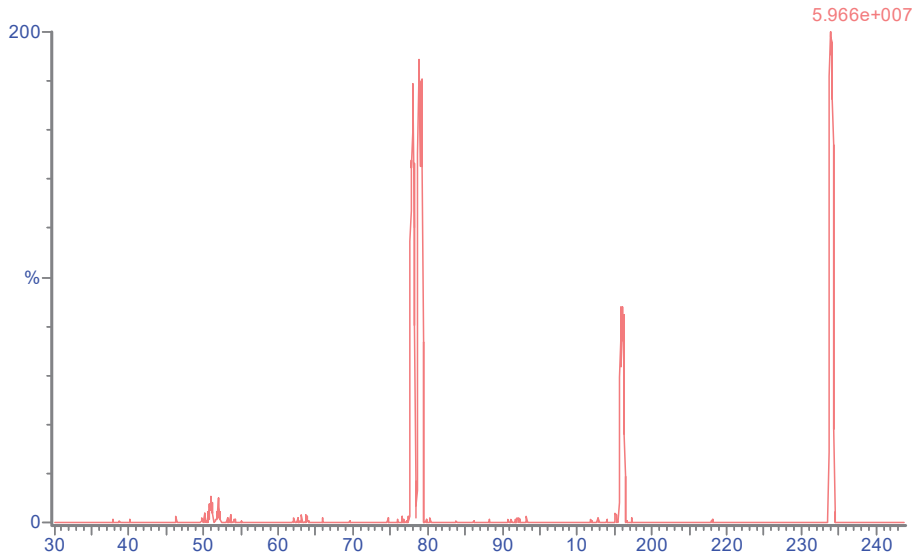

Optimized Daughter Spectrum (at Collision Energy 18eV)

Appendix F

Calibration curves

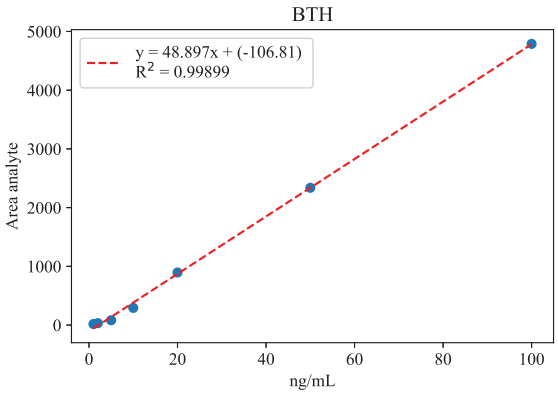
BTH
y = 48.897x + (-106.81)
R² = 0.99899
Area analyte
ng/mL

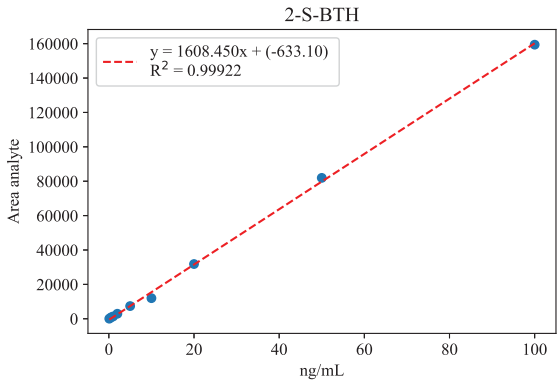
2-S-BTH
y = 1608.450x + (-633.10)
R² = 0.99922
Area analyte
ng/mL

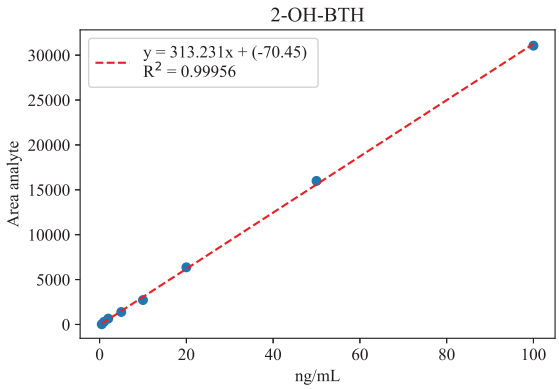
2-OH-BTH
y = 313.231x + (-70.45)
R² = 0.99956
Area analyte
ng/mL

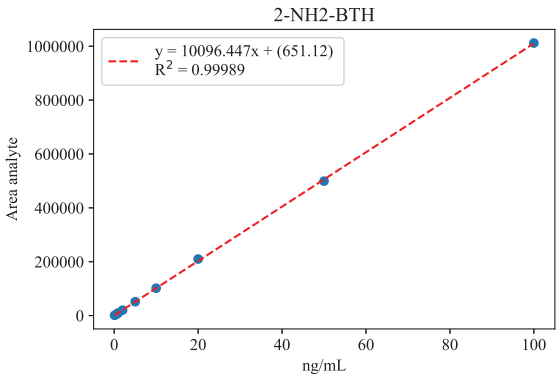
2-NH2-BTH
y = 10096.447x + (651.12)
R² = 0.99989
Area analyte
ng/mL

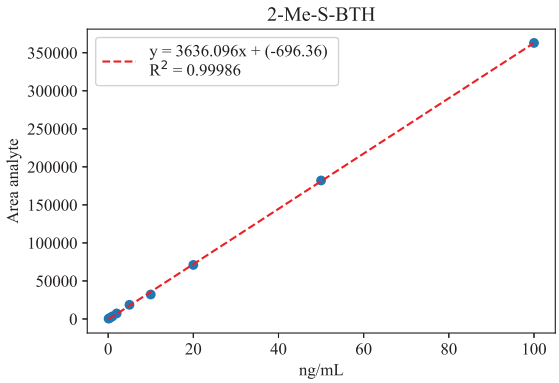
2-Me-S-BTH
y = 3636.096x + (-696.36)
R² = 0.99986
Area analyte
ng/mL

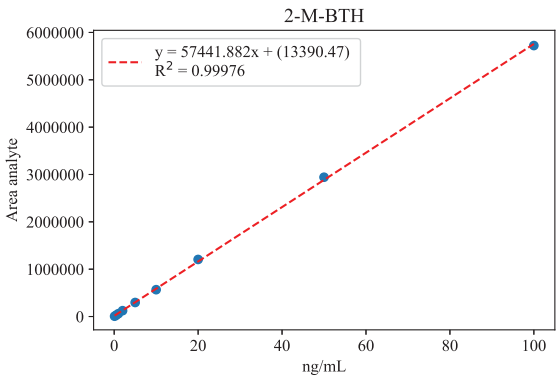
2-M-BTH
y = 57441.882x + (13390.47)
R² = 0.99976
Area analyte
ng/mL

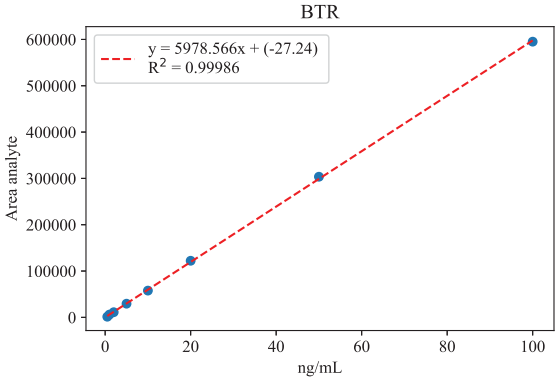
BTR
y = 5978.566x + (-27.24)
R² = 0.99986
Area analyte
ng/mL

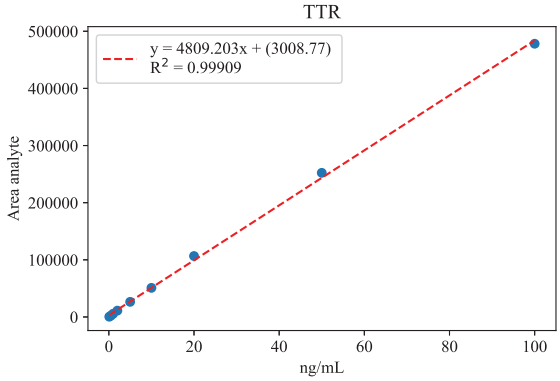
TTR
y = 4809.203x + (3008.77)
R² = 0.99909
Area analyte
ng/mL

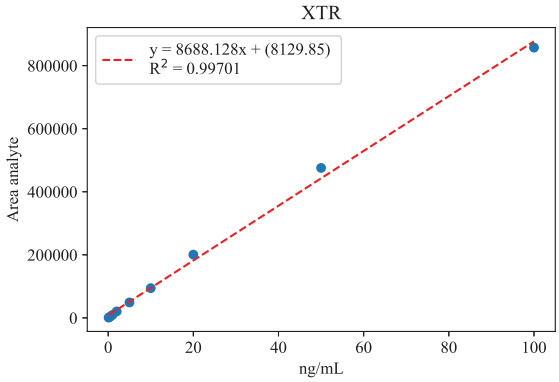
XTR
y = 8688.128x + (8129.85)
R² = 0.99701
Area analyte
ng/mL

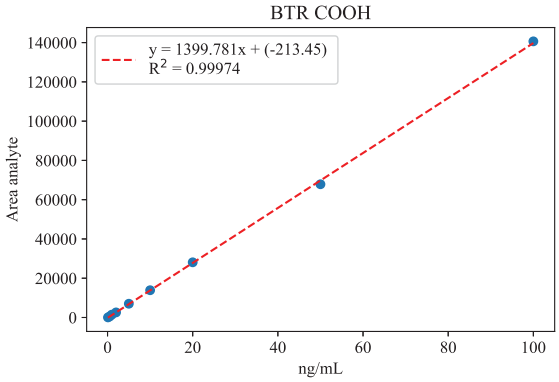
BTR COOH
y = 1399.781x + (-213.45)
R² = 0.99974
Area analyte
ng/mL

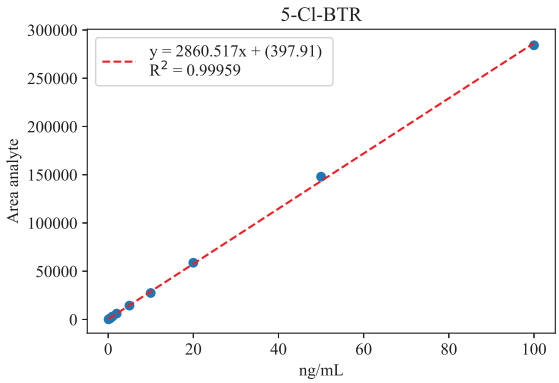
5-Cl-BTR
y = 2860.517x + (397.91)
R² = 0.99959
Area analyte
ng/mL

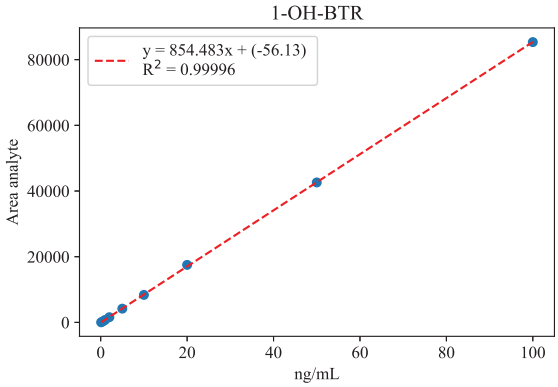
1-OH-BTR
y = 854.483x + (-56.13)
R² = 0.99996
Area analyte
ng/mL

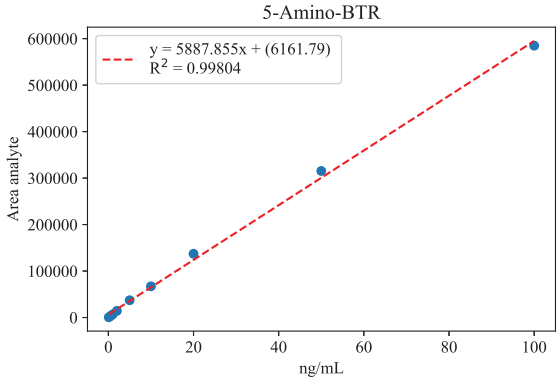
5-Amino-BTR
y = 5887.855x + (6161.79)
R² = 0.99804
Area analyte
ng/mL

Appendix G

ICP-MS parameters

Table G.1: Specifications for ICP-MS, Element 2 from Thermo Scientific

Instrumental part	Specification
Autosampler	SC2 DX equipped with a dustcover with ULPA filter
Sample injector	prepFAST
Nebulizer	PFA-ST with approx. volume range from 50-700μl/min.
Spray chamber	Quarts baffled micro cyclonic, with dual gas inlet type (ESI – ES-3452-111-11)
Cooling	PC^{3x} - Peltier cooling and heated inlet system.
Torch	Quarts Demountable with o-rings
Injector	Quarts 2.5 mm with o-rings, (ES-1024-0250)
Sample cone	Aluminium (ES-3000-18032)
Skimmer cone	Aluminium type X-skimmer (ES-3000-1805 X)
Radio frequency(RF)-power	1350 W

Table G.2: Gas flow settings for ICP-MS

Type of gas	Flow (L/min)
Cool gas	15.5
Auxiliary gas	1.1
Sample gas 1 (nebulizer)	0.75
Sample gas 2 (T-connection)	0.55
Additional gas (10% methane in Argon)	0.0004 corresponds to approx. 0.04% in the sample

Appendix H

Principal component analysis (PCA) data

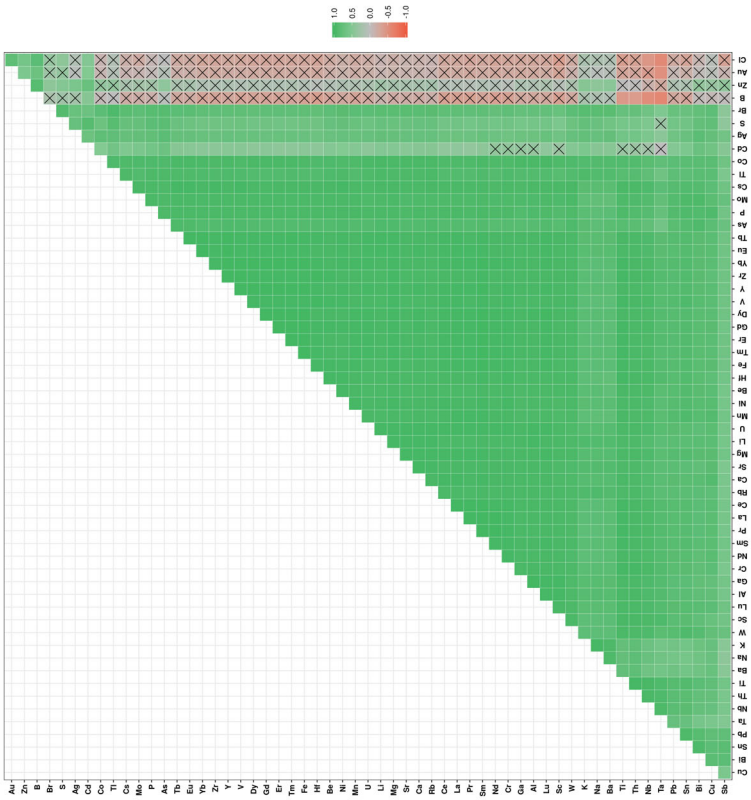

Figure H.1: Correlations of concentration (log) of elements used for PCA

Metals

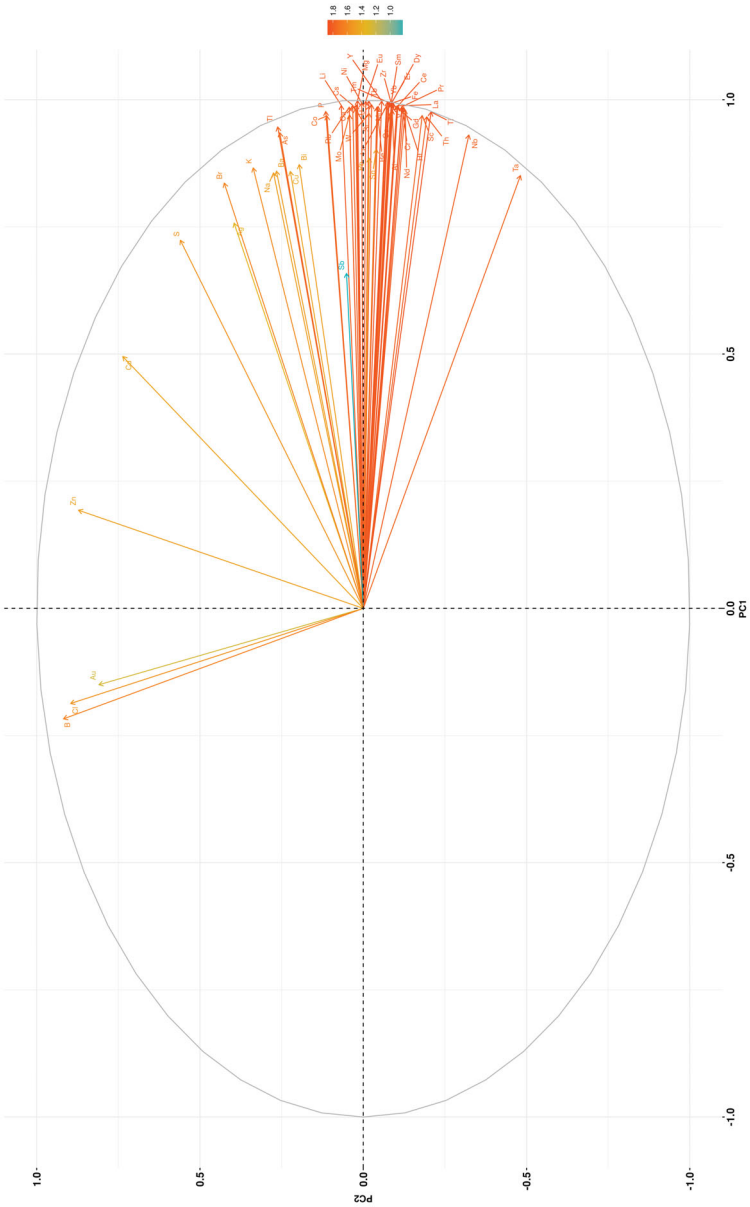

Figure H.2: Detailed loading plot for PCA elements

Benzothiazoles and benzotriazoles

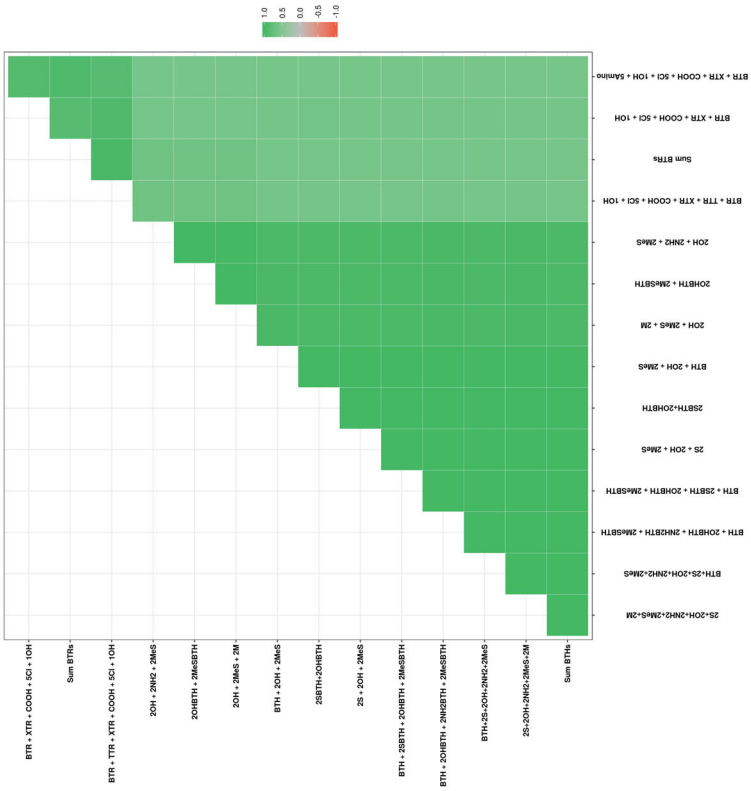

Figure H.3: Correlations of concentration (log) of BTHs and BTRs used for PCA

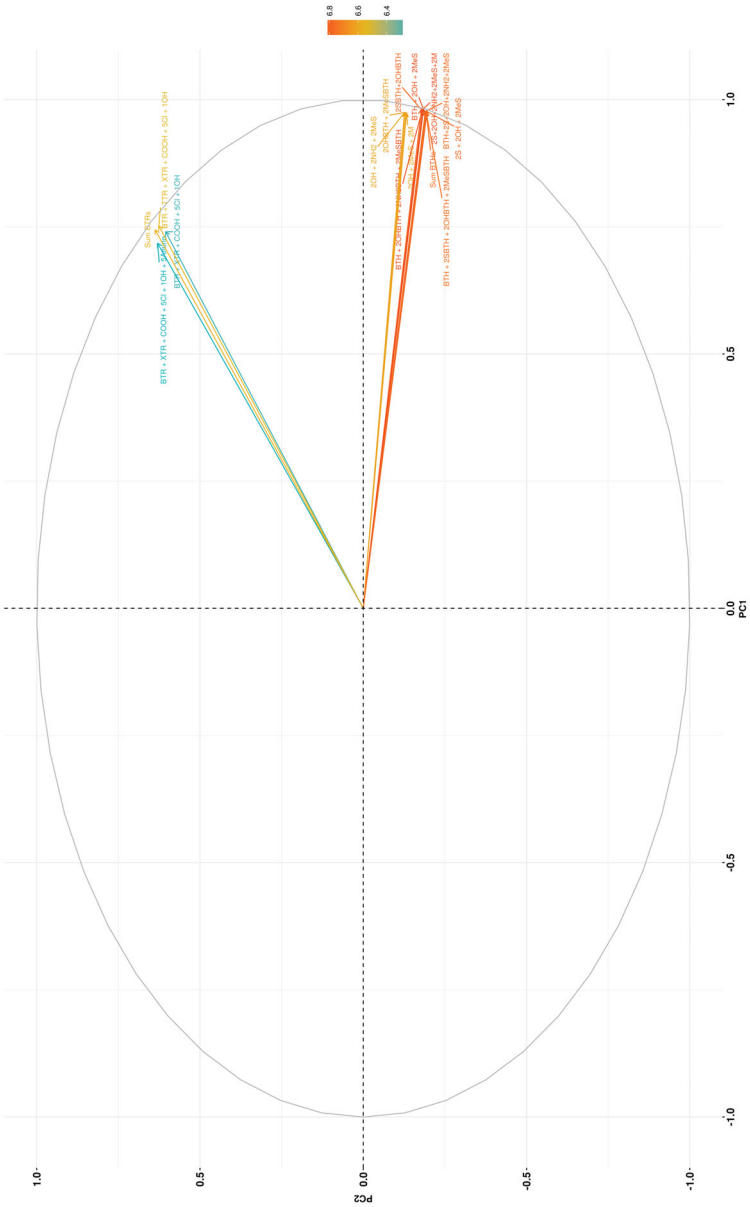

Figure H.4: Detailed loading plot for PCA of BTHs and BTRs in turbid road dust samples

Metals, Benzothiazoles and benzotriazoles

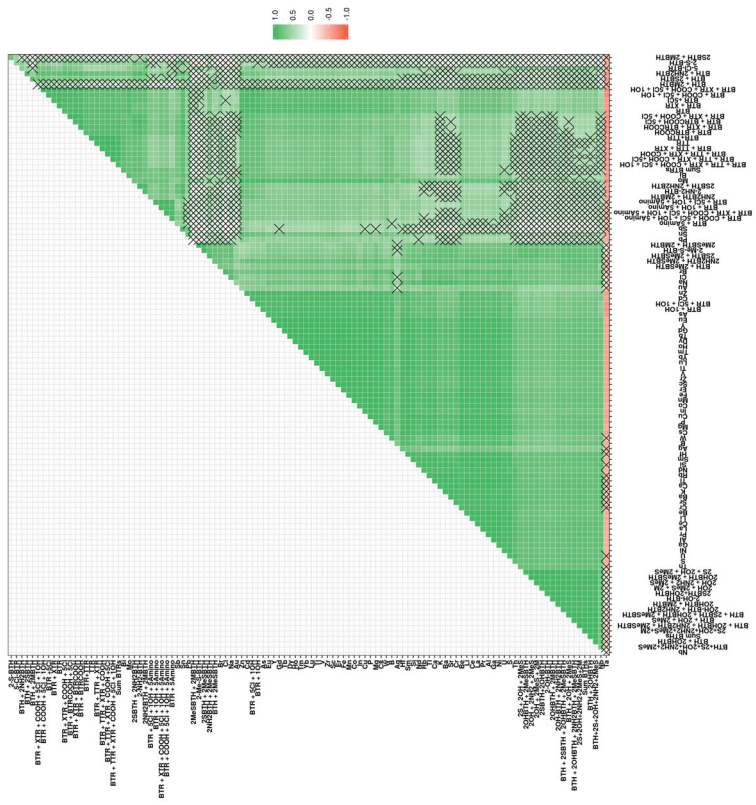

Figure H.5: Correlations of concentration (log) of elements, BTHs and BTRs used for PCA

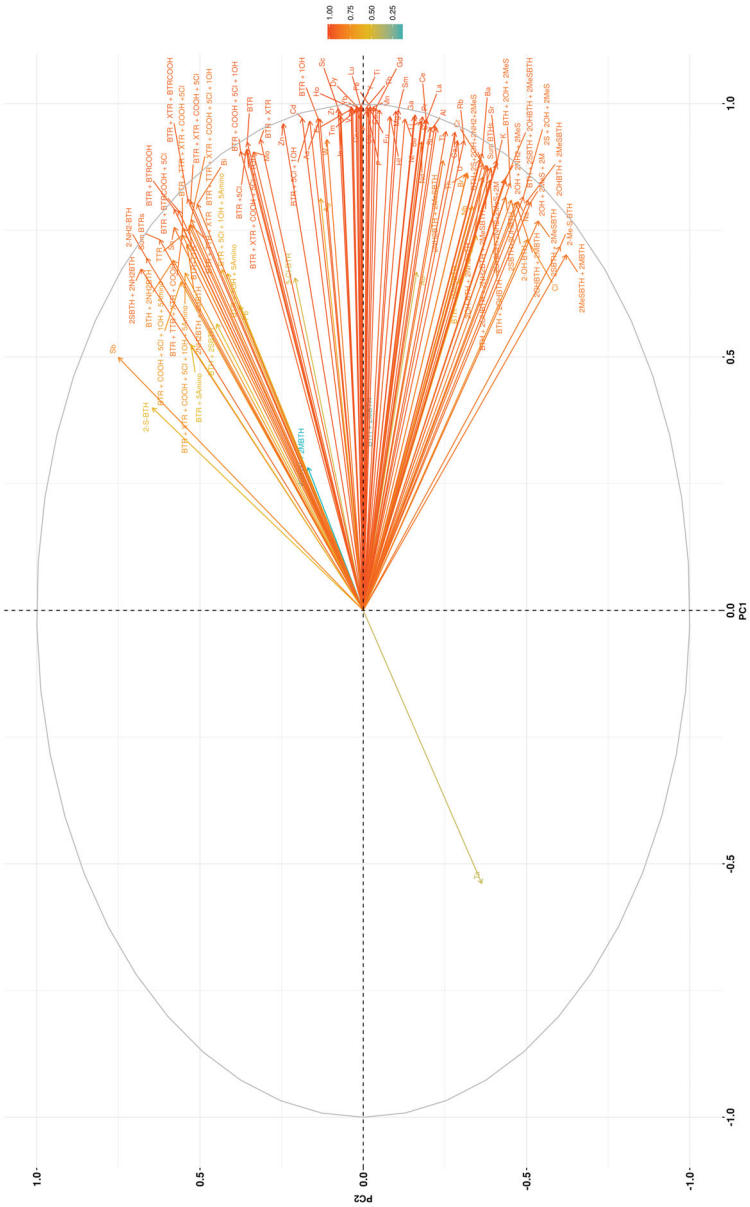

Figure H.6: Detailed loading plot for PCA of elements, BTHs and BTRs in turbid road dust samples